UCLouvain

FACULTE DES SCIENCES

Faculté des sciences

On Arctic Curve Phenomena in the Six-Vertex and Related Models

Mémoire présenté en vue de l'obtention du grade académique de

Master [120] en sciences physiques, finalité approfondie

Auteur : Nathan Vanbeneden
Promoteur : Prof. Christian Walmsley Hagendorf (IRMP/GPP)
Lecteurs : Prof. Philippe Ruelle (IRMP/GPP)
Prof. Jan Govaerts (IRMP/CP3)
École de Physique, IRMP, GPP

Année académique 2023-2024

Remerciements

Je tiens à remercier infiniment le Professeur Christian Walmsley Hagendorf, mon promoteur, pour son temps, son soutien constant et sa patience mise à rude épreuve par ma gestion de mail chaotique. Merci de m'avoir aidé tout le long de mon parcours universitaire, je ne serai probablement pas arrivé là où je suis sans le temps que vous m'avez accordé pendant le projet de fin de bachelier.

Je remercie également les Professeurs Philippe Ruelle et Jan Govaerts. J'ai particulièrement apprécié nos discussions lors de la pré-défense.

Merci à ma famille et à mes amis qui ont toujours cru en moi (tout en surestimant grandement mes capacités) sans jamais lâcher prise. Même si certains d'entre vous n'aiment pas cette phrase : vous m'avez sauvé !

Contents

List of Figures

Chapter 1

Introduction

The six-vertex model is a famous integrable model in statistical mechanics. We can use it to describe the thermodynamics of ice in two dimensions. The model is connected to numerous other systems [3], such as domino tiling of the Aztec diamond [18], alternating sign matrices [25, 26], height functions, non-intersecting paths, etc... Its thermodynamics depends on the chosen boundary conditions, unlike most statistical models. With a particular choice on a square lattice, called domain-wall boundary conditions, some regions of the domain are frozen in a fixed state as the number of vertices tends to infinity. The boundary of those frozen regions is called the *arctic curve*.

The six-vertex model is not the only model with arctic curve. Colomo and Sportiello devised a method to compute its expression, called the *tangent method* [13]. The method uses a relation between the six-vertex model and a set of non-intersecting paths. It is applicable to other models that relate in a similar way to a set of paths.

A simple model closely connected to the six-vertex model is the three-colour model. A three-colouring is given by attributing a colour to each face of a graph in such a way that any two adjacent faces have different colours [17]. Numerical simulations suggest that this model (with domain-wall boundary conditions) possesses frozen regions and an arctic curve. The initial aim of this work was to investigate the arctic curve in the three-colour model on a particular domain with a reflecting end.

In chapter 2, we give the basic definitions of the models we study, together with some of their properties. We then explain the tangent method and the algorithm we used to sample configurations under some choice of weights.

In chapter 3, we follow an article from Di Francesco [16] to compute the arctic curve of the six-vertex model on a square grid with domain-wall boundary conditions. We use the tangent method. We then briefly compare the results with the numerical simulations.

In the final chapter, we turn our attention to a generalisation of the six-vertex model, called the eight-vertex solid-on-solid (8VSOS) model. We use the relation between its partition function to the one of the three-colour model given by Hietala during her PhD thesis [19, 20]. We furthermore study a particular case of the 8VSOS model, unrelated to the three-colour model. This specialisation greatly simplifies

the formulas, since the partition function reduces to a product.

Chapter 2

The Models and the Tangent Method

In section 2.1, we provide the definition of the six-vertex model and some of its boundary conditions. We furthermore discuss the degrees of freedom for fixed boundary conditions together with the thermodynamic of the system. We introduce other models related to the six-vertex model in section 2.2. We dedicate the last section 2.3 to the tangent method and an explanation of the algorithm used to sample configurations.

2.1 Definitions

In this thesis, we only consider planar and connected graphs. For any graph G, we write $V(G)$ its set of vertices, and $E(G)$ the set of edges. For each $n \in \mathbb{N}_*$, we also define $V_n(G)$ as the set of vertices of G with degree equal to n. We denote $\mathcal{F}(G)$ the dual graph of G, *i.e.* the graph defined by the faces of G, where two faces form an edge if they are adjacent. We write the set of faces of G by $F(G) = V(\mathcal{F}(G))$. In the case of rectangular grids, we consider the vertices as elements of $\mathbb{Z}^2$ and the faces in the set $(1/2 + 1/2) + \mathbb{Z}^2$. Then, we separate faces when there exists a point lying on an edge of G, even if they should be the same face according to the definition of the dual graph.

We begin our discussion with an exposure of the six-vertex model. It is a statistical model originally created to understand the thermodynamics of ice. In ordinary ice, the crystalline structure of the water molecules is approximately a three-dimensional hexagonal lattice [31]. The oxygen atoms place themselves on the vertices of the lattice, but the hydrogen atoms are not fixed. A simple model is to consider that each of the hydrogen atoms of a molecule is bounded to its oxygen atom and is positioned on the edges between this oxygen atom and its nearest neighbours. Moreover, each edge can only have one hydrogen atom.

The six-vertex model is an approximation of this system on a two-dimensional grid G, seen as a graph. The vertices represent the oxygen atoms, and oriented edges represent the bounded hydrogen atoms. The orientation points towards the bounded atom. Because the graph has degree four, every vertex has two ingoing edges and

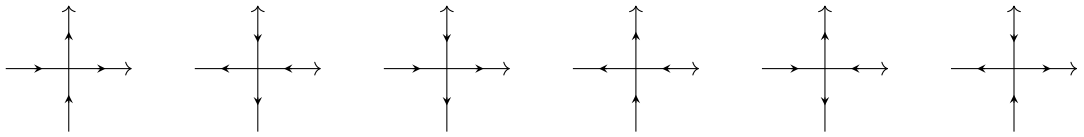

Figure 2.1: Types of vertices of the six-vertex model

two outgoing ones. We call this property the *ice rule*. An orientation of the graph G is a *six-vertex configuration* if it satisfies the ice rule at every vertex. This rule leaves only six possible local configurations around the vertices, called $a_\pm, b_\pm$ and $c_\pm$ (see figure 2.1). We depict the orientation by arrows.

For any vertex v and six-vertex configuration ω, we denote the vertex type of v in ω as $t(v,\omega)$. We associate a weight W_t to each vertex of type $t \in \{a_\pm, b_\pm, c_\pm\}$. We define the weight of ω as the product of all the vertex weights of the configuration.

$$W(\omega) = \prod_{v \in V_4(G)} W_{t(v,\omega)} = \prod_{t \in \{a_\pm, b_\pm, c_\pm\}} W_t^{N_t(\omega)}. \tag{2.1}$$

where $N_t(\omega)$ is the number of t-vertices in ω. The partition function Z over a set of configurations Ω is the sum of the weights over Ω, *i.e.* $Z = \sum_{\omega \in \Omega} W(\omega)$. When the vertex weights are positive, this defines a probability measure by asking that the probability of finding a configuration ω be

$$\mathbb{P}(\omega) = \frac{1}{Z} W(\omega). \tag{2.2}$$

With this definition, we understand why it is only necessary to consider connected graphs. Suppose that the set of connected components $[G]$ of G has finite cardinality greater than 2. For each $c \in [G]$, we define Ω_c as the set of functions in Ω restricted to c. We furthermore write $Z_c = \sum_{\omega \in \Omega_c} W(\omega)$ and define the marginal probabilities $\mathbb{P}_c$ by

$$\mathbb{P}_c \colon \Omega_c \mapsto [0,1] \colon \varpi \mapsto \sum_{\substack{\omega \in \Omega \\ \omega_{|c} = \varpi}} \mathbb{P}(\omega). \tag{2.3}$$

The set Ω is in bijection with the cartiesian product $\prod_{c \in [G]} \Omega_c$. Hence, we compute using (2.1) for all $\omega \in \Omega$

$$\mathbb{P}_c(\omega_{|c}) = \frac{1}{Z_c} W(\omega_{|c}), \quad \mathbb{P}(\omega) = \prod_{c \in [G]} \mathbb{P}_c(\omega_{|c}). \tag{2.4}$$

We have independence. In what follows, we abuse notation and refer to the weights W_t simply as t.

As it will be important later, we add some structure to the model. With the current definition of the vertices, if we rotate figure 2.1 by 90 degrees, the vertices change. The vertex a_+ becomes b_- (or b_+ depending on the direction of rotation), etc. The types of vertices are only defined if we specify an orientation of the plane (the paper).

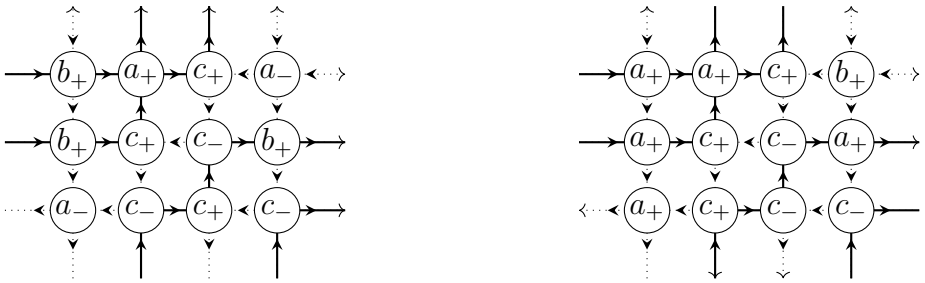

Figure 2.2: Two identical six-vertex configurations with different line orientations. Note that the type of vertices changes.

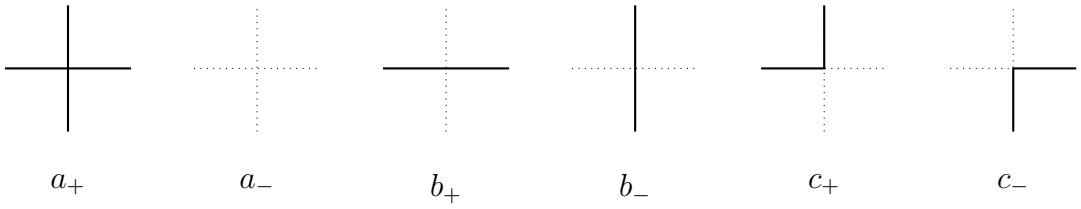

Figure 2.3: Types of vertices of the six-vertex model in the path picture.

We change this by attributing an orientation to each line of the graph, depicted with the arrows on the boundary of the edges in figure 2.1. We find the type of a vertex by rotating the local configuration so that the line orientation match the ones of figure 2.1. Note that the line orientations have nothing to do with the orientations of the edges defining the six-vertex model.

The added structure allows us to create more complex configurations, for example by alternating the line orientations (see figure 2.2).

There is another useful way to understand the six-vertex model. Instead of depicting the orientations as arrows, we draw a thick line if the orientation on an edge points east or north, and we draw dotted lines otherwise (see figure 2.3). Thanks to the ice rule, we can interpret this picture as a set of paths between adjacent vertices on the graph where each step goes either right or up (or the opposite) [30]. A different choice of directions for the drawing prescription would give different paths going in other directions. Note that in this representation, we do not take into account the line orientation. The representation in the path picture is always drawn with the paper's orientation, as if the horizontal lines were oriented to the right and the vertical ones upward. To determine the type of vertex, we generally need to translate the drawing in the arrow picture. Sometimes, we draw the configurations with arrows and paths, as in figure 2.2

2.1.1 Boundary Conditions

For now, we did not specify the space of configuration Ω. The most elementary choice is the set of every possible configuration. Most of the time, we work with every possible configuration that satisfy some boundary conditions.

We study a particular case of fixed boundary condition called *domain-wall* boundary conditions [24]. They are defined on a square grid and such that the orientation on the horizontal boundary edges enters the square grid and the arrow on the vertical

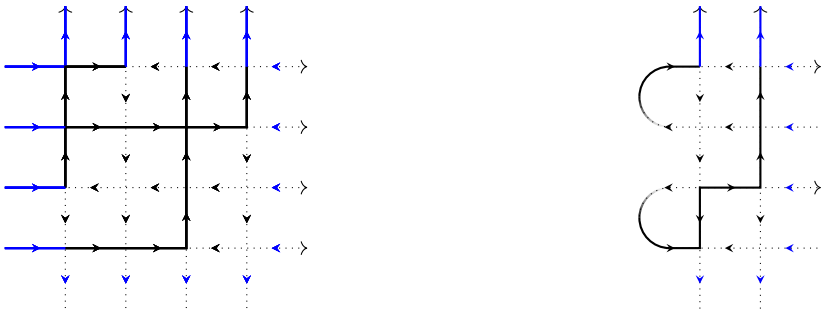

Figure 2.4: Two configurations of the six-vertex model with domain-wall boundary conditions (left) on a square lattice (right) with a reflecting end. The blue arrows and edges indicate the boundary conditions.

Figure 2.5: Types of turn of the six-vertex models with a reflecting end. The point in the middle of the half circle is the turn, but we do not draw it.

outer edges points outside (or the opposite). In terms of paths, this translates to drawing thick lines on the occidental and septentrional border and none on the other. Figure 2.4 illustrates a configuration with a reflecting end.

Boundary conditions with a reflecting end are an other option [12, 34]. There, we attach the exterior parts of two boundary edges together at a vertex v, and we ask the orientations of the edges to be such that one arrow points towards v and one away from v. We call such a vertex v a *turn*. We do not represent it on the figures, but we indicate the turns with an arc of circle. The orientation is reflected back from one line to the other in the opposite direction. We ask the line orientation of the two connected lines to be opposite so that we can see them as one line that turns back. We have two possible turns, k_+ and k_- (see figure 2.5). We generalise the previous six-vertex model by attributing a weight $W_{k_\pm}$ to the turns $k_\pm$. We write $K(G)$ the set of turns of G and define the weight of a configuration ω as

$$W(\omega) = \prod_{v \in V_4(G)} W_{t(v,\omega)} \prod_{k \in K(G)} W_{t(k,\omega)} = \prod_{t \in \{a_\pm, b_\pm, c_\pm, k_\pm\}} W_t^{N_t(\omega)}. \tag{2.5}$$

The right part of figure 2.4 illustrates a configuration with a reflecting end.

Although there are multiple other types of boundary conditions of great interest, we restrict ourselves only to domain-wall boundary conditions on a square grid of size $n \times n$ and domain-wall boundary conditions with a reflecting end on a rectangular grid of size $2n \times n$.

2.1.2 Degrees of Freedom and Flips

Despite the apparent six degrees of freedom, the six-vertex model has some conserved quantities that allow to reduce the number of different weights. In the six-vertex

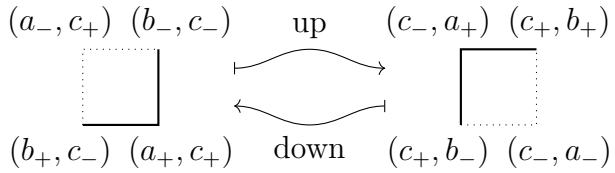

Figure 2.6: The possible vertices around each corner of a flippable face. Each pair of vertices is mapped to their corresponding type after the flip.

model with fixed boundary conditions, we only need to consider the *symmetric* case, where $t_+ = t_-$ for each vertex-type t. We can show this by combinatorial means with the path picture, but we here choose a different approach based on the important algorithm for this thesis. We only consider six-vertex models on rectangular grids.

Consider a six-vertex configuration ω with fixed boundary conditions. Suppose we have a face of the lattice with a path coming from the down left corner to the down right one and then proceeding upward. If we pull the path to cross the up left corner instead of the down right corner, we obtain a new six-vertex configuration. We can do the same operation in the opposite direction. We call such a transformation a *flip*, specifically a flip *up* for the one defined above and a flip *down* for the opposite (see figure 2.6). We write the function that flips a configuration around the face f by F_f (if the flip is not possible on a configuration, F_f acts as the identity on it).

We define an order on the paths of ω. A path p is greater than an other q if its starting point is either above or to the left of the start of q. In other words, we count the paths by beginning on the upper left corner, going down until we reach the bottom line, and then continuing to the right. From the configuration ω, we use a sequence of flip up to pull the first path north and west to its maximum. Then we proceed to do the same with the second path, etc, ... In this way, we create a configuration ω_- from a finite sequence of flips applied to ω,

$$\omega_- = F_{f_n} \dots F_{f_1} \omega. \tag{2.6}$$

This procedure produces the same configuration ω_- from any initial configuration ω. Hence, for an other configuration ω', there is a finite sequence of flips such that

$$\omega_- = F_{f'_{n'}} \dots F_{f'_1} \omega'. \tag{2.7}$$

As the flips are invertible, $F_f^{-1} = F_f$, we can pass between any two configurations ω, ω' by a sequence of flips

$$\omega' = F_{f'_1} \dots F_{f'_{n'}} F_{f_n} \dots, F_{f_1} \omega. \tag{2.8}$$

We are now ready to find the conserved quantities. We define for convenience the notation $\delta t = N_{t_+} - N_{t_-}$ for $t \in \{a, b, c\}$. Consider a flip on a face f. Figure 2.6 shows the possible vertex configuration on the corner of the face and their mapping under a flip. Looking at every possibility, we find some invariant quantities. On the upper left corner, either a a_- is mapped to c_- or c_+ is mapped to a_+. Hence

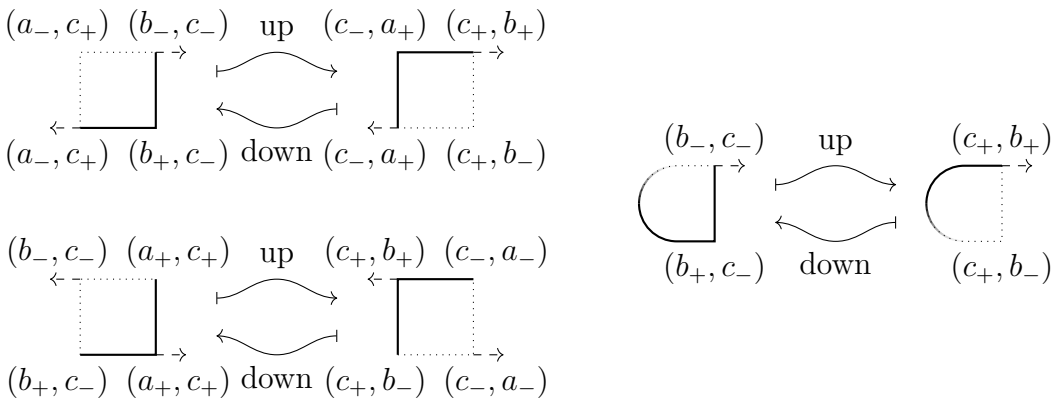

Figure 2.7: The possible vertices and turns around each corner of a flippable face. Each pair of vertices is mapped to their corresponding types after the flip.

this adds one to the value of δa. Conversely, the contribution of a flip on the down right corner subtracts one from δa. Because the two other corners of the face never have a a-vertex and those four vertices are the only ones modified by the flip, the quantity δa is invariant under the flips.

$$\delta a = (\delta a) \circ F_f, \quad \text{for every face } f. \tag{2.9}$$

With the same argument, we find two other invariant quantities, namely δb and δc. Because any two configurations are connected through a sequence of flips, the variables δt are the same for every configuration, *i.e.* they are conserved. These invariants allow us to rewrite the general system as the symmetric one.

The general partition function with fixed boundary conditions is

$$\begin{aligned} Z(a_\pm, b_\pm, c_\pm) &= \prod_{t\in\{a,b,c\}} \left(\frac{t_+}{t_-}\right)^{\delta t/2} \sum_{\omega\in\Omega} \prod_{t\in\{a,b,c\}} \sqrt{t_+ t_-}^{N_t(\omega)} \\ &= \prod_{t\in\{a,b,c\}} \left(\frac{t_+}{t_-}\right)^{\delta t/2} Z^{\mathrm{Sym}}\left(\sqrt{a_+a_-}, \sqrt{b_+b_-}, \sqrt{c_+c_-}\right). \end{aligned} \tag{2.10}$$

Therefore, we have the following theorem.

Proposition 2.1. *The six-vertex model on a square grid with fixed boundary condition is equivalent to the symmetric model with the weight of each family of vertices given by their geometric mean in the initial model, $t = \sqrt{t_+t_-}$ for $t \in \{a, b, c\}$.*

For more general boundary conditions, such as the periodic boundary conditions, the model is not as simple. Nevertheless, in the case of a reflecting end, as described above, we still have two conserved quantities restricting δb and δc. With the help of figure 2.7 and a similar argument as before, we find that δb and $\delta c - \delta k$ are invariant under a flip. The following theorem is important for Section 4.

Theorem 2.2. *The six-vertex model with domain-wall boundary condition and a reflecting end satisfy*

$$\delta b + \frac{n(n+1)}{2} = 0, \quad \delta c = \delta k \tag{2.11}$$

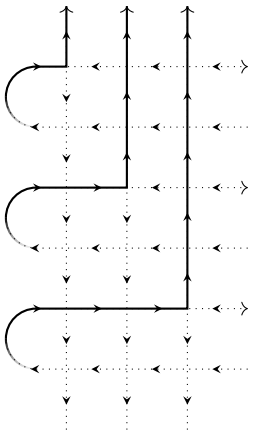

Figure 2.8: A particular six-vertex configuration with domain-wall boundary conditions and a reflecting end. Recall that one needs to be careful with the line orientations to obtain the type of vertices.

Proof. As previously shown, we know that δb and $\delta c - \delta k$ are invariant the same for every configuration. We thus only need to compute their values with one particular state. For example, we find the value from the configuration depicted in figure 2.8. We have

$$N_{c_+} = n = N_{k_+}, \quad , N_{c_-} = 0 = N_{k_-}, \quad , N_{b_+} = \frac{(n-1)n}{2}, \quad N_{b_-} = n^2. \tag{2.12}$$

This concludes the proof. □

2.1.3 Thermodynamics and Arctic Curves

In the six-vertex and other related models, we consider the configurations embedded inside a chosen fixed domain. In that sense, when we take the limit as n tends to infinity, we scale the whole configuration, and the density of vertex increases. We sometimes refer to this limit as the *scaling limit*. Most of the time, in statistical mechanics, the thermodynamic limit of the system does not depend on the particular choice of boundary conditions. This does not apply to the six-vertex model. Lieb and Sutherland first solved the symmetric model with periodic boundary conditions in 1967 [29, 35]. The probabilities are invariant under a rescaling of every weight; hence, it is enough to know the values a/c and b/c to describe the system. The macroscopic properties depend only on one parameter Δ defined as

$$\Delta = \frac{a^2 + b^2 - c^2}{2ab}. \tag{2.13}$$

When $|\Delta| > 1$, the system is ordered and frozen in two possible configurations in the thermodynamic limit. Those minimal-energy states contain only vertices that belong to the family with the biggest weight. When the dominant weights are a,or b, the vertices are all the same in the allowed configurations, and the system is in the *ferroelectric phase*. Conversely, if c is the biggest weight, the vertices alternate between c_+ and c_- as two of the same c-vertices can not be adjacent. This is the

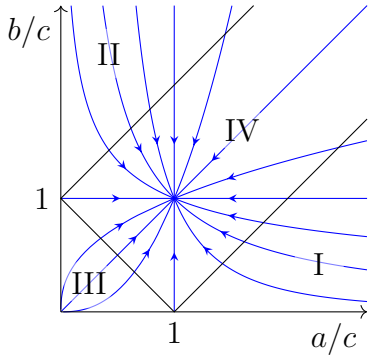

Figure 2.9: The phase diagram of the six-vertex model with periodic and domain-wall boundary conditions. Region I and II are the ferroelectric phases, region III is the antiferroelectric phase and region IV is the disordered phase. The blue lines indicate the change of weight with temperature. As the temperature increases, the points converge to $(1, 1)$.

anti-ferroelectric phase. The system is in the *disordered phase* if $|\Delta| < 1$. Then, many configurations contribute to the system.

The complete phase diagram is illustrated in figure 2.9 [3], with its temperature flow (the trajectories of $(a^\beta, b^\beta, c^\beta)$ as the inverse temperature β decreases). The free energy per unit site has a singularity as it crosses the boundary of the regions.

In the case of domain-wall boundary condition, the system has the same phase diagram as with periodic boundary condition [23, 8], but its properties are different [14]. In the ferroelectric phase, there is only one allowed configuration. As previously, they maximise the number of a or b vertices. They are given by the only configurations with only c vertices on the diagonal or anti-diagonal.

In a random configuration of the disordered phase, the neighbourhood of a corner contains only one type of vertex. In the configuration's core, however, the configurations are disordered. As the size of the grid increases, the probability of finding a vertex different than its neighbours around the corner goes to zero. Those regions are called *frozen*. The aim of this work is to study the boundary of these domains, called the *arctic curve*. Figure 2.10 shows a random configuration. Aggarwal [1] proved the existence of the arctic curve when $a = b = c$, but no proof exist for general weights.

In the anti-ferroelectric phase, the behaviour is similar. The system favours configurations with the greatest number of c-vertices, but the boundary condition restricts the vertices. A typical configuration has frozen regions around the corners enclosing a disordered region, allowing the emergence of second ordered region in the core of the square. The latter region contains only c-vertices.

2.2 Related Models

We present some simpler models whose set of configurations is equivalent to the one of the six-vertex model. We also introduce a generalisation of the six-vertex model. The definitions are inspired by [27].

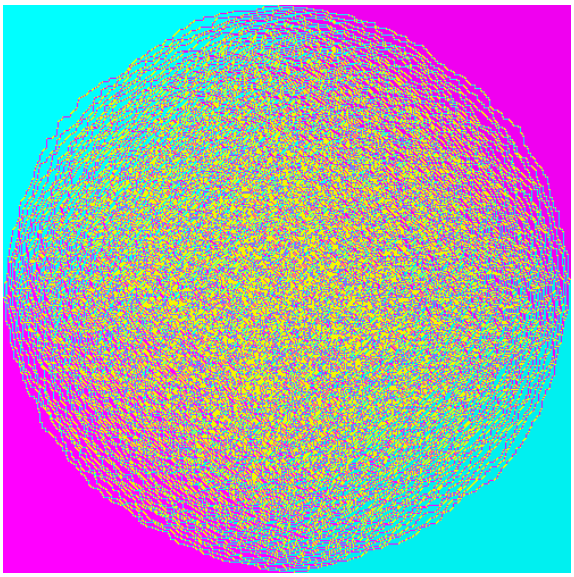

Figure 2.10: A random configuration in the six-vertex model with domain-wall boundary condition on a square grid of size 500. We color each vertex with respect to their family a, b or c, a is blue, b is magenta, and c is yellow. The weights are $a_\pm = b_\pm = 1$ and $c_\pm = \sqrt{2}$. There is a frozen region around the four corners of the square. With these weights, the arctic curve is a circle.

2.2.1 Solid-on-Solid Model

A *height map* on a graph G is a map h from G to $\mathbb{Z}$. We furthermore ask h to differ by one for each two adjacent vertices :

$$h(u) - h(v) \in \{-1, 1\} \quad \text{for all } u, v \in V(G) \text{ such that } \{u, v\} \in E(G). \tag{2.14}$$

With the specialisation, we also call a height map a *solid-on-solid* configuration. We define probabilities on the model by attributing weights W_t depending on the value t that the height map takes. We write $N_q(h)$ the number of vertices $v \in V(G)$ such that $h(v) = q \in \mathbb{Z}$. The complete weight of a configuration h is the product of the weights at each vertices.

$$W(h) = \prod_{v \in V(G)} W_{h(v)} = \prod_{q \in \mathbb{Z}} W_q^{N_q(h)}. \tag{2.15}$$

With a particular choice of boundary conditions, the six-vertex and solid-on-solid models are equivalent (when the graph is simply connected). We can construct a height map h on $F(G)$ from any six-vertex configuration ω on G in the following way. We choose a particular face $f \in F(G)$ and a value $h(f) \in \mathbb{Z}$. A face f' adjacent to f sharing the edge e takes the value $h(f) + 1$ if the arrow of ω on e points to the left with respect to an observer travelling from f to f'; otherwise, we fix $h(f') = h(f) - 1$ (of course, the opposite prescription also works). This procedure extends h to a function over $F(G)$. The ice-rule ensures that h is well defined: If we circle around a vertex, we see two arrows pointing to the left and two to the right; hence, h goes back to its initial value. The inverse operation is possible, even when $F(G)$ is not simply connected. A height map h and a six-vertex configuration ω are

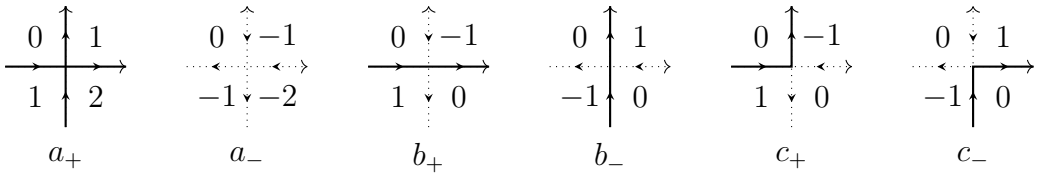

Figure 2.11: The local height configuration around the six possible vertices. The height on the upper right corner is fixed to zero. If the latter face has a non zero value h_0, add h_0 to each face to obtain the associated configuration.

Figure 2.12: A height map and a three-colouring coherent with the same six-vertex configuration as in figure 2.4. Both configurations have domain-wall boundary condition.

coherent if we can obtain one from the other by the algorithm described previously. Figure 2.11 illustrates the configurations around the six possible vertices.

As we study the six-vertex model with domain-wall boundary conditions, we use the related restriction on the external edges (see figure 2.12). The height map rises as we follow the septentrional border and then drops back, going down on the eastern column. The height maps are defined up to a constant, so we fix the value $h = 0$ on the upper leftmost face. Note that in the reflecting case, the turns alternate the direction of the horizontal arrows. Hence one face out of two on the western border is fixed to zero.

2.2.2 Three-Colouring

Graph colouring is an important subject in mathematics with many open problems [22, 17]. For $n \in \mathbb{N}_*$, a n-colouring of a graph G is a function c over $V(G)$ to $\{0, \dots, n\}$ such that two adjacent vertices do not share the same value, *i.e.*

$$c(u) \neq c(v) \quad \text{for all } u, v \in V(G) \text{ such that } \{u, v\} \in E(G). \tag{2.16}$$

In this context, we are not interested in the usual question of existence of such colourings. We consider the set of all possible n-colourings on a graph G, potentially specifying some boundary conditions, and define the statistic of the model by attributing weights W_q to each colour $q \in \{0, \dots, n-1\}$. As usual, the weight of a configuration is the product of the individual weights over all vertices.

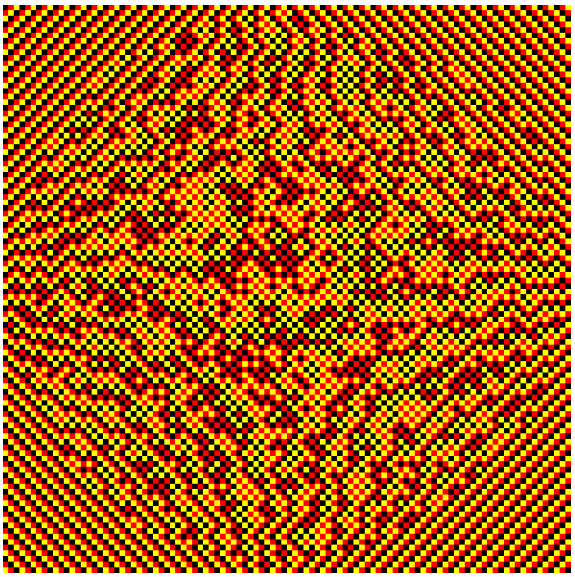

Figure 2.13: A random three-colouring with domain-wall boundary conditions on a square lattice of size 102. The configuration is generated with a uniform probability distribution ($a = b = c$).

$$W(c) = \prod_{v \in V(G)} W_{c(v)} = \prod_{q \in \{0,\dots,n-1\}} W_q^{N_q(c)}, \tag{2.17}$$

where $N_q(c)$ is the number of vertices $v \in V(G)$ such that $c(v) = q \in \{0, \dots, n-1\}$. We study the special case $n = 3$. If we take a height map from the preceding subsection modulo 3, we obtain a 3-colouring, or three-colouring.

As in the previous subsection, we consider boundary conditions analogous to domain-wall boundary conditions. In this case, the colours cycle on the border of the domain (see figure 2.12).

When $W_0 = W_1 = W_2$, every configuration has the same probability. In this particular case, we recover the results known for the six-vertex model with $a = b = c$ and know that the model has an arctic curve. With general colour weights, the existence of an arctic curve is unknown. Numerical simulations suggest that frozen regions and arctic curves occur in the three-colour model (figure 2.13). The frozen regions are made of diagonal lines with constant colour, cycling with the border of the square. Moreover, when the weights do not take the same value, the sampled configurations indicate the presence of a possible third region in the core. This is similar to the six-vertex model in the anti-ferroelectric phase. We did not investigate this property analytically.

2.2.3 Six-Vertex Solid-on-Solid Model

The *six-vertex solid-on-solid* model, or briefly the 6VSOS model, is a generalisation of the six-vertex model that uses its relation with the other systems. A configuration is the combination of a six-vertex configuration ω and a coherent height map h. This time, the weight around a vertex v depends on the type of vertex and the value of the height function in the upper left face of v with respect to the line orientation as

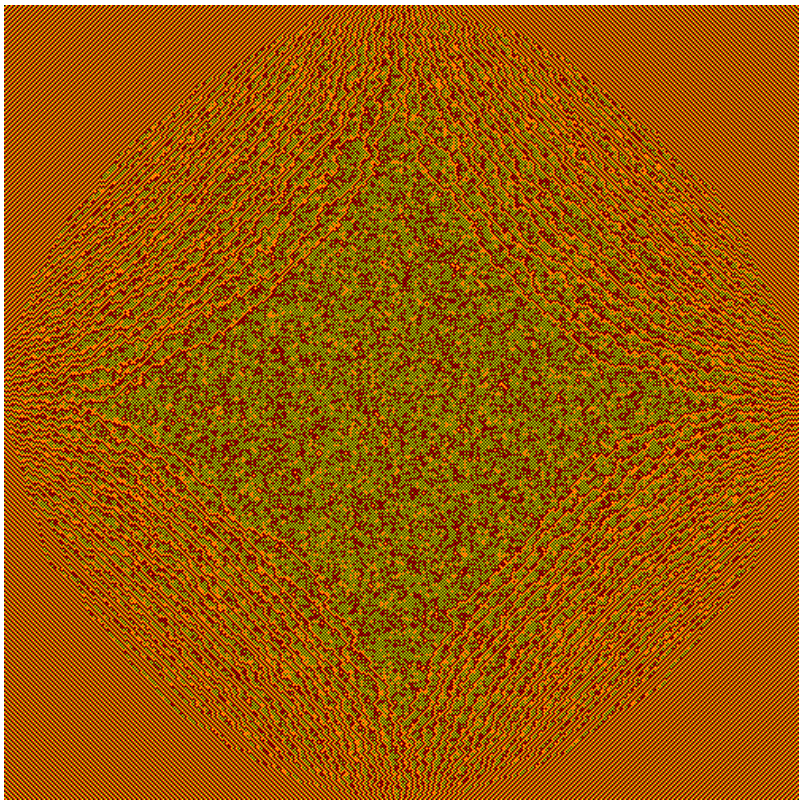

Figure 2.14: A random three-colouring with domain-wall boundary conditions on a square lattice of size 500. The colours are 0 = black, 1 = yellow, and 2 = red. The configuration is generated with colour weights $W_0 = 1, W_1 = 1/2, W_2 = 1/4$.

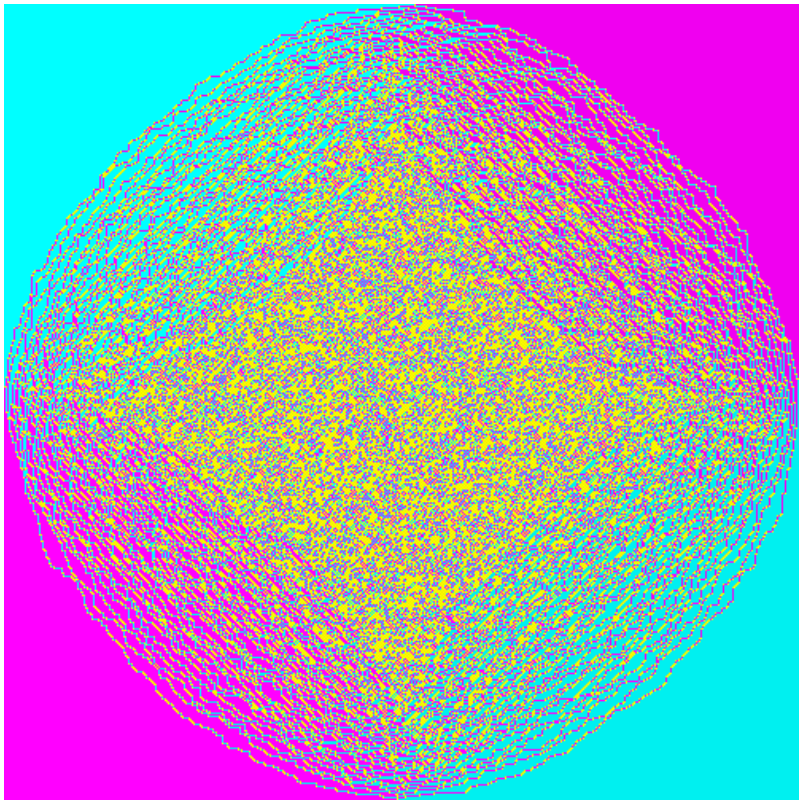

Figure 2.15: The six-vertex configuration corresponding to the three-colouring of figure 2.14. We color each vertex with respect to their family a, b or c, a is blue, b is magenta, and c is yellow.

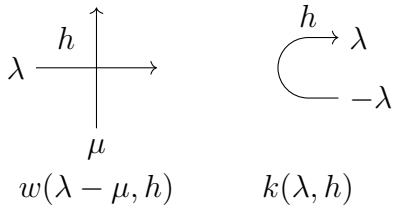

Figure 2.16: The dependence of the vertex weight on the height map and the spectral parameters. We denote the weight function of the vertex by w.

in figure 2.16 (do not mind the λ and μ for now). The relevant height for the weight of a turn k is the one on the face above k.

2.2.4 Inhomogeneities

So far, we have only considered the six-vertex model, where the vertex weights do not depend on their position in the graph. The partition function of the six-vertex model with domain-wall boundary condition was found by adding some inhomogeneity [21]. To each line of the domain, labelled by i, we associate a parameter λ_i. Similarly, we add a variable μ_j for each column j. We call λ_i and μ_j the spectral parameters. We chose a set of functions w_t for $t \in \{a_\pm, b_\pm, c_\pm\}$. The weight of vertex of type t with spectral parameters λ and μ as in figure 2.16 is

$$W_t = w_t(\lambda - \mu). \tag{2.18}$$

With some clever choice of continuous weight parametrisation w_t, it is possible to compute the partition function of the inhomogeneous model. We then find the homogeneous partition function by taking the homogeneous limit where every line has the same spectral parameter (same for the columns). We use such expressions of the partition function in section 3.1.3.

When there is a reflecting end, the horizontal spectral parameters are attributed to each pair of lines connected by a turn. The upper line takes the value λ while the other has the parameter $-\lambda$. As for the vertices, we define functions w_k for $k \in \{k_\pm\}$. The weight of a turn k with spectral parameter λ as in 2.16 is $w_k(\lambda)$.

We can generalise this to the six-vertex solid-on-solid model. When the functions parametrising the weights are elliptic (see Chapter 4), we actually call this system the *eight-vertex solid-on-solid* model, or 8VSOS model. Despite what the name suggests, there are still only six vertices in the model (and maybe two turns if we consider a reflecting end).

2.3 The Tangent Method

So far, the discussion has been mostly about definitions and some observations without any computations. We are interested in a method to obtain an expression for the arctic curve. We use the tangent method devised by Colomo and Sportiello [13].

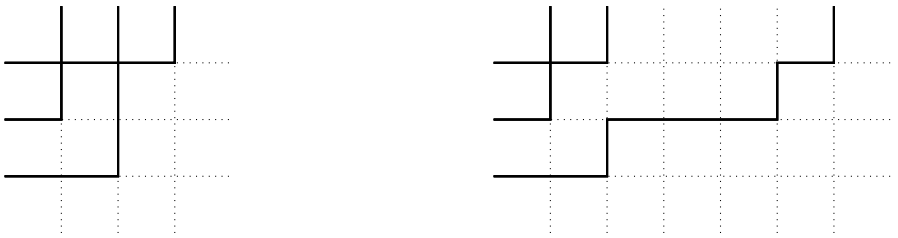

Figure 2.17: Two different configurations from a square lattice of size 3 (left) in the initial domain, (right) in the extended domain with $\lambda = 2$

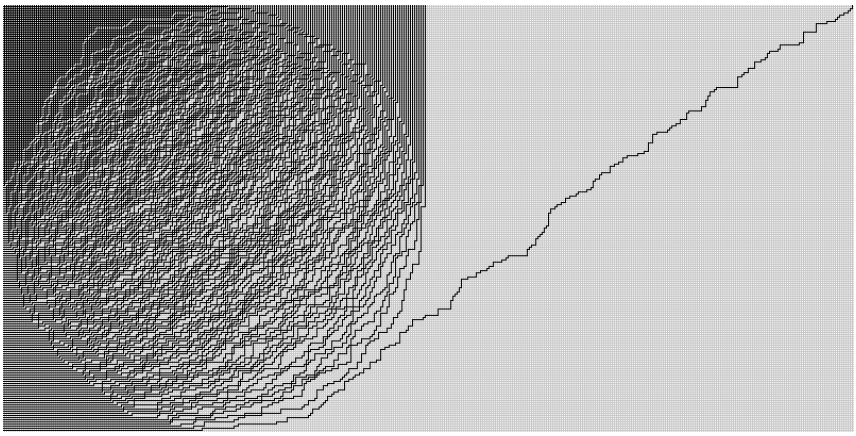

Figure 2.18: A random configuration in the path picture of the extension of the six-vertex model with domain-wall boundary condition with an initial square grid of size 200 and $\lambda = 2$. The left part is similar to a random configuration of the initial system, and the free path on the right part is approximately a straight line.

We have seen the appearance of the arctic curve by images depicting the different types of vertices in some random six-vertex configuration. The path picture gives more insight into the situation. With our previous choice of path direction, *i.e.* going north or east, the southeast region of the square is empty of lines. For fixed domain size, the lowest path of the configuration gives an approximate boundary of the frozen region. The arctic curve is this lowest path in the scaling limit. The tangent method uses this representation to compute the arctic curve. We illustrate the idea of the method with the specific example of domain-wall boundary conditions. We can apply it to other models that exhibit the same type of bijection with path configurations.

Consider the simple six-vertex model with domain-wall boundary conditions on a square grid. Recall that in the path picture, the boundary conditions are such that a path begins at every line on the left boundary and ends at every edge of the upper boundary. We create a new system by extending the square on its right to create a rectangle of chosen ratio $1 + \lambda$, with $\lambda \in \mathbb{Q}^+$. We impose the same boundary condition such that the path begins at every possible position on the left boundary and all the upper ones that belong to the initial square except the rightmost one. We finally add a path on the upper boundary on the rightmost corner of the rectangle. We effectively took the initial boundary conditions and pulled the rightmost endpoint further to the right (see figure 2.17).

A random configuration of this new system has a similar form as the one portrayed in

figure 2.18. The modified path takes the shape of a straight line on the extension of the domain, and a similar shape as the arctic curve on the left part. This illustrates the two hypotheses of the tangent method :

1. In the scaling limit, the rightmost path is the union of an arctic curve $\mathcal{A}(\lambda)$ and a line segment escaping from tangentially from $\mathcal{A}(\lambda)$ to the upper right corner of the rectangle.
2. The arctic curve $\mathcal{A}(\lambda)$ coincides with a section of the arctic curve $\mathcal{A}$ of the initial system.

The first hypothesis is proved [15], but the second one is more complicated to verify in general.

The tangent method allows us to compute the arctic curve. To do this, we need to study two functions:

1. The *refined partition function* $Z_{n,k}$, also called the *one-point function*. It is the partition function of the initial model of size n with the addition constraint that the rightmost path comes from the left to the right column at the line k.
2. The *path partition function* $Y_{k,\ell}$. It is the partition function of the extension of ℓ rows of the domain with the requirement that a path enters the extension at the line k.

With those definitions, we can write the partition function of the extended system as

$$Z^{\tan}_{n,\ell} = \sum_{k=1}^{n} Z_{n,k} Y_{k,\ell} C_k, \tag{2.19}$$

where C_k is some factor that we can easily compute from the right column of the configurations contributing to $Z_{n,k}$[1]. To study the scaling limit, we fix the parameter λ and consider the limit of $Z^{\tan}_{n,\lambda n}$ as n tends to infinity :

$$Z^{\tan}_{n,\ell} = \sum_{k=1}^{\lambda n} Z_{n,k} Y_{k,\lambda n} C_k, \tag{2.20}$$

According to the tangent method, the probability of obtaining a straight line tangent to the arctic curve tends to one in the scaling limit. Hence, for each $\lambda \in \mathbb{Q}^+$, there should be a κ that dominates as the sum tends to infinity. We can find this parameter κ via asymptotic analysis.

Once we find κ, we obtain the equation of the line tangent to the arctic curve. As this can be done for every $\lambda \in \mathbb{Q}^+$, we gain a family of lines whose envelope is the arctic curve $\mathcal{A}$. We define the slope P and the intercept I as the functions of λ such that the tangent lines are given by the equation

$$y - P(\lambda)x - I(\lambda) = 0. \tag{2.21}$$

[1]One may absorb the constant C_k in the definitions of $Z_{n,k}$.

We supose that we can extend smoothly P and I to $\lambda \in \mathbb{R}^+$. Then, the envelope of this family of lines also satisfy

$$P'(\lambda)x + I'(\lambda) = 0. \tag{2.22}$$

Hence, we obtain the expression of the arctic curve as the parametrisation

$$\lambda \mapsto (-I'(\lambda)/P'(\lambda), I(\lambda) - P(\lambda)I'(\lambda)/P'(\lambda)). \tag{2.23}$$

We dedicate the next chapter to the computation of the arctic curve using the tangent method in the six-vertex model with domain-wall boundary conditions on a square grid.

2.3.1 Simulations

To heuristically investigate the arctic curve phenomenon on the six-vertex and other models, we use numerical simulations. Because the number of configurations grows very quickly as the size of the domain increases, we cannot simply generate every possible configuration and take one at random after computing each probability. The algorithm we used is widely inspired by [2] and Jean-François de Kemmeter's master thesis [14]. The method uses the flips defined in subsection 2.1.2.

The algorithm is based on the concept of Markov chains.
Definition 2.3. *A Markov chain is a sequence of random variables $(Y_n)_{n\in\mathbb{N}}$ on a space Ω such that the probability distribution $\boldsymbol{P}$ of Y_n knowing $Y_0, \dots, Y_{n-1}$ depends only on the value taken by Y_{n-1}, i.e. for all configurations $\omega \in \Omega$ we have*

$$\boldsymbol{P}(Y_n = \omega \mid Y_0 = \omega_0, \dots Y_{n-1} = \omega_{n-1}) = \boldsymbol{P}(Y_n = \omega \mid Y_{n-1} = \omega_{n-1}). \tag{2.24}$$

The Markov chain is strongly irreducible if there exists an $n \in \mathbb{N}$ such that for every greater natural number n we have $\boldsymbol{P}(Y_n = \omega) > 0$ for all $\omega \in \Omega$. The Markov chain is homogeneous if the distribution of X_n knowing X_{n-1} does not depend on $n \in \mathbb{N}$.

In the case of a homogeneous Markov chain, we can understand Y_n as the application of a random function X n times. We define this function by

$$\boldsymbol{P}(X(\omega) = \omega_0) = \boldsymbol{P}(Y_1 = \omega \mid Y_0 = \omega_0). \tag{2.25}$$

The Markov chain then satisfies $Y_n = X^n Y_0$ for each $n \in \mathbb{N}$.

An homogeneous Markov chain has a stationary distribution π associated if there exists a measure π such that

$$\pi(\omega) = \sum_{\varpi\in\Omega} \pi(\varpi)\boldsymbol{P}(X(\varpi) = \omega), \quad \text{for all } \omega \in \Omega. \tag{2.26}$$

Markov chains arise in numerous parts of physics. For our purpose, we can use them to approximate distributions using the following theorem, which is a specific case of [28, Theorem 4.9]

Theorem 2.4. *Let $(Y_n)_{n\in\mathbb{N}}$ be a homogeneous and strongly irreducible Markov chain. If the chain has a stationary distribution π, we have for all $\omega, \omega_0 \in \Omega$*

$$\lim_{n\to\infty} \boldsymbol{P}(Y_n = \omega \mid Y_0 = \omega_0) = \pi(\omega). \tag{2.27}$$

Our aim is to create such a Markov chain that converges to the stationary distribution $\pi = \mathbb{P}$.

To define our own Markov chain, we first consider a fixed configuration ω_0 and we repeatedly apply some unknown random function X to it. To obtain the required stationary distribution, we impose the *detailed balance condition*

$$\mathbb{P}(\omega)\boldsymbol{P}(X(\omega) = \varpi) = \mathbb{P}(\varpi)\boldsymbol{P}(X(\varpi) = \omega),, \quad \text{for all } \omega, \varpi \in \Omega. \tag{2.28}$$

In this way, we obtain Equation 2.26. We define our function X by first choosing a random face under some distribution d and then flip the face, if possible, with flip probability P_f in a way to satisfy the detailed balance condition. We use two different choices of X:

1. We choose a face at random from the N possible ones and flip it with probability given by

$$P_f(X(\omega) = \omega) = \min\left(1, \frac{\mathbb{P}(F_f(\omega))}{\mathbb{P}(\omega)}\right). \tag{2.29}$$

2. We choose a face at random in the $N(\omega)$ possible flippable faces of ω and flip it with probability given by

$$P_f(X(\omega) = \omega) = \min\left(1, \frac{N(\omega)\mathbb{P}(F_f(\omega))}{N(F_f(\omega))\mathbb{P}(\omega)}\right). \tag{2.30}$$

The second scheme is useful when we deal with an initial configuration ω_0 with only a small number of flippable faces. In this case, the first algorithm would usually miss the flippable faces, and it would take time to move away from ω_0. The ratio $\mathbb{P}(F_f(\omega))/\mathbb{P}(\omega)$ is quick to compute as it only depends on the weights around the face f. In the three-colour model, it is only the ratio of the weights of the new colour to the previous one:

$$\frac{\mathbb{P}(F_f(\omega))}{\mathbb{P}(\omega)} = \frac{W_{F_f(\omega(f))}}{W_{\omega(f)}}. \tag{2.31}$$

We only consider weights of our models such that every configuration ω has a non zero probability $\mathbb{P}(\omega)$. Recall from section 2.1.2 that we can obtain any configuration from a sequence of flip applied on ω_0. Hence, for the two schemes, the Markov chain is strongly irreducible. Then, by the theorem 2.4, we can approximate $\mathbb{P}$ by considering $X^n(\omega_0)$ for some n sufficiently large.

We implemented the algorithm on a computer using Python and C++. We define the initial six-vertex configuration as one of the two configurations in figure 2.19.

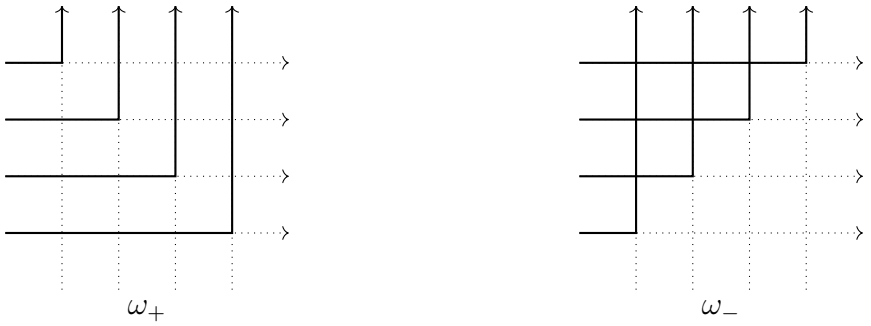

Figure 2.19: Path representation of the two initial conditions used in the sampling algorithm on a square grid of size 4.

The up flips have no effect on the configuration ω_- on the right, whereas the down flips do not affect the left configuration ω_+. We need to apply $(n-1)n(n+1)/6$ up flips on ω_+ to recover ω_- on a square grid of size n. This is the maximum number of times one has to flip to travel between two configurations. We wish to be able to obtain any configuration with the algorithm. Hence, we ask the number of flips made by the algorithm to behave at least as Cn^3. We sampled the configurations with the choice $C = 10^4$.

Chapter 3

Arctic Curves in the Six-Vertex Model

In this chapter, we follow [16] to compute the arctic curve in the six-vertex model with domain-wall boundary conditions in the disordered phase. In section 3.1, we study some properties of the model. We compute the free energy per site f, the refined partition function $Z_{n,k}$ and the path partition function $Y_{k,\ell}$. We then obtain the arctic curve via the tangent method in section 3.2. Finally, in section 3.3, we give the expression of the arctic curve with a reflecting end. We conclude by briefly plotting some sampled six-vertex configurations.

3.1 Domain-Wall Boundary Conditions

3.1.1 Weight Parametrisation

In this section, we consider the six-vertex model on a square grid of size n in the disorered phase, as defined in the previous chapter. We denote respectively u_i and v_j the spectral parameters associated with the i^{th} line and the j^{th} column. Let $\eta \in (0, \pi/2)$. We work with the following parametrisation of the vertex weights.

$$a_\pm(u) = \sin(u+\eta) = a(u), \quad b_\pm(u) = \sin(u-\eta) = b(u), \quad c_\pm(u) = \sin(2\eta) = c. \tag{3.1}$$

We chose $u \in (\eta, \pi - \eta)$ so that the weights are all positive.

With parametrisation (3.1), the partition function Z has the following symmetry. In the ferroelectric and anti-ferroelectric phases, we write the weights in terms of hyperbolic functions.

Lemma 3.1. *The partition function of the six vertex model with weights as in equation* (3.1) *and spectral parameter u is symmetric under the map $u \mapsto \pi - u$.*

Proof. This follows immediately from the symmetry $u \mapsto \pi - u$ of each weight a, b and c. □

3.1.2 Properties

We begin the discussion with some elementary properties that will be useful in the subsequent sections. We recall the two configurations $\omega_\pm$ of section 2.3.1 (see figure 2.19).

Lemma 3.2. *The configuration ω_+ is the only one without a-vertices. Similarily, ω_- is the only configuration without b-vertices.*

Proof. We first prove the case without a-vertices. Consider the leftmost column on a square grid of size n. The paths must continue on each line and one must end on the upper border. Because a-vertices are not allowed, the upper vertex is a $c-+$ and every other bellow are b_+-vertices. The same argument applied on the upper collumn shows that every vertices on the right of the c_+ is of type b_-. The remaining unkown vertices form a six-vertex model with domain wall boundary conditions on the square grid of size $n-1$. The lemma follows by induction on n. The proof for the other case is similar. □

With the help of the previous lemma, we immediately compute the partition function when a (or b) equals zero.

Corollary 3.3. *The partition function of the homogeneous six-vertex model on a square grid of size n with domain-wall boundary condition specialises to $(b_+b_-)^{n(n-1)/2}c_+^n$ when $a_+ = a_- = 0$ and to $(a_+a_-)^{n(n-1)/2}c_+^n$ when $b_+ = b_- = 0$.*

Proof. Consider the case $a_+ = a_- = 0$. By lemma 3.2, only one configuration contributes to the partition function. Moreover, this configuration has $n(n-1)/2$ b_+ vertices, n c_+ vertices and $n(n-1)/2$ b_- vertices. Thus the partition function is $(b_+b_-)^{n(n-1)/2}c_+^n$.

The argument is similar when $b_+ = b_- = 0$. □

Proposition 3.4. *In the six-vertex model on a square grid of size n with domain-wall boundary condition, each frontier line and column has exactly one c-type vertex.*

Proof. Consider the bottommost line of the square. The boundary conditions imply that each vertex on this line has an outgoing vertex below it. The leftmost vertex has a right-going arrow on its left, whereas the rightmost vertex has a left-going arrow on its right. Therefore, there has to be a vertex on the edge such that the arrow on its left is right-going and the one on its right is directed to the left. This is a c_+-vertex.

Suppose there is at least another vertex on the edge that has two opposite arrows on its left and right. This is the case if and only if this vertex is of type c. Consider the nearest one to the previous c_+ vertex. By hypothesis, it is the nearest vertex that changes the direction of the horizontal arrow; thus, its left arrow is left-going and the arrow on its right is right-going. Thus this vertex is a c_- vertex. This is impossible because of the boundary condition. Therefore, there is no other c-type vertex on this edge.

The same argument applies to the other boundaries of the square. □

3.1.3 Inhomogeneous and Homogeneous Partition Function

We consider the inhomogeneous six-vertex model with weights defined by the functions 3.1. Korepin found a recurrence relation that satisfy the sequence of partition function $(Z_n)_{n\in\mathbb{N}}$ [24]. This relation allowed Izergin, Coker and Korepin to find the expression of the partition function [21]. This expression is the *Izergin-Korepin* formula.

Theorem 3.5. *The partition function of the inhomogeneous six-vertex model on a square grid of size n with domain-wall boundary condition with weights as in equation* (3.1) *is*

$$Z_n(u,v) = \det\left[\frac{c}{a(u_i-v_j)b(u_i-v_j)}\right]_{1\le i\le n}^{1\le j\le n} \frac{\prod_{i,j=1}^{n} a(u_i-v_j)b(u_i-v_j)}{\prod_{1\le i<j\le n}\sin(u_i-u_j)\sin(v_j-v_i)}. \tag{3.2}$$

We aim to take the homogeneous limit of 3.2. To get rid of the singularities in the denominator of the factor on the right, we use divided difference operators [32].

Definition 3.6. *The divided difference operators $\mathcal{D}_k$ for $k \in \mathbb{N}$ are defined for all functions f by $\mathcal{D}_0 f = f$ and recursively for $k \in \mathbb{N}_*$ by*

$$\mathcal{D}_k f(x_0,\dots,x_k) = \frac{\mathcal{D}_{k-1}f(x_0,\dots,x_{k-2},x_k) - \mathcal{D}_{k-1}f(x_0,\dots,x_{k-1})}{x_k - x_{k-1}}. \tag{3.3}$$

For example, $\mathcal{D}_1$ gives back to the usual difference quotient

$$\mathcal{D}_1 f(x,y) = \frac{f(y)-f(x)}{y-x}. \tag{3.4}$$

One of the most important properties of the divided difference operator is linked to interpolation polynomials. We have the following theorem.

Theorem 3.7. *Let $f\colon \mathbb{R}\to\mathbb{R}$ be a function and distinct numbers $x_0,\dots,x_k \in \mathbb{R}$. The unique interpolation polynomial P of f at the nodes $x_0,\dots,x_k$ of degree at most $k-1$ is*

$$P(x) = \sum_{\ell=0}^{k} \mathcal{D}_\ell f(x_0,\dots,x_\ell) \prod_{q=0}^{\ell-1}(x-x_q). \tag{3.5}$$

Proof. The statement is trivially true when $k = 0$. Supose that the theorem holds for some $k \in \mathbb{N}$. Let P be the interpolation polynomial of f at the nodes $x_0,\dots,x_k$ and Q the interpolation polynomial at the nodes $x_1,\dots,x_{k-1},x_{k+1}$. Consider the polynomial defined by

$$R(x) = \frac{P(x)(x_{k+1}-x) + Q(x)(x-x_k)}{x_{k+1}-x_k}. \tag{3.6}$$

Direct computation shows that R satisfies $R(x_\ell) = f(x_\ell)$ for all $\ell \in \{0,\dots,k+1\}$. Because R is of degree at most k, R is the unique interpolating polynomial of f of degree at most k at the nodes $x_0,\dots,x_{k+1}$. We have

$$R(x) = P(x) + \frac{Q(x)-P(x)}{x_{k+1}-x_k}(x-x_k). \tag{3.7}$$

By hypothesis on P and Q, they can be written in the form of theorem (3.5), from which we find

$$\begin{aligned}\frac{Q(x)-P(x)}{x_{k+1}-x_k} &= \frac{\mathcal{D}_k f(x_0,\dots,x_k)-\mathcal{D}_k f(x_0,\dots,x_{k-1},x_{k+1})}{x_{k+1}-x_k}\prod_{\ell=0}^{k-1}(x-x_\ell)\\ &= \mathcal{D}_{k+1}f(x_0,\dots,x_{k+1})\prod_{\ell=0}^{k-1}(x-x_\ell).\end{aligned} \tag{3.8}$$

Therefore, R is of the form of theorem 3.5. By induction, the theorem is true for all $k \in \mathbb{N}$. □

To end the discussion about divided difference operators, we state the following important theorem relating these operators with usual derivatives. (3.4) is a particular case of this relation.

Theorem 3.8. *Let $k \in \mathbb{N}_*$, $f\colon \mathbb{R} \to \mathbb{R}$ be a C^k function, and distinct points $x_0,\dots,x_k \in \mathbb{R}$. Denote $x_- = \min\{x_0,\dots,x_k\}$ and $x_+ = \max\{x_0,\dots,x_k\}$. There exist $\xi \in [x_-,x_+]$ such that*

$$\mathcal{D}_k f(x_0,\dots,x_k) = \frac{1}{k!}f^{(k)}(\xi). \tag{3.9}$$

Proof. We assume that $i<j$ implies $x_i<x_j$, else we permute the variable names. For all $i \in \{0,\dots,k\}$, x_i is a root of $P-f$. By the mean value theorem, for all $\ell \in \{0,\dots,k-1\}$, there exist $\xi_\ell \in (x_\ell, x_{\ell+1})$ such that $P'(\xi_\ell)-f'(\xi_\ell)=0$. So $P'-f'$ has at least $k-1$ roots in the interval $[x_-,x_+]$. Applying the same argument for each derivative shows that there exist $\xi \in [x_-,x_+]$ such that $P^{(k)}(\xi)-f^{(k)}(\xi)=0$. Therefore, it follows that

$$\mathcal{D}_k f(x_0,\dots,x_k) = \frac{1}{k!}P^{(k)}(\xi) = \frac{1}{k!}f^{(k)}(\xi). \tag{3.10}$$

□

We can now write the expression of the homogeneous limit of 3.2. The expression is a corollary of the more general proposition.

Proposition 3.9. *Let $k \in \mathbb{N}_*$, $u,v \in \mathbb{R}$ and $f\colon \mathbb{R}^2 \to \mathbb{R}$ a function k times differentiable at (u,v). The function $F\colon \mathbb{R}^2 \to \mathbb{R}$ defined by*

$$F(u,v) = \lim_{u_1,\dots,u_k \to u}\ \lim_{v_1,\dots,v_k \to v} \frac{\det\left[f(u_i,v_j)\right]_{1\le i\le k}^{1\le j\le k}}{(u_j-u_i)(v_j-v_i)} \tag{3.11}$$

is equal to the determinant

$$F(u,v) = \frac{1}{\prod_{\ell=1}^{k-1}\ell!^2}\det\left[\partial_1^i\partial_2^j f(u,v)\right]_{0\le i\le k-1}^{0\le j\le k-1}. \tag{3.12}$$

Proof. For $j \in \{1, \dots, k\}$, we denote f_j the function

$$f_j \colon \mathbb{R} \to \mathbb{R} \colon x \mapsto f(x, v_j). \tag{3.13}$$

Consider the matrix $\big[f(u_i, v_j)\big]_{1 \le i \le k}^{1 \le j \le k}$. Subtract the first line from all the others below. By linearity, take the factor $1/(u_1 - u_j)$ out of the prefactor and multiply the j^{th} line by it. Then proceed similarly for the second line, and by induction on all the other lines. The remaining matrix has components

$$\mathcal{D}_{i-1} f_j(u_1, \dots, u_i). \tag{3.14}$$

By theorem 3.8, there exists $\xi_i \in [u_-, u_+]$ such that

$$\mathcal{D}_{i-1} f_j(u_1, \dots, u_i) = \frac{1}{(i-1)!} f_j^{(i-1)}(\xi_i). \tag{3.15}$$

In the limit $u_1, \dots, u_n \to u$, we have $\xi_i \to u$ for all $i \in \{0, \dots, n-1\}$. Therefore, taking this limit, the determinant becomes the determinant of a matrix with components

$$\frac{1}{(i-1)!} f_j^{(i-1)}(u) = \frac{1}{(i-1)!} \partial_1^{i-1} f(u, v_j). \tag{3.16}$$

Using the same argument to the columns for the v variables and pulling out the factorial for each line completes the proof. □

The homogeneous limit of the partition function 3.2 follows immediately.

Corollary 3.10. *Let $\Gamma = \{-\eta, \eta\} + 2\pi\mathbb{Z}$ and $m \colon \mathbb{R} \backslash \Gamma \to \mathbb{R} \colon x \mapsto c/a(x)b(x)$. Define the function*

$$D_n \colon \mathbb{R} \backslash \Gamma \to \mathbb{R} \colon x \mapsto \det\big[m^{(i+j)}(x)\big]_{1 \le i \le n-1}^{1 \le j \le n-1}. \tag{3.17}$$

The partition function of the homogeneous six-vertex model on a square grid of size n with domain-wall boundary conditions for $u, v \in \mathbb{R}$ with $u - v \neq \pm\eta$ is

$$Z_n(u, v) = \frac{a(u-v)^{n^2} b(u-v)^{n^2}}{\prod_{k=1}^{n-1} k!^2} D_n(u - v). \tag{3.18}$$

Proof. We rewrite the partition function of theorem 3.5 as

$$\begin{aligned} \prod_{i,j=1}^{n} a(u_i - v_j) b(u_i - v_j) \prod_{1 \le i < j \le n} \left[\frac{(u_i - u_j)(v_j - v_i)}{\sin(u_i - u_j) \sin(v_j - v_i)} \right] \\ \times \frac{(-1)^{n(n-1)/2}}{\prod_{1 \le i < j \le n} (u_j - u_i)(v_j - v_i)} \det\big[m(u_i - v_j)\big]_{1 \le i \le n}^{1 \le j \le n}. \end{aligned} \tag{3.19}$$

By proposition 3.9 with $f(u, v) = m(u - v)$, the homogeneous limit takes the form

$$\frac{a(u-v)^{n^2} b(u-v)^{n^2}}{\prod_{k=0}^{n-1} k!^2} (-1)^{n(n-1)/2} \det\big[(-1)^j m^{(i+j)}(u - v)\big]_{0 \le i \le n-1}^{1 \le j \le n-1}. \tag{3.20}$$

We pull out the factor $(-1)^j$ for each column, which cancels the $(-1)^{n(n-1)/2}$ term outside the determinant. This proves the claim. □

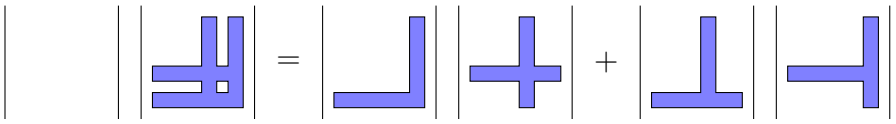

Figure 3.1: An illustration of the Desnanot-Jacobi identity (Equation (3.22)). The blue lines and columns indicate the ones removed from the matrices.

We use the notation D_n as in the corollary in this whole section. Note that the partition function only depends on the difference of u and v. We therefore abuse notation and write $Z_n(u-v)$ instead of $Z_n(u,v)$.

For some specific values of the spectral parameters, the partition function takes a simple form.

Lemma 3.11. *For each n, the homogeneous partition function of the six-vertex model with domain-wall boundary condition satisfy*

$$Z_n(\pm\eta) = \sin(2\eta)^{n^2} = c^{n^2}. \tag{3.21}$$

Proof. We have $b(\eta) = 0$ and $a(\eta) = c$. By corollary 3.3, the partition function is $Z_n(\eta) = c^{n^2} = \sin(2\eta)^{n^2}$. The argument is similar when $u - v = -\eta$. □

3.1.4 Homogeneous Free Energy

Our aim is to study the asymptotic of the partition function as n tends to infinity. Korepin and Zinn-Justin first computed the free energy per site in [23]. Bleher and Fokin wrote a rigorous proof for the asymptotic in the disordered phase [9]. Their approach is based on the theory of random matrices. Bleher and Liechty later combined the results with the other phases [7, 5, 6, 4] in their book [8]. In this section, we do not follow this point of view and give a less rigorous derivation of the free energy per site. We follow [16].

In this setting, we find the large n limit using a recurrence relation provided using the Desnanot-Jacobi identity.

Theorem 3.12 (Desnanot-Jacobi identity)**.** *Let $M \in \mathbb{R}^{n\times n}$ be a matrix and for I, J two subsets of $\{1,\dots,n\}$. We write M_I^J the submatrix of M without the lines indexed in I and columns indexed in J. Then we have*

$$\begin{aligned}\det(M)\det\left(M^{\{n-1,n\}}_{\{n-1,n\}}\right) = \det\left(M^{\{n-1\}}_{\{n-1\}}\right)\det\left(M^{\{n\}}_{\{n\}}\right)\\ - \det\left(M^{\{n-1\}}_{\{n\}}\right)\det\left(M^{\{n\}}_{\{n-1\}}\right).\end{aligned} \tag{3.22}$$

A proof of this relation can be found in [11]. Identity (3.22) allows us to write a differential equation for the determinants D_n.

Proposition 3.13. *For each $n \in \mathbb{N}_*$, we have*

$$D_{n+1}D_{n-1} = D_n^2(\ln D_n)'' \quad \text{for all } n \in \mathbb{N}_*. \tag{3.23}$$

Proof. For each $x \in \mathbb{C}$, let M_n be the matrix defining $D_n(x)$ and $\zeta(x)$ be the first line of M_n. Viewing the determinant as a volume form, we have

$$D_n(x) = \det(\zeta(x), \zeta'(x), \dots, \zeta^{(n-1)}(x)). \tag{3.24}$$

By multilinearity and antisymmetry, the derivative of D_n is

$$D_n'(x) = \det(\zeta(x), \zeta'(x), \dots, \zeta^{(n-2)}(x), \zeta^{(n)}(x)) = \det\left((M_{n+1})_{\{n\}}^{\{n+1\}}\right). \tag{3.25}$$

We apply the same argument to the columns, giving

$$D_n'(x) = \det\left((M_{n+1})_{\{n+1\}}^{\{n\}}\right), \qquad D_n''(x) = \det\left((M_{n+1})_{\{n\}}^{\{n\}}\right). \tag{3.26}$$

Combining these equations with the Desnanot-Jacobi identity (3.22), we find

$$D_{n+1}(x)D_{n-1}(x) = D_n(x)D_n''(x) - D_n'(x)^2 = D_n(x)(\ln D_n)''. \tag{3.27}$$

This concludes the proof. □

We translate this relation in terms of the partition function.

Corollary 3.14. *The rescaled partition function $\mathcal{Z}_n(x) = Z_n(x)/a(x)^{n^2}b(x)^{n^2}$ of the homogeneous six-vertex model on a square grid of size n with domain-wall boundary conditions satisfy the recurrence relation*

$$\mathcal{Z}_{n+1}(x)\mathcal{Z}_{n-1}(x) = \frac{1}{n^2}\mathcal{Z}_n(x)^2(\ln \mathcal{Z}_n)''(x). \tag{3.28}$$

Proof. By corollary 3.10, the rescaled partition function is

$$\mathcal{Z}_n(x) = \frac{1}{\prod_{k=1}^{n-1} k!^2} D_n(x). \tag{3.29}$$

The relation then follows directly from proposition 3.13. □

We aim to compute the dominant term of the partition function, given by the free energy per site f defined through

$$f(x) = \lim_{n\to\infty} -\frac{1}{n^2}\ln Z_n(x) = -\ln(a(x)b(x)) + \lim_{n\to\infty} -\frac{1}{n^2}\ln \mathcal{Z}_n(x). \tag{3.30}$$

We thus write $\mathcal{Z}_n(x) = \exp(-n^2 f_r(x) + R_n(x))$, where the rest $R_n = o(n^2)$ as n tends to infinity. We neglect the rest R_n and substitute $\mathcal{Z}_n(x)$ in corollary 3.14. We obtain the differential equation

$$\mathrm{e}^{-2f_r(x)} = -f_r''(x). \tag{3.31}$$

To compute the solution, we need two additional conditions. We determine those using our knowledge of the partition function at certain values of the spectral parameters. We have $a(\eta) = c$ and $b(\eta) = 0$. By lemma 3.11, $f(\eta) = -\ln(c)$ and we thereby obtain

$$\lim_{x\to\eta} f_r(x) = \lim_{x\to\eta} \ln(a(x)b(x)) + f(x) = -\infty. \tag{3.32}$$

The same argument at $x \to \pi - \eta$ gives $\lim_{x\to\pi-\eta} f_r(x) = -\infty$. We write $\alpha = \pi/(\pi - 2\eta)$. The solution to the differential equation (3.31) with the two previous initial conditions is

$$f_r(x) = \ln\left(\frac{1}{\alpha}\sin(\alpha(x-\eta))\right). \tag{3.33}$$

This provides the following conjecture.

Conjecture 3.15. *Let $\alpha = \pi/(\pi - 2\eta)$. The free energy per unit size of the homogeneous six-vertex model on a square grid with domain-wall boundary conditions is*

$$f(x) = -\ln(a(x)b(x)) + \ln\left(\frac{1}{\alpha}\sin\left(\alpha(x-\eta)\right)\right). \tag{3.34}$$

3.1.5 Partially Homogeneous Limit

In order to study the refined partition functions $Z_{n,k}$ as defined in the previous chapter (section 2.3), we consider the *partially homogeneous* limit of the spectral parameters. Every line and every column takes the same spectral parameter except for the last column, which has a shift of ξ. The partition function is

$$\tilde{Z}_n(u,v,\xi) = \lim_{\substack{u_1,\dots,u_n\to u\\ v_1,\dots,v_{n-1}\to v\\ v_n\to v+\xi}} Z_n(u_1,\dots,u_n,v_1,\dots,v_n). \tag{3.35}$$

Similarly to the homogeneous case, we write the limit as a factor times the determinant of a matrix M. The matrix M is essentially the same except for the last column, which depends on the new parameter ξ. We define $M(x,\xi)$ the matrix with entries for $i,j \in \{0,\dots,n-1\}$ given by

$$\begin{aligned} M(x,\xi)_{i,j} &= m^{(i+j)}(x), \quad i \in \{0,\dots,n-1\},\ j \in \{0,\dots,n-2\},\\ M(x,\xi)_{i,n-1} &= m^{(i)}(x-\xi), \quad i \in \{0,\dots,n-1\}. \end{aligned} \tag{3.36}$$

We furthermore denote $\tilde{D}_n(x,\xi) = \det M(x,\xi)$.

Theorem 3.16. *Let $x,\xi \in \mathbb{R}$, m as in corollary 3.10. The partially homogeneous partition function of the six-vertex model on a square grid of size n with domain-wall boundary conditions takes the form*

$$\tilde{Z}_n(u,v,\xi) = \frac{(-1)^{n-1}(n-1)!}{\sin(\xi)^{n-1}}\left[\frac{a(u-v-\xi)b(u-v-\xi)}{a(u-v)b(u-v)}\right]^n \frac{\tilde{D}_n(u-v,\xi)}{D_n(u-v)} Z_n(u-v). \tag{3.37}$$

Proof. The proof is essentially the same as the one of corollary 3.10. We follow the same steps as the proof of 3.10, until we use proposition 3.9. Then, we apply the same technique as in the proof of the latter proposition 3.9, except for the last column. Finally, we take the partially homogeneous limit. We obtain

$$\begin{aligned} \tilde{Z}_n(u,v,\xi) = {} & \frac{a(u-v)^{n(n-1)}b(u-v)^{n(n-1)}}{\prod_{k=1}^{n-1}k!^2}\frac{(n-1)!a(u-v-\xi)^n b(u-v-\xi)^n}{\sin(\xi)^{n-1}}\\ & \times(-1)^{n(n-1)/2}\det\left[(-1)^j m^{(i+j)}(u-v)\middle|m^{(i)}(u-v-\xi)\right]_{0\le i\le n-1}^{0\le j\le n-2}. \end{aligned} \tag{3.38}$$

We pull the factor $(-1)^j$ out of the determinant, leaving us with the overall factor $(-1)^{n-1}$. We obtain the expression of the theorem by comparison with the homogeneous partition function (3.18). □

As before, $\tilde{Z}_n(u,v,\xi)$ depends only on the difference $u-v$ and ξ. We thus write $\tilde{Z}_n(u-v,\xi)$ instead of $\tilde{Z}_n(u,v,\xi)$. The recurrence relation of the function $\tilde{D}_n$ gives us insight into its asymtotics as n goes to infinity.

Proposition 3.17. *For all $n \in \mathbb{N}_*$, we have*

$$\tilde{D}_{n+1}(x,\xi)D_{n-1}(x) = D_n(x)\partial_1\tilde{D}_n(x,\xi) - \tilde{D}_n(x,\xi)D_n'(x). \tag{3.39}$$

Proof. Let M be the matrix defining $\tilde{D}_{n+1}(x,\xi)$. We note that

$$D_n(x) = \det\left(M^{\{n+1\}}_{\{n+1\}}\right), \quad \tilde{D}_n(x,\xi) = \det\left(M^{\{n\}}_{\{n+1\}}\right). \tag{3.40}$$

We write respectively ζ and ρ the line of the matrix defining $\tilde{D}_n(x,\xi)$ and $D_n(x)$. We see the determinant as a volume form and compute by multilinearity and antisymmetry

$$\begin{aligned}
\partial_1\tilde{D}_n(x,\xi) &= \partial_1\det(\zeta,\partial_1\zeta,\dots,\partial_1^{(n-2)}\zeta,\partial_1^{(n-1)}\zeta)\\
&= \det(\zeta,\partial_1\zeta,\dots,\partial_1^{(n-2)}\zeta,\partial_1^{(n)}\zeta) = \det\left(M^{\{n\}}_{\{n\}}\right),\\
D_n'(x) &= (\det(\rho,\rho',\dots,\rho^{(n-2)},\rho^{(n-1)}))'\\
&= \det(\rho,\rho',\dots,\rho^{(n-2)},\rho^{(n)}) = \det\left(M^{\{n+1\}}_{\{n\}}\right).
\end{aligned} \tag{3.41}$$

The proposition then follows from the Desnanot-Jacobi identity 3.12. □

As in the homogeneous limit, we use the differential equation to compute the asymptotic of the partition function. The current equation involves D_n together with $\tilde{D}_n$. We rewrite the differential equation in terms of $\tilde{Z}_n$ and Z_n.

Corollary 3.18. *Define the ratio*

$$\mathcal{H}_n(x,\xi) = \left(\frac{a(x)b(x)}{a(x-\xi)b(x-\xi)}\right)^n \frac{\tilde{Z}_n(x,\xi)}{Z_n(x)} = \frac{(-1)^{n-1}(n-1)!}{\sin(\xi)^{n-1}}\frac{\tilde{D}_n(x,\xi)}{D_n(x)}. \tag{3.42}$$

These functions satisfy the recurrence relation

$$\frac{\mathcal{H}_{n+1}(x,\xi)}{\mathcal{H}_n(x,\xi)}\frac{\mathcal{Z}_{n+1}(x)\mathcal{Z}_{n-1}(x)}{\mathcal{Z}_n(x)^2} + \frac{1}{n\sin(\xi)}\partial_1(\ln\mathcal{H}_n)(x,\xi) = 0. \tag{3.43}$$

Proof. The recurrence relation of proposition 3.17 divided by $\tilde{D}_n(x,\xi)D_n(x)$ is

$$\begin{aligned}
\frac{\tilde{D}_{n+1}(x,\xi)}{D_n(x)}\frac{D_n(x)}{\tilde{D}_n(x,\xi)}\frac{D_{n+1}(x)D_{n-1}(x)}{D_n(x)^2} &= \partial_1(\ln\tilde{D}_n)(x,\xi) - (\ln D_n)'(x)\\
&= \partial_1\left(\ln\frac{\tilde{D}_n}{D_n}\right)(x,\xi).
\end{aligned} \tag{3.44}$$

We obtain the statement by substituting the expression of $\mathcal{H}_n$ (3.42) and by using (3.29). □

For the asymptotic of $\mathcal{H}_n$, we consider the ansatz

$$\mathcal{H}_n(x,\xi) = \exp(-n\sin(\xi)\psi(x,\xi)). \tag{3.45}$$

We substitute this expression in the recurrence relation of corollary 3.18 and the leading-order torm of $\mathcal{Z}_n$ 3.15 to obtain

$$\sin(\xi)\left(\frac{\alpha}{\sin(\alpha(x-\eta))}\right)^2 = \partial_1\big[\exp(\sin(\xi)\psi(x,\xi))\big]. \tag{3.46}$$

As before, we need an initial condition to solve this equation. At $x = \eta+\xi$, the weight of the vertices in the right column of the partially homogeneous system all have spectral parameter η. Thus, only the configurations without any b-vertices on the right column contribute to the partition function. The only possible configurations are the ones with a c-vertex on the upper right position and a-vertices at every other position on the corresponding line and column. The set of possible configurations in the untouched square of size $n-1$ are all the configurations of the six-vertex model with domain-wall boundary conditions. Thus, we use $a(\eta) = c$ and write

$$\tilde{Z}_n(\eta+\xi,\xi) = a(\eta+\xi)^{n-1}c^n Z_{n-1}(\eta+\xi). \tag{3.47}$$

We use the previous conjecture 3.15 and forget about the rest of $Z_n = \exp(-n^2 f)$ to compute

$$\frac{Z_{n-1}(\eta+\xi)}{Z_n(\eta+\xi)} = \mathrm{e}^{2nf(\eta+\xi)}. \tag{3.48}$$

Hence, we compute, for $x\xi \neq 0$,

$$\begin{aligned} -\sin(\xi)\psi(\eta+\xi,\xi) &= \lim_{n\to\infty}\frac{1}{n}\ln(\mathcal{H}_n(\eta+\xi,\xi)) \\ &= \lim_{x\to\eta+\xi}\ln\left(\frac{a(\eta+\xi)^2 b(\eta+\xi)c}{a(\eta)b(x-\xi)}\right) + 2f(\eta+\xi) \\ &= \infty \end{aligned} \tag{3.49}$$

Hence, we have $\exp(\sin(\xi)\psi(\eta+\xi,\xi)) = 0$. We write $\alpha = \pi/(\pi-2\eta)$ and integrate the differential equation

$$\begin{aligned} \mathrm{e}^{\sin(\xi)\psi(x,\xi)} &= \sin(\xi)\int_{\eta+\xi}^{x}\left(\frac{\alpha}{\sin(\alpha(y-\eta))}\right)^2 \mathrm{d}y = \alpha\sin(\xi)\left[\cot(\alpha\xi) - \cot(\alpha(x-\eta))\right] \\ &= \frac{\alpha\sin(\xi)\sin(\alpha(x-\eta-\xi)}{\sin(\alpha\xi)\sin(\alpha(x-\eta))}. \end{aligned} \tag{3.50}$$

This argument leads to the conjecture

Conjecture 3.19. *Define the ratio*

$$H_n(x,\xi) = \frac{\tilde{Z}_n(x,\xi)}{Z_n(x)} = \left(\frac{a(x-\xi)b(x-\xi)}{a(x)b(x)}\right)^n \mathcal{H}_n(x,\xi). \tag{3.51}$$

The limit $\lim_{n\to\infty}(\ln H_n(x,\xi))/n$ *exists and equals*

$$\lim_{n\to\infty}\frac{1}{n}\ln H_n(x,\xi) = \ln\left(\frac{\sin(\alpha\xi)\sin(\alpha(x-\eta))a(x-\xi)b(x-\xi)}{\alpha\sin(\xi)\sin(\alpha(x-\eta-\xi))a(x)b(x)}\right). \tag{3.52}$$

To apply the tangent method, we extend the domain. Consider a rectangular domain of size n by $n+\ell$ with the same boundary conditions as before, except for the $n, \ldots, n+\ell-1$ vertices on top where the arrow points down (see figure 3.2). We write the partition function of this domain with homogeneous weights as $Z^{\tan}_{n,\ell}(u-v)$. Our aim is to characterise this function.

First of all, we note the relation between the refined partition functions $Z_{n,k}$ and the partially homogeneous partition function $\tilde{Z}_n$.

Proposition 3.20. *The following equation holds*

$$\tilde{Z}_n(x,\xi) = \sum_{k=1}^{n} Z_{n,k}(x) \left[\frac{a(x-\xi)}{a(x)}\right]^{k-1} \left[\frac{b(x-\xi)}{b(x)}\right]^{n-k}. \tag{3.53}$$

Proof. Consider a configuration ω of the six-vertex model. By proposition 3.4, there always exists a $k \in \{1, \ldots, n\}$ such that ω contributes to $Z_{n,k}$. We write Ω_k the set of configurations that contributs to $Z_{n,k}$. The sets $\Omega_1, \ldots, \Omega_n$ define a partition over the set of configuration Ω. Because of the domain-wall boundary conditions, the vertices on the right column below the c-vertex are a-vertices and the ones above are b-vertices. □

We define the ratio $H_{n,k}$ by

$$H_{n,k}(x,\xi) = \frac{b(x)}{c} \left[\frac{a(x)}{b(x)}\right]^{n-k} \frac{Z_{n,k}(x)}{Z_n(x)}. \tag{3.54}$$

Corollary 3.21. *The following relation holds*

$$H_n(x,\xi) = \frac{c}{b(x)} \left[\frac{a(x-\xi)}{a(x)}\right]^{n-1} \sum_{k=1}^{n} H_{n,k}(x) \left[\frac{b(x-\xi)}{a(x-\xi)}\right]^{n-k}. \tag{3.55}$$

Proof. We find the stated expression by direct computation when substituting the definition of $H_{n,k}$ and H_n is proposition 3.20. □

We see that H_n is a function times a polynomial in $t(x,\xi) = b(x-\xi)/a(x-\xi)$. We invert the relation and computing the coefficients using Cauchy's theorem. We first need the following property:

Proposition 3.22. *The function $t\colon \mathbb{C} \to \mathbb{C}\colon z \mapsto b(z)/a(z)$ has image $\mathbb{C}\backslash\{e^{\pm 2i\eta}\}$ and for all $z, w \in \mathbb{C}$, the equality $t(z) = t(w)$ implies $z - w \in \pi\mathbb{Z}$.*

Proof. We have $t(z+\pi) = t(z)$ for all $z \in \mathbb{C}$. Hence, we obtain the image by looking at values for $z \in [0,\pi) + i\mathbb{R}$. We write $z = x + iy$ with $x, y \in \mathbb{R}$. We consider the image of vertical lines: $\mathrm{Re}(z) = x \in \mathbb{R}$.

The union of the lines at $x = \pi - \eta$ and $\pi/2 - \eta$ is mapped to the line $x = \cos(2\eta)$ without the points $\exp(\pm 2i\eta)$. Let $x \in [0, 2\pi)\backslash\{\pi/2 - \eta, \pi - \eta\}$ and define $C(x) = \sin(2x)/\sin(2x + 2\eta)$. After some algebra, we find

$$|t(z) - C(x)|^2 = \frac{\sin(2\eta)^2}{\sin(2x+2\eta)^2} = R(x)^2. \tag{3.56}$$

Therefore, the image of the line $\mathrm{Re}(z) = x$ is a subset of the circle of centre $C(x)$ and radius $R(x)$. Moreover, we compute

$$t(x) \in \mathbb{R}, \quad \lim_{y\to\pm\infty} t(x + \mathrm{i}y) = \exp(\pm 2\mathrm{i}\eta), \quad \partial_y t(x + \mathrm{i}y) = \frac{\mathrm{i}\sin(2\eta)}{\sin(z+\eta)^2}. \tag{3.57}$$

As $\partial_y t(x + \mathrm{i}y) \neq 0$, the image of the vertical line $\mathrm{Re}(z) = x$ is the arc of circle of centre $C(x)$ and radius $R(x)$ that contains $t(x)$ and stops just before $\exp(\pm 2\mathrm{i}\eta)$. For every $w \in \mathbb{C}\backslash(\cos(2\eta) + \mathrm{i}\mathbb{R})$, there always exist such an arc of circle S such that $w \in S$. Hence, the image of t is $\mathbb{C}\backslash\{\mathrm{e}^{\pm 2\mathrm{i}\eta}\}$.

Let $z, w \in \mathbb{C}$ such that $t(z) = t(w)$. This implies, after some algebra

$$\sin(z - w)\sin(2\eta) = 0. \tag{3.58}$$

Because $\eta \in (0, \pi/2)$, we have $z - w \in \pi\mathbb{Z}$. □

We can thus invert t if we restrict ξ to some domain. But we have to be careful, as the factor $a(x - \xi)$ outside the sum in equation (3.55) is not invariant under the change $\xi \mapsto \xi + \pi$. Nevertheless, if we restrict n to the odd natural numbers, $n \in 1 + 2\mathbb{Z}$, then the exponent gets rid of the apparent factor -1 and the function is well defined.

Proposition 3.23. *Let $x \in \mathbb{R}$, $t_x \colon \mathbb{C} \to \mathbb{C} \colon z \mapsto t(x - z)$. The function t_x is locally invertible, and the function $f \colon \mathrm{Im}\, t \to \mathbb{C}$ defined by*

$$f(z) = \frac{c}{b(x)}\left[\frac{a(x - t_x^{-1}(z))}{a(x)}\right]^{n-1} \sum_{k=1}^{n} H_{n,k}(x) z^{n-k} \tag{3.59}$$

is well-defined and holomorphic on $\mathrm{Im}\, t$ when n is odd. Moreover, it satisfies

$$H_n(x, t_x^{-1}(z)) = f(z), \quad \textit{for all } z \in \mathrm{Im} t. \tag{3.60}$$

Proof. By Proposition 3.22, t_x is injective on any open ball of radius less than $\pi/2$. Hence it is locally invertible. Moreover, we compute the derivative of t

$$t'(z) = \frac{\sin(2\eta)}{\sin(z + \eta)\sin(z - \eta)}. \tag{3.61}$$

We see that t' is never zero and contains only simple poles when $\eta \in (0, \eta)$. Hence, any local inverse of t is homomorphic on its local domain.

Proposition 3.22 gives us $t(z) = t(w)$ if $z - w \in \pi\mathbb{Z}$. Additionally, we have $f(z+\pi) = f(z)$; therefore, the function $f \circ t_x^{-1}$ extends to the whole plane, except at the points $z = \mathrm{e}^{\pm 2\mathrm{i}\eta}$. By the chain rule, the derivative of $f \circ t_x^{-1}$ exists at every point of its domain, and hence the function is holomorphic. □

Now that we have shown that this function is holomorphic, we can use Cauchy's theorem to extract the coefficients $H_{n,k}$.

Theorem 3.24. *For $n \in 1 + 2\mathbb{Z}$ and for any loop $\gamma \colon S^1 \to \mathrm{Im}\, t$ encircling once the origin, without enclosing the points $\mathrm{e}^{\pm 2\mathrm{i}\eta}$, we have*

$$H_{n,k}(x) = \frac{1}{2\pi\mathrm{i}} \int_{\tilde{\gamma}} \frac{b(x)}{c}\left[\frac{a(x)}{a(x - t_x^{-1}(z))}\right]^{n-1} \frac{H_n(x, t_x^{-1}(z))}{z^{n-k+1}} \mathrm{d}z. \tag{3.62}$$

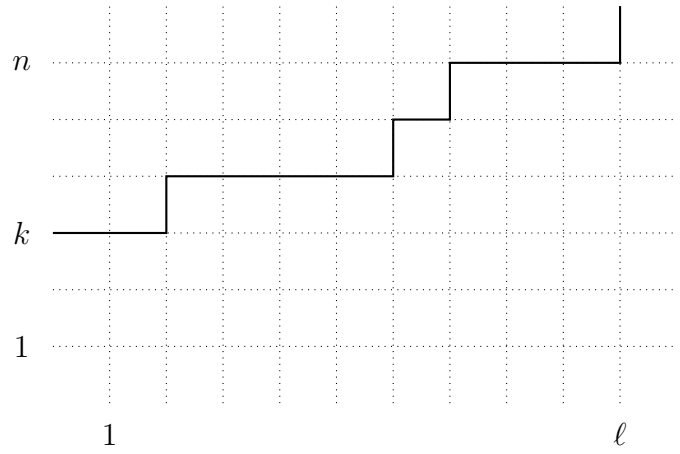

Figure 3.2: Exemple of the extension of the six-vertex model in path representation.

Proof. By proposition 3.23, we have

$$\sum_{k=1}^{n} H_{n,k}(x) z^{n-k} = \frac{b(x)}{c} \left[\frac{a(x)}{a(x - t_x^{-1}(z))} \right]^{n-1} H_n(x, t_x^{-1}(z)). \tag{3.63}$$

This is a holomorphic function of z in $\operatorname{Im} t$. The theorem follows from Cauchy's theorem. □

3.1.6 Path Partition Function

In this section, we consider the extension of the domain defined for the partition function. Consider the six-vertex model on a $\ell \times n$ rectangular grid. We choose boundary conditions such that one path travels to the right on the left boundary at a vertical position $n - k + 1$, and one goes upward on the upper right corner, see figure 3.2. We write the partition function of this domain by $Y_{k,\ell}(a, b, c)$.

Consider a configuration of the extended domain. We can see the unique path of this configuration as a sequence of steps of size 1. Each step is either horizontal (going right) or vertical (going up). We denote a horizontal step by H and a vertical step by V. We write a path of N steps as $\alpha = (\alpha_0, \alpha_1, \ldots, \alpha_N) \in \{H, V\}^{N+1}$. For each vertex v on the path, the step that ends on the v and the step that begins at v give the weight of the vertex. This defines a function $w \colon \{H, V\} \to \{b, c\}$. We use linear algebra to compute the partition function of this part of the domain. Let V be the vector space generated by H and V, and $h, v \in \mathbb{C}$. We define a map $\imath \colon \{H, V\} \to \{h, v\}$ and a linear operator $E \colon V \to V$ by

$$\imath(H) = h, \quad \imath(V) = v, \quad E(\alpha) = \sum_{\beta \in \{H,V\}} w(\alpha, \beta) \imath(\beta) \beta \tag{3.64}$$

We call E the *transfer matrix*, or the *evolution operator*. In the basis (H, V) and considering the six-vertex model with weights a, b and c, the operator E is

$$E = \begin{pmatrix} hb & hc \\ vc & vb \end{pmatrix}. \tag{3.65}$$

The connection between E and the generating function of the partition functions $Y_{k,\ell}$ is given in the following proposition.

Proposition 3.25. *For a vector x, we write x^* its dual. For each $\alpha, \beta \in \{H, V\}$ and $N \in \mathbb{N}$, the function $V^*(E^N(H))$ is the polynomial of degree N in the variables h and v given by*

$$V^*(E^N(H)) = \sum_{\substack{k,\ell \in \mathbb{N}_* \\ k+\ell = N+1}} Y_{k,\ell}(1, b, c) h^{\ell-1} v^{n-k+1}. \tag{3.66}$$

Proof. The coefficients of E are monomials of degree one in h and v. Thus each component of E^N are polynomials that are sums of monomials of h and v of degree N.

Let $k, \ell \in \mathbb{N}_*$ such that $n + \ell - k = N$. Define the set

$$\Pi^{N+1} = \{\alpha \in \{H, V\}^{N+1} \mid \alpha_0 = H,\, \alpha_N = V\}, \tag{3.67}$$

And Π_k^{N+1} the subsets of Π^{N+1} with only $n - k + 1$ element V. The set $\{\Pi_k^{N+1} \colon k \in \{1, \dots N\}\}$ is a partition of Π^{N+1}. Consider $Y_{k,\ell}(1, b, c)$. As $a = 1$, the weight of each configuration is the product of the weight of the vertices lying on the path.

$$Y_{k,N-n+k}(1, b, c) = \sum_{\alpha \in \Pi_k^{N+1}} \prod_{q=1}^{N} w(\alpha_{q-1}, \alpha_q). \tag{3.68}$$

On the other hand, by definition of the transfer matrix 3.64, the component of E^N is

$$V^*(E^N(H)) = \sum_{\alpha \in \Pi^{N+1}} \prod_{q=1}^{N} w(\alpha_{q-1}, \alpha_q) \imath(\alpha_q) \tag{3.69}$$

The product $\prod_{q=1}^{N} \imath(\alpha_q)$ depends only on the number of horizontal and vertical steps. For any configuration in Π_k^{N+1}, the product equals $h^{N-n+k-1} v^{n-k+1}$. We substitute this relation in (3.69) and use (3.68) to obtain

$$\begin{aligned} V^*(E^N(H)) &= \sum_{k=1}^{N} \sum_{\alpha \in \Pi_k^{N+1}} \left[\prod_{q=1}^{N} w(\alpha_{q-1}, \alpha_q) \right] h^{N-k} v^k \\ &= \sum_{k=1}^{N} \sum_{\alpha \in \Pi_k^{N+1}} Y_{k,N-n+k} h^{N-n+k-1} v^{n-k+1}. \end{aligned} \tag{3.70}$$

The proposition follows with $\ell = N - n + k$. □

To extract the coefficients, one could try to compute E^N explicitly. Another method is to take the series $\sum_{N \in \mathbb{N}} E^N$ which converges to the inverse of a two-by-two matrix, which is easy to compute.

Proposition 3.26. *When $h^2 + v^2 < 1/(b^2 + c^2)$, we have*

$$V^*((\mathrm{Id} - E)^{-1}(H)) = \sum_{k,\ell \in \mathbb{N}} Y_{k,\ell} h^{\ell-1} v^{n-k+1}. \tag{3.71}$$

Proof. The ℓ^2 norm of E is $(h^2+v^2)(b^2+v^2)$. Therefore, the series $\sum_{n\in\mathbb{N}} E^N$ converges when $h^2+v^2 < 1/(b^2+c^2)$. The series is

$$\sum_{n\in\mathbb{N}} E^N = (\mathrm{Id}-E)^{-1}. \tag{3.72}$$

By proposition 3.25 and because $V^*(H)=0$, we have

$$V^*((\mathrm{Id}-E)^{-1}(H)) = V^*\left(\sum_{N\in\mathbb{N}_*} E^N(H)\right) + V^*(H) = \sum_{k,\ell\in\mathbb{N}} Y_{k,\ell} h^{\ell-1} v^{n-k+1}. \tag{3.73}$$

This concludes the proof □

We extract the coefficients by explicitly computing the inverse of $\mathrm{Id}-E$.

Proposition 3.27. *The partition function $Y_{k+1,\ell+1}(1,b,c)$ is given by*

$$Y_{k,\ell+1}(1,b,c) = \sum_{t=0}^{\min\{\ell,n-k\}} \binom{\ell}{t} \binom{\ell+n-k-t}{\ell} c(c^2-b^2)^t b^{\ell+n-k-2t}. \tag{3.74}$$

Proof. We use expression (3.65) to compute the determinant of $\mathrm{Id}-E$

$$\det(\mathrm{Id}-E) = (1-vb)\left(1-\frac{h}{1-vb}(b+c^2-b^2)\right). \tag{3.75}$$

The component of the inverse of $\mathrm{Id}-E$ is $H^*(E-\mathrm{Id})(V)$ divided by the determinant of $\mathrm{Id}-E$

$$V^*(\mathrm{Id}-E)^{-1}(H) = \frac{vc}{(1-vb)\left(1-\frac{h}{1-vb}(b+(c^2-b^2)v)\right)}. \tag{3.76}$$

We expand the denominator in h as a geometric series

$$\begin{aligned} V^*(\mathrm{Id}-E)^{-1}(H) &= \sum_{p\in\mathbb{N}} \frac{vc}{(1-vb)^{p+1}}(b+(c^2-b^2)v)^p h^p \\ &= \sum_{p\in\mathbb{N}}\sum_{t=0}^{p} \binom{p}{t} \frac{c}{(1-vb)^{p+1}}(c^2-b^2)^t b^{p-t} v^{t+1} h^p. \end{aligned} \tag{3.77}$$

We use the kth power of the geometric series

$$\frac{1}{(1-x)^k} = \sum_{q\in\mathbb{N}} \binom{k+q-1}{q} x^q \tag{3.78}$$

on the denominator that still depends on v and obtain

$$\begin{aligned} V^*(\mathrm{Id}-E)^{-1}(H) &= \sum_{p,q\in\mathbb{N}}\sum_{t=0}^{p} \binom{p}{t}\binom{p+q}{q} c(c^2-b^2)^t b^{p+q-t} v^{t+q+1} h^p \\ &= \sum_{p,q\in\mathbb{N}}\sum_{t=0}^{\min\{p,q\}} \binom{p}{t}\binom{p+q-t}{p} c(c^2-b^2)^t b^{p+q-2t} v^{q+1} h^p \end{aligned} \tag{3.79}$$

By proposition 3.26, $V^*(\mathrm{Id}-E)^{-1}(H)$ is the generating function of the elements $\{Y_{k,\ell}\colon k,\ell\in\mathbb{N}_*\}$. We compare the coefficients and obtain

$$Y_{k,\ell+1}(1,b,c)=\sum_{t=0}^{\min\{\ell,n-k\}}\binom{\ell}{t}\binom{\ell+n-k-t}{\ell}c(c^2-b^2)^t b^{\ell+n-k-2t}. \tag{3.80}$$

□

We obtain the general expression of $Y_{k,\ell}(a,b,c)$. For all $w\in\mathbb{C}$, the partition function $Y_{k,\ell}$ satisfy

$$Y_{k,\ell}(wa,wb,wc)=w^{n\ell}\,Y_{k,\ell}(a,b,c). \tag{3.81}$$

Hence we obtain the following corollary.

Corollary 3.28. *The partition function $Y_{k+1,\ell+1}(a,b,c)$ for $a\neq 0$ is given by*

$$Y_{k,\ell+1}(a,b,c)= a^{n(\ell+1)}\sum_{t=0}^{\min\{\ell,n-k\}}\binom{\ell}{t}\binom{n+\ell-k-t}{\ell}\frac{c}{a}\left(\frac{c^2-b^2}{a^2}\right)^t\left(\frac{b}{a}\right)^{n+\ell-k-2t}. \tag{3.82}$$

3.2 The Arctic Curve

We do not attempt to rigorously prove the results of this section. We write $f\simeq_{n\to\infty} g$ if $f/g=\mathcal{O}(1)$ as n tends to infinity. We consider that ℓ is divisible by n and write $\lambda n=\ell$. The partition function of the extended domain described in the previous chapter is (up to an overall irrelevant factor)

$$Z^{\tan}_{n,\lambda n}(x)=\sum_{k=1}^{n}H_{n,k}(x)Y_{k,\lambda n}(1,b(x)/a(x),c(x)/a(x)). \tag{3.83}$$

We obtain the dominating position k in the sum by studying the asymptotic of $H_{n,k}$ and $Y_{k,\lambda n}$. We guess that we can use the steepest descent method on the contour integral (3.24) and that its dominant part is located in the region where conjecture 3.19 is valid. We then have, with $k=\kappa n$,

$$H_{n,\kappa n}(x)\underset{n\to\infty}{\simeq}\int_{\tilde\gamma}\mathrm{e}^{-nS_H(x,\kappa,t_x^{-1}(z))}\mathrm{d}z, \tag{3.84}$$

where S_H is the function defined by

$$S_H(x,\kappa,\xi)=\ln\left(\frac{\alpha\sin(\xi)\sin(\alpha(x-\eta-\xi)b(x)}{\sin(\alpha\xi)\sin(\alpha(x-\eta))b(x-\xi)}\right)+(1-\kappa)\ln(t_x(\xi)). \tag{3.85}$$

To apply the method of steepest descent, we compute the saddle point ξ_* of $S_H(x,\kappa,\xi)$. This point satisfies the equation

$$\cot(\xi_*)+\cot(x-\eta-\xi_*)-\alpha\cot(\alpha(x-\eta-\xi_*))-\alpha\cot(\alpha\xi_*)=(\kappa-1)\frac{t_x'(\xi_*)}{t_x(\xi_*)}. \tag{3.86}$$

In this way, we obtain

$$H_{n,\kappa n}(x)\underset{n\to\infty}{\simeq}\mathrm{e}^{-nS_H(x,\kappa,\xi_*)} \tag{3.87}$$

For the extension of the domain, we naively approximate the sum of equation (3.68) as an integral, use Stirling's approximation of the Gamma function, and apply the steepest descent method. We write $\beta = b(x)/a(x)$ and $\gamma = c/a(x)$. We have

$$\begin{aligned} Y_{\kappa n,\lambda n}(1,b,\gamma) &\underset{n\to\infty}{\simeq} \int_0^{\min\{\lambda,1-\kappa\}n} \binom{\lambda n}{t}\binom{(1+\lambda-\kappa)n-t}{\lambda n}\gamma(\gamma^2-\beta^2)^t\beta^{(1+\lambda-\kappa)n-2t}\mathrm{d}t \\ &\underset{n\to\infty}{\simeq} \int_0^{\min\{\lambda,1-\kappa\}} \mathrm{e}^{-nS_Y(\tau,\kappa,\lambda)}\mathrm{d}\tau \end{aligned} \tag{3.88}$$

with the function S_Y defined by

$$\begin{aligned} S_Y(\tau,\kappa,\eta) = &-(1+\lambda-\kappa-\tau)\ln(1+\lambda-\kappa-\tau)+\tau\ln\tau+(\lambda-\tau)\ln(\lambda-\tau) \\ &+(1-\kappa-\tau)\ln(1-\kappa-\tau)-\tau\ln(\gamma^2-\beta^2)-(1+\lambda-\kappa-2\tau)\ln(\beta). \end{aligned} \tag{3.89}$$

The minimiser τ_* of S_Y satisfy the equation

$$\frac{(1+\lambda-\kappa-\tau)\tau\beta^2}{(\lambda-\tau)(1-\kappa-\tau)(\gamma^2-\beta^2)} = 1. \tag{3.90}$$

In this way, we obtain the heuristic asymptotic

$$Y_{\kappa n,\lambda n}(1,\beta,\gamma) \underset{n\to\infty}{\simeq} \mathrm{e}^{-nS_Y(\tau_*,\kappa,\lambda)}. \tag{3.91}$$

With these assumptions, we hope the extended partition function takes the form

$$Z^{\tan}_{n,\lambda n}(x) \underset{n\to\infty}{\simeq} \sum_{k=1}^{n} \mathrm{e}^{-n(S_H(x,\kappa,\xi_*)+S_Y(\tau_*,\kappa,\lambda)} \underset{n\to\infty}{\simeq} \int_0^1 \mathrm{e}^{-n(S_H(x,\kappa,\xi_*)+S_Y(\tau_*,\kappa,\lambda)}\mathrm{d}\kappa. \tag{3.92}$$

As before, we find the dominant term κ_* using the steepest descent method. If we simply forget about the fact that ξ_* and τ_* implicitly depend on κ, the stationary point satisfy

$$\frac{(1+\lambda-\kappa_*-\tau)\beta}{(1-\kappa_*-\tau)t_x(\xi_*)} = 1. \tag{3.93}$$

We extract the value of $(1-\kappa_*)/\lambda$ from (3.90) and (3.93),

$$\frac{1-\kappa_*}{\lambda} = \frac{\gamma^2-\beta^2}{\beta t_x(\xi_*)+\gamma^2-\beta^2} - \frac{\beta}{\beta-t_x(\xi_*)}. \tag{3.94}$$

We use the parametrisation (3.1) and the expression of $t(z) = b(z)/a(z)$ to find, after some algebra,

$$\frac{1-\kappa_*}{\lambda} = \frac{\sin(x-\xi_*-\eta)\sin(x-\xi_*+\eta)}{\sin(\xi_*)\sin(\xi_*-2\eta)}. \tag{3.95}$$

We now have a heuristic expression for the slope of the dominant path for a fixed λ. Equation (3.95) suggests that we instead write κ_* and λ in terms of ξ_* instead of everything in terms of λ.

We consider the scaling limit $n \to \infty$ where the original square domain is $[-1,0]\times[0,1]$, and the extension is in the set $\mathbb{R}^+\times[0,1]$. In this way, the lines of the tangent

method intercept the points $(0, \kappa_*)$ and $(\lambda, 1)$. For some fixed ξ_*, this is the line given by the set of points $(x, y) \in \mathbb{R}^2$ that satisfy

$$F(\xi_*) = y - \frac{1 - \kappa_*(\xi_*)}{\lambda(\xi_*)} x - \kappa_*(\xi_*) = 0 \tag{3.96}$$

The tangent method states that the envelope of this set of curves is the arctic curve. The slope P and the intercept I of (3.96) are

$$\begin{aligned} P(\xi) &= -\frac{\sin(x - \xi - \eta)\sin(x - \xi + \eta)}{\sin(\xi)\sin(\xi - 2\eta)}, \\ I(\xi) &= 1 - (\cot(\xi) + \cot(x - \eta - \xi) - \alpha \cot(\alpha(x - \eta - \xi)) - \alpha \cot(\alpha\xi)) \\ &\quad \times \frac{\sin(x - \xi - \eta)\sin(x - \xi + \eta)}{\sin(2\eta)}. \end{aligned} \tag{3.97}$$

The tangent method leads to the following conjecture.

Conjecture 3.29. *The arctic curve in the southeast region of the six-vertex model on the square lattice with domain wall boundary conditions with the weight parametrisation* (3.1) *is given by the parametric curve*

$$\gamma\colon (u + \eta - \pi, 0) \to [-1, 0] \times [0, 1]\colon \xi \mapsto \left(\frac{I'(\xi)}{P'(\xi)}, I(\xi) - P(\xi)\frac{I'(\xi)}{P'(\xi)} \right) \tag{3.98}$$

We obtained a section of the artic curve, the boundary south-east region in this specific case. To obtain the boundary of another region, we could change our convention for the direction of the paths and repeat the whole chapter for each of the three left directions. Each time we would obtain a different part of the curve. However, there is a trick to avoid such computation. If we were interested in the north-east region, we would have to consider paths travelling to the right and downward. This is equivalent to considering the previous model reflected with respect to a centred horizontal line. Such a reflection transforms the a-vertices into b-vertices, and vice versa. Thus the statistic of the reflected domain if we interchange the weights a and b. With the parametrisation (3.1), this amounts to mapping u to $\pi - u$. Hence, we can obtain the four branches of the arctic curve from Equation (3.98). Figure 3.3 illustrates a sampled configuration when the parameters are $\eta = \pi/4$, $u = \pi/2$ and $v = 0$.

3.2.1 Reflecting End

We give the expression (without derivation) of the arctic curve in the six-vertex model with a reflecting-end. We scale the domain in the rectangle $[-1, 0] \times [0, 2]$. In the homogeneous limit, the value of the a and b vertices depends on which line they lie. We need the five different possible weights to remain positive.

$$a\colon \begin{cases} \sin(u - v + \eta), \\ \sin(u + v - \eta) \end{cases} \qquad b\colon \begin{cases} \sin(u - v - \eta), \\ \sin(u + v + \eta) \end{cases} \qquad c\colon \sin(2\eta). \tag{3.99}$$

We can choose the range of the parameters as $\eta \in (0, \pi/2)$, $u \in (\eta, \pi - \eta)$ and $|v| \in (0, \pi/2 - \eta - |u - \pi/2|)$. The derivation of the expression of the arctic curve

is essentially the same as in the previous section of this chapter, with more computation. In this case, the result does not only depend on the difference $x = u - v$. The differential equations analogous to (3.23) and (3.39) become partial differential equations in the variables u and v. The transfer matrix E (3.64) is promoted to a 4×4 matrix because the weights now depend on the parity of the lines. Remarkably, the arctic curve does not depend on the turn weights [16]. Thus, we choose to fix the reflecting end; we only consider the case where one of the turn weights is zero. The slope P and the intercept I of the familly of lines are

$$\begin{aligned} P(\xi) &= 2\frac{\sin(u-v-\eta-\xi)\sin(u-v+\eta-\xi)\sin(u+v-\eta+\xi)\sin(u+v+\eta+\xi)}{\sin(\xi-2\eta)\sin(\xi)(\cos(2\eta)-\cos(2\eta)-\cos(2u)\cos(2v+2\xi))}, \\ I(\xi) &= 2\Big[\cot(u-v-\eta-\xi)+\cot(\xi)+\cot(\xi+2v)-\cot(u+v+\eta+\xi) \\ &\quad -\alpha\big(\cot(\alpha(u-v-\eta-\xi))+\cot(\alpha\xi)+\cot(\alpha(\xi+2v))-\cot(\alpha(u+v-\eta+\xi))\big)\Big] \\ &\quad \times \frac{\sin(u-v-\eta-\xi)\sin(u-v+\eta-\xi)\sin(u+v-\eta+\xi)\sin(u+v+\eta+\xi)}{\sin(2\eta)(\cos(2\eta)-\cos(2\eta)-\cos(2u)\cos(2v+2\xi))}. \end{aligned} \tag{3.100}$$

Conjecture 3.30. *The arctic curve in the north-east region of the six-vertex model with domain-wall boundary conditions and a fixed reflecting end with the weight parametrisation* (3.1) *is given by the parametric curve*

$$\gamma\colon (u-v+\eta-\pi,0) \to [-1,0]\times[0,1]\colon \xi \mapsto \left(\frac{I'(\xi)}{P'(\xi)}, I(\xi) - P(\xi)\frac{I'(\xi)}{P'(\xi)}\right) \tag{3.101}$$

We can obtain the southeast branch of the artic curve with a similar trick as in the last subsection. We need to reflect the solution and make the substitution

$$u \mapsto \pi - u, \quad v \mapsto -v. \tag{3.102}$$

From the numerical result of the next section, there seems to be a frozen region on the left side of the domain. However, we cannot find the west branches of the curve via the tangent method. The reflecting end forces the vertices of this frozen region to periodically change in the vertical direction. In terms of paths, each line out of two has a path going to the left. This is true for the four possible conventions of the path directions. The region is not empty of lines and thus cannot simply use the tangent method. Finding this part of the arctic curve is an open problem.

3.3 Simulations

In this subsection, we compare some analytical expressions of the arctic curves with random configurations generated via the algorithm described at the end of the previous chapter. In each image illustrating the vertices of the six-vertex model, the colour blue indicates a vertex of type a, magenta for the b's and yellow for the c vertices. On the square grid with the choice of parameters $\eta = \pi/4$ and $u - v = \pi/2$, the arctic curve is an inscribed circle (figure 3.3).

For all $\eta \in (0, \pi/2)$ and when $u = \pi/2$ and $v = 0$, the east part of the arctic curve with a reflecting end is the double of the arctic curve of the six-vertex model on the

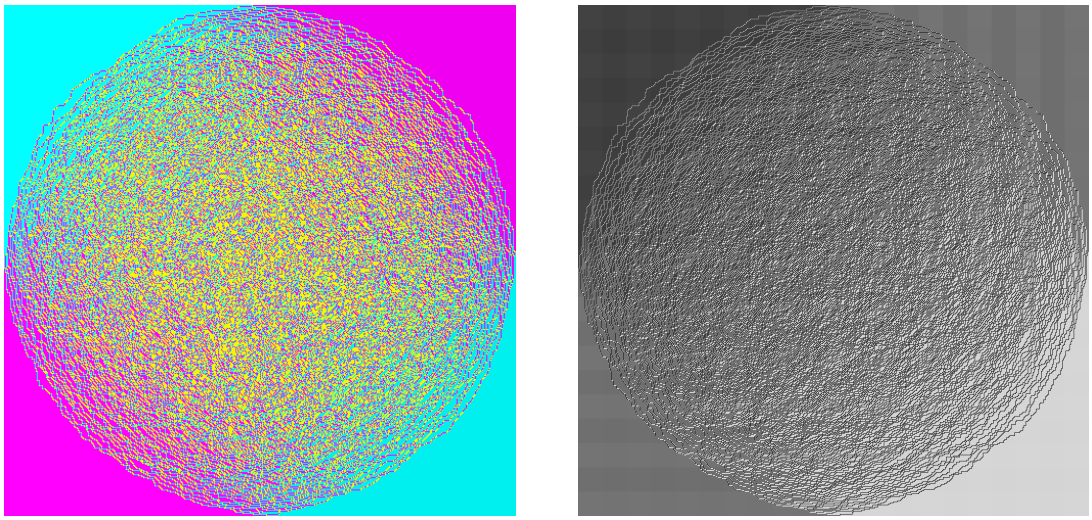

Figure 3.3: A random configuration of the six-vertex model with domain-wall boundary conditions on a square grid of size 500. The parameters are $\eta = \pi/4$, $u = \pi/2$ and $v = 0$. With these parameters, the arctic curve is a circle.

square. Hence, for $\eta = \pi/3$, we recover the arc of circle. At $\eta = \pi/4, u = 3\pi/4$ and $v = 0$, no configurations can occur because $a = 0$ regardless of the parity of the line. However, the arctic curve is defined in the limit as u tends to $3\pi/4$, with η and v fixed. We find an ellipse inscribed in the square. Figure 3.4 illustrates a configuration when $u = \pi/2+\pi/4.05$. Figure 3.5 shows an asymmetric configuration.

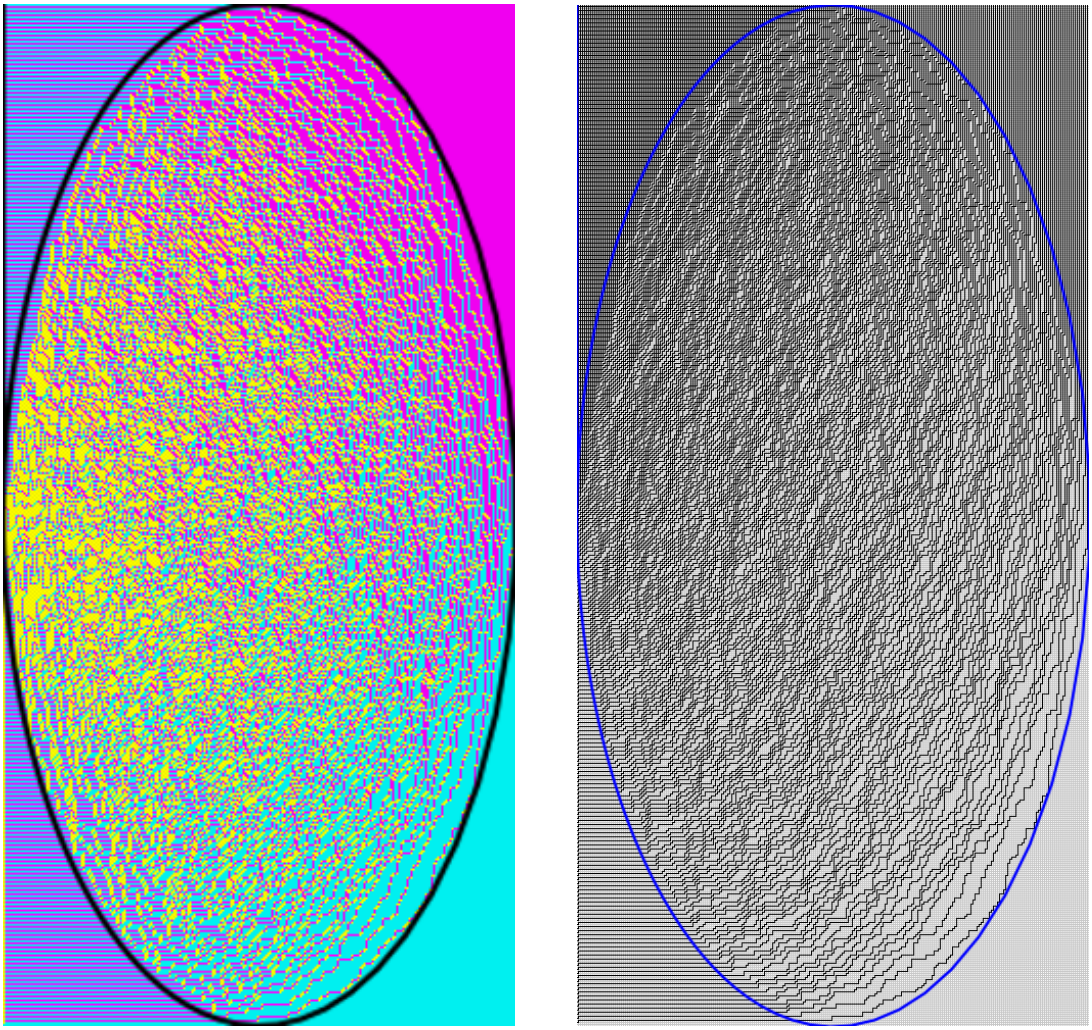

Figure 3.4: A random configuration of the six-vertex model with domain-wall boundary condition and a reflecing end on a 250×500 grid. The parameters are $\eta = \pi/4$, $u = \pi/2 + \pi/4.05$ and $v = 0$. With these parameters, the arctic curve is (almost) an ellipse. The left part of the drawn line is the analytic continuation of the arctic curve on the right.

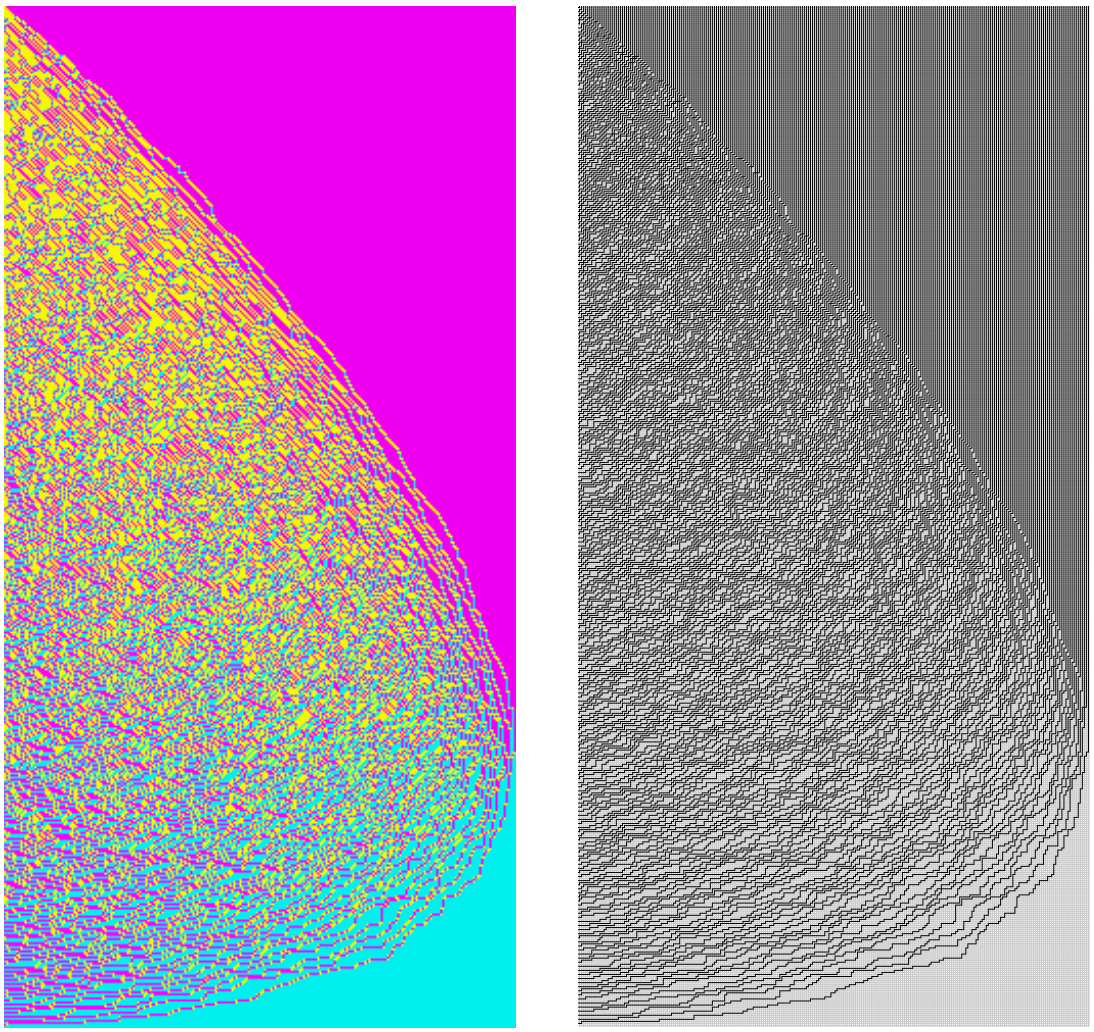

Figure 3.5: A random configuration of the six-vertex model with domain-wall boundary condition and a reflecting end on a 250×500 grid. The parameters are $\eta = \pi/4$, $u = \pi/2$ and $v = -\pi/5$. With these parameters, the arctic curve is not symmetric under the reflection orthogonal to the central horizontal line.

Chapter 4

The Eight-Vertex Solid-on-Solid and Three-Colour Model

In this chapter, we turn our attention to the generalizaton of the six-vertex model introduced in 2.2.3 with a reflecting end. In section 2.2.3, we introduce the Jacobi theta functions. We use the theta functions to parametrise the weights of the model. We also write the expression of the partition function. Section 4.2 follows Hietala's article [19] to obtain a relation between the partition functions of the 8VSOS and three-colour model. In section 4.3, we specialise the parameters of the 8VSOS model to study an other system whose vertex weights depend on the parity of the line and column.

4.1 The Eight-Vertex Solid-on-Solid Model

In this section, we consider the 8VSOS model as defined in 2.2.4. We study it on a rectangular lattice with a reflecting end. We follow Linnea Hietala's convention and reverse the flow of the arrows on the boundary of the domain-wall (see the boundary conditions in figure 4.1). Moreover, we reverse the rule to increase or decrease the value of a height map when crossing an edge. We also then consider the (down left) path representation (see figure 4.2). In essence, only the direction of the arrow changes. The horizontal spectral parameters are labelled $\vec{\lambda} = (\lambda_1, \dots, \lambda_n)$ and the vertical ones are $\vec{\mu} = (\mu_1, \dots, \mu_n)$. We denote the local height near a vertex by z, and ζ is a parameter describing the weight of the turns. We also introduce a parameter ρ to manipulate the height of the upper left corner. We still write 0 in the illustration, but ρ appears in the formula for the weights. We denote h_ω the height map associated with a six-vertex configuration ω.

The weight of the 8VSOS vertices is parametrised by theta function. More specifically, we write them in terms of the Jacobi theta functions. We begin this chapter with a very brief introduction to the Jacobi theta functions.

4.1.1 Jacobi Theta Functions

The vertex weights of the six-vertex model are written in terms of trigonometric functions. In the eight-vertex model SOS, we write them with elliptic functions.

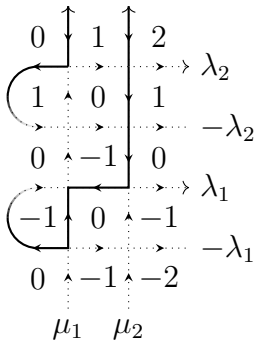

Figure 4.1: A particular six-vertex configuration with domain-wall boundary conditions and a reflecting end.

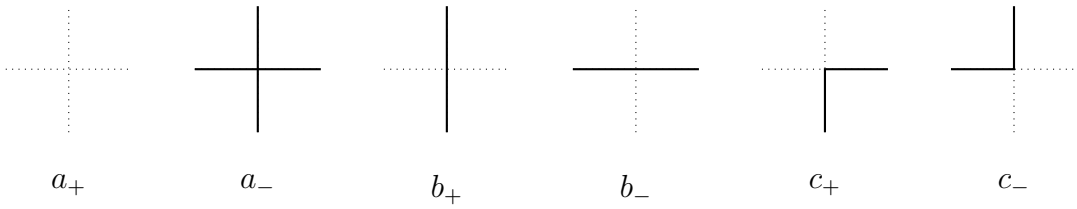

Figure 4.2: Types of vertices of the six-vertex model in the path picture with (down left) convention.

There are multiple conventions for such functions. We work with the conventions for the Jacobi theta functions of Whittaker and Watson [36]. Most of the properties in this subsection come from those references.

In this section, for any variable denoted by τ, we write $p = \mathrm{e}^{\mathrm{i}\pi\tau}$ and use the condensed notation $p^x = \mathrm{e}^{\mathrm{i}\pi\tau x}$ for all $x \in \mathbb{C}$. We usually abuse notations and write dependencies in τ in terms of p.

Definition 4.1 (Jacobi theta function)**.** *The Jacobi theta functions $\vartheta_1, \vartheta_2, \vartheta_3$ and ϑ_4 are defined as*

$$\begin{aligned}
\vartheta_1(x \mid \tau) = \vartheta_1(x,p) &= -\mathrm{i}\sum_{n\in\mathbb{Z}} (-1)^n p^{(n+1/2)^2} \mathrm{e}^{(2n+1)\mathrm{i}x}, \\
\vartheta_2(x \mid \tau) = \vartheta_2(x,p) &= \sum_{n\in\mathbb{Z}} p^{(n+1/2)^2} \mathrm{e}^{(2n+1)\mathrm{i}x}, \\
\vartheta_3(x \mid \tau) = \vartheta_3(x,p) &= \sum_{n\in\mathbb{Z}} p^{n^2} \mathrm{e}^{2n\mathrm{i}x}, \\
\vartheta_4(x \mid \tau) = \vartheta_4(x,p) &= \sum_{n\in\mathbb{Z}} (-1)^n p^{n^2} \mathrm{e}^{2n\mathrm{i}x}.
\end{aligned} \tag{4.1}$$

We direct the reader interested in an introduction to the Jacobi theta function to the appendix of the master thesis of Sandrine Brasseur [10]. In this subsection, we state some of the relevant properties of the Jacobi theta function without proof. We write $\vartheta_i(x) = \vartheta_1(x,p)$ when there is no possible confusion. The first Jacobi theta function is odd, whereas the three other are even.

Proposition 4.2. *The Jacobi theta functions $\vartheta_1, \vartheta_2, \vartheta_3$ and ϑ_4 satisfy the relations*

$$\vartheta_1(x+\pi/2,p) = \vartheta_2(x,p), \qquad \vartheta_3(x+\pi/2,p) = \vartheta_4(x,p), \tag{4.2}$$
$$\vartheta_2(x+\pi/2,p) = -\vartheta_1(x,p), \qquad \vartheta_4(x+\pi/2,p) = \vartheta_3(x,p), \tag{4.3}$$

and ϑ_1 and ϑ_4 are related by

$$\vartheta_4(x \pm \pi\tau/2, p) = \pm \mathrm{i} p^{-1/4} \mathrm{e}^{\mp \mathrm{i} x} \vartheta_1(x,p). \tag{4.4}$$

The Jacobi theta functions satisfy the *addition rule*
Proposition 4.3. *The following equation holds*

$$\vartheta_1(x+y)\vartheta_1(x-y)\vartheta_4(0)^2 = \vartheta_1(x)^2\vartheta_4(y)^2 - \vartheta_4(x)^2\vartheta_1(y)^2. \tag{4.5}$$

We also use a *duplication formula.*
Proposition 4.4. *The Jacobi theta functions satisfy the equation*

$$\vartheta_1(2x,p^2) = \frac{G(p^2)}{G(p)^2}\vartheta_1(x,p)\vartheta_2(x,p). \tag{4.6}$$

As this expression in not in the references, we give a proof in appendix A.
Proposition 4.5. *The first Jacobi theta function satisfy the equation*

$$\Psi(x) = \frac{G(p)^3}{G(p^3)}\vartheta_1(3x,p^3) = \vartheta_1(x,p)\vartheta_1\left(x+\frac{2\pi}{3},p\right)\vartheta_1\left(x+\frac{4\pi}{3},p\right). \tag{4.7}$$

As with the previous proposition, the proof is in appendix A.

The first Jacobi theta function is an element of a bigger class of function called *theta functions.*
Definition 4.6. *A holomorphic function $f\colon \mathbb{C} \to \mathbb{C}$ is a Theta function of order n, nome p and norm r if f satisfies for all $x \in \mathbb{C}$*

$$f(x+\pi) = (-1)^n f(x), \quad f(x+\mathrm{i}\pi\tau) = (-p)^{-n}\mathrm{e}^{-2\mathrm{i}(nx+r)}f(x). \tag{4.8}$$

We denote the set of all theta functions of order n, nome p and norm r by $\Theta_n(r)$.

The most important property for us of the set $\Theta_n(r)$ is its finite-dimensional vector space structure. The proof can be found in [33][1]
Theorem 4.7. *For all $n \in \mathbb{N}_*$ and $r \in \mathbb{C}$, the set $\Theta_n(r)$ is a vector space of dimension n.*

4.1.2 Partition Function

The vertex-weights of the 8VSOS model have the additional dependency in the height parameter h. When a vertex is oriented as in figure 4.3, the weight depends on the height h on the upper-left neighbouring face. The weights are described in terms of the spectral parameters λ, μ, and two additional parameters η and ρ.

[1] One needs to translate the definition of theta function in A_{n-1} theta functions.

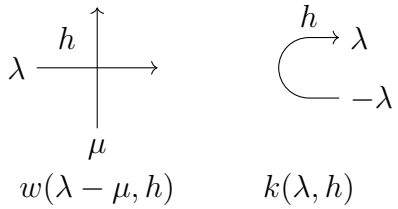

Figure 4.3: The dependence of the vertex weight on the height map and the spectral parameters. We denote the weight function of the vertex by w.

Definition 4.8. *Let $\lambda, \mu, \eta, \rho, h, \zeta \in \mathbb{C}$ and define $z = \rho + \eta h$ and $x = \lambda - \mu$. The weight associated with local configurations as in figure 4.3 are*

$$a(x,h) = \vartheta_1(x+\eta), \quad b_\pm(x,h) = \frac{\vartheta_1(x)\vartheta_1(z \mp \eta)}{\vartheta_1(z)}, \quad c_\pm(x,h) = \frac{\vartheta_1(\eta)\vartheta_1(z \pm x)}{\vartheta_1(z)}. \tag{4.9}$$

The weights of the turns are

$$k_+(\lambda,h,\zeta) = \frac{\vartheta_1(z+\zeta-\lambda)}{\vartheta_1(z+\zeta+\lambda)}, \quad k_-(\lambda,h,\zeta) = \frac{\vartheta_1(\zeta-\lambda)}{\vartheta_1(\zeta+\lambda)}. \tag{4.10}$$

Note that for each turn $h = 0$, and, hence, we can replace z by ρ because we fixed $h = 0$ on the upper left face. The partition function of the 8VSOS is written in terms of a determinant, as in the six-vertex model. We modify the partition function written in Linnea Hietala's paper [19].

Theorem 4.9 (Partition function)**.** *For $n \in \mathbb{N}$, define the matrix $K \in \mathbb{C}^{n\times n}$ with components*

$$K_{ij} = \frac{1}{\vartheta_1(\lambda_i+\mu_j+\eta)\vartheta_1(\lambda_i-\mu_j+\eta)\vartheta_1(\lambda_i+\mu_j)\vartheta_1(\lambda_i-\mu_j)}. \tag{4.11}$$

The partition function of the eight-vertex model solid-on-solid with domain-wall boundary condition and a reflecting end with weights (4.8) *is*

$$\begin{aligned} &Z_n(\vec{\lambda},\vec{\mu},\rho,\zeta) \\ &= \vartheta_1(\eta)^n \prod_{i=1}^{n} \frac{\vartheta_1(2\lambda_i)\vartheta_1(\zeta-\mu_i)\vartheta_1(\rho+\zeta+\mu_i)\vartheta_1(\rho+(2i-n-2)\eta)}{\vartheta_1(\zeta+\lambda_i)\vartheta_1(\rho+\zeta+\lambda_i)\vartheta_1(\rho+(n-i)\eta)} \\ &\times \frac{\prod_{i,j=1}^{n}\vartheta_1(\lambda_i+\mu_j+\eta)\vartheta_1(\lambda_i-\mu_j+\eta)\vartheta_1(\lambda_i+\mu_j)\vartheta_1(\lambda_i-\mu_j)}{\prod_{i<j}\vartheta_1(\lambda_i+\lambda_j+\eta)\vartheta_1(\lambda_i-\lambda_j)\vartheta_1(\mu_j+\mu_i)\vartheta_1(\mu_j-\mu_i)} \det K. \end{aligned} \tag{4.12}$$

This expression differs from [19] as the weight parametrisation is written in terms of other functions. The translation in terms of the weight parametrisation (4.3) is in appendix A. The similarities with the partition function of the six-vertex model with a reflecting end lead us to hope that we could find the arctic curve of the 8VSOS model with the tangent method.

We abuse notation and write $Z(\lambda_*, \mu_*, \rho, \zeta) = Z(\vec{\lambda}, \vec{\mu}, \rho, \zeta)$ when $\lambda_i = \lambda_*$ and $\mu_i = \mu_*$ for all $i \in \{1, \dots, n\}$.

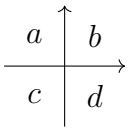

Figure 4.4: The different faces around a vertex.

4.2 The Three-Colour Model

In this section, we investigate the relation between the 8VSOS model and the three-colour model. The 8VSOS model has a strong connection with the three-colour model on a rectangular domain with a reflecting end. As we know the partition function of the 8VSOS model by theorem 4.9, we use this relation to find the partition function of the three-colour model. The discussion of this section is based on the first paper of Linnea Hietala's thesis [19].

We define Ω_n the set of possible three-colourings on the rectangle with $n+1$ columns of colourable faces. To uncover the relation, we create a new parametrisation of the weights. We define a function $f\colon \mathbb{Z}^4 \to \mathbb{R}$ as

$$f(x_1, x_2, x_3, x_4) = \frac{3(x_1 + x_3) - (x_2 + x_4)}{4}. \tag{4.13}$$

For every vertex v, we write a, b, c, d the height on the faces around v as in figure 4.4. We define another function

$$\tilde{w}_\omega(v) = \frac{\vartheta_1(\rho + f(a,b,c,d)\eta)}{\vartheta_1(\rho + a\eta)}. \tag{4.14}$$

The partition function of the 8VSOS model when $\lambda_i = -\eta/2$ and $\mu_i = 0$ can be written in terms of the functions $\tilde{w}_\omega$. We write $\Omega_{n,k}$ the subset of configurations that has exactly k positive turns and $K_\pm(\zeta) = k_\pm(-\eta/2, 0, \zeta)$.

Lemma 4.10. *When $\lambda = -\eta/2$ and $\mu = 0$, the homogeneous partition function of the 8VSOS model with a reflecting end satisfy*

$$\frac{Z_n(-\eta/2, 0, \rho, \zeta)}{(-1)^{n(n+1)/2}\vartheta_1(\eta/2)^{2n^2}} = \sum_{k=0}^{n} \sum_{\omega \in \Omega_{n,k}} \left(\frac{\vartheta_1(\eta)}{\vartheta_1(\eta/2)}\right)^{N_c(\omega)} \left[\prod_{v \in V(\mathcal{B})} \tilde{w}_\omega(v)\right] K_+(\zeta)^k K_-(\zeta)^{n-k}. \tag{4.15}$$

Proof. We compute the expression of (4.14) and compare it with the weights of definition (4.8)

$$\tilde{w}_\omega(v) = \begin{cases} a(-\eta/2, h)/\vartheta_1(\eta/2) & \text{if } v \text{ is a } a\text{-vertex,} \\ -b_\pm(-\eta/2, h)/\vartheta_1(\eta/2) & \text{if } v \text{ is a } b_\pm\text{-vertex,} \\ c_\pm(-\eta/2, h)/\vartheta_1(\eta) & \text{if } v \text{ is a } b_\pm\text{-vertex,} \end{cases} \tag{4.16}$$

We thus obtain by definition of the partition function

$$Z(-\eta/2,0,\rho,\zeta) = \vartheta_1(\eta/2)^{2n^2} \sum_{k=0}^{n} \sum_{\omega\in\Omega_{n,k}} (-1)^{N_b(\omega)} \left(\frac{\vartheta_1(\eta)}{\vartheta_1(\eta/2)}\right)^{N_c(\omega)} \times \left[\prod_{v\in V(\mathcal{B})} \tilde{w}_\omega(v)\right] K_+(\zeta)^k K_-(\zeta)^{n-k}. \tag{4.17}$$

We use proposition 2.1 to obtain for any configuration ω

$$(-1)^{N_b(\omega)} = (-1)^{n(n+1)/2}. \tag{4.18}$$

We substitute (4.18) in (4.17) and conclude the proof. □

To find a relation between the 8VSOS model and the three-colour model, we specify $\eta = -4\pi/3$. We define the functions $K^\rho_\pm$ and T_i for $i \in \{0,1,2\}$ by

$$K^\rho_\pm(\zeta) = \vartheta_1\left(\rho \mp \frac{2\pi}{3}\right) K_\pm(\zeta), \quad T_i = \frac{1}{\vartheta_1(\rho + 2i\pi/3)^3}. \tag{4.19}$$

We also define

$$A_n = \begin{cases} 1 & \text{if } n \equiv 0 \mod 3, \\ \dfrac{\vartheta_1(\rho+4\pi/3)}{\vartheta_1(\rho)} & \text{if } n \equiv 1 \mod 3, \\ \dfrac{\vartheta_1(\rho+2\pi/3)\vartheta_1(\rho+4\pi/3)}{\vartheta_1(\rho)^2} & \text{if } n \equiv 2 \mod 3. \end{cases} \tag{4.20}$$

We write $Z^3_{n,k}(t_0,t_1,t_2)$ the partition function of the three-colour model with configurations $\Omega_{n,k}$ and weights t_0, t_1 and t_2.

Theorem 4.11. *The 8VSOS model and the three-colour model are related by the equation*

$$Z_n(2\pi/3,0,\rho,\zeta) = \vartheta_1(2\pi/3)^{2n^2}(-1)^{n(n-1)/2}\vartheta_1(\rho)^{n+3}\Psi(\rho)^{2n(n+1)}A_n \times \sum_{k=0}^{n} K^\rho_+(\zeta)^k K^\rho_-(\zeta)^{n-k} Z^3_{n,k}(T_0,T_1,T_2). \tag{4.21}$$

Proof. With $\eta = -4\pi/3$, we apply the Proposition 4.2 to compute $\vartheta_1(x+\pi) = -\vartheta_1(x)$ to compute the form of the new weights (4.14)

$$\tilde{w}_\omega(v) = \frac{\vartheta_1(\rho-(a+c)\pi+(b+d)\pi/3)}{\vartheta_1(\rho-4a\pi/3)} = (-1)^{a+b+c+d}\frac{\vartheta_1(\rho-2(b+d)\pi/3)}{\vartheta_1(\rho+2a\pi/3)}. \tag{4.22}$$

Because a, b, c and d are the heights of the faces adjacent to the vertex v, the parity of a and b is different from the parity of c and d. Hence $a+b+c+d$ is even. Therefore,

$$\tilde{w}_\omega(v) = \frac{\vartheta_1(\rho-2(b+d)\pi/3)}{\vartheta_1(\rho+2a\pi/3)}. \tag{4.23}$$

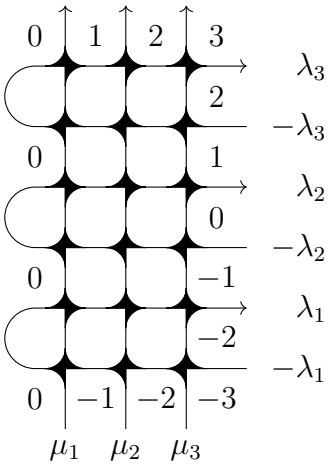

Figure 4.5: Configuration of the 8VSOS model on a rectangular grid with $n = 3$ with a reflecting end. The shadow region near each vertex v indicates the faces a, b, and d.

Also, b and d differ only by 1. So b is not congruent to d modulo 3. We find by checking every possibility that $-(b+d), b$ and d are three non congruent numbers modulo 3. We thus obtain

$$\vartheta_1(\rho - 2(b+d)\pi/3)\vartheta_1(\rho + 2b\pi/3)\vartheta_1(\rho + 2d\pi/3) \\ = \vartheta_1(\rho)\vartheta_1(\rho + 2\pi/3)\vartheta_1(\rho + 4\pi/3). \quad (4.24)$$

We substitute (4.24) into the expression of the weights (4.23) and use Proposition 4.5 to finally compute

$$\tilde{w}_\omega(v) = \frac{\Psi(\rho)}{\vartheta_1(\rho + 2a\pi/3)\vartheta_1(\rho + 2b\pi/3)\vartheta_1(\rho + 2d\pi/3)}. \quad (4.25)$$

With this representation, we can see the product over all vertices of (4.15) as a product over the faces instead. Every vertex adds the weights of three adjacent faces. The interior faces all have three vertices contributing (see figure 4.5), so the product of $\tilde{w}_\omega(v)$ over all vertices $v \in V(\mathcal{B})$ is, up to a factor A_n depending on the faces on the boundary, the product given by

$$\prod_{v \in V(\mathcal{B})} \tilde{w}_\omega(v) = B_n \Psi(\rho)^{2n^2} \prod_{f \in F(\mathcal{B})} \frac{1}{\vartheta_1(\rho + 2h_\omega(f)\pi/3)^3}. \quad (4.26)$$

We compute explicitly the factor B_n in appendix B. We find

$$B_n = \vartheta_1(\rho)^{n+3}\vartheta_1\left(\rho + \frac{2\pi}{3}\right)^{n-k}\vartheta_1\left(\rho + \frac{4\pi}{3}\right)^{k}\Psi(\rho)^{2n}A_n, \quad (4.27)$$

with A_n as in (4.20). By definition, the partition function of the three-colour model with weights T_0, T_1 and T_2 is

$$Z^3_{n,k}(T_0, T_1, T_2) = \sum_{\omega \in \Omega_{n,k}} \prod_{f \in F(\mathcal{B})} \frac{1}{\vartheta_1(\rho + 2h_\omega(f)\pi/3)^3}. \quad (4.28)$$

Moreover, by Proposition 2.1, we have for $\omega \in \Omega_{n,k}$

$$\left(\frac{\vartheta_1(\eta)}{\vartheta_1(\eta/2)}\right)^{N_c(\omega)} = \left(\frac{\vartheta_1(4\pi/3)}{\vartheta_1(2\pi/3)}\right)^{2N_{c+}(\omega)-2k-n} = (-1)^{-n}. \tag{4.29}$$

We substitute (4.26), (4.28) and (4.29) into the equation of Lemma 4.10 and obtain

$$\begin{aligned} Z_n(2\pi/3,0,\rho,\zeta) &= \vartheta_1(2\pi/3)^{2n^2}(-1)^{n(n-1)/2}\vartheta_1(\rho)^{n+3}\Psi(\rho)^{2n(n+1)}A_n \\ \times \sum_{k=0}^{n} \vartheta_1(\rho+4\pi/3)^k K_+(\zeta)^k \vartheta_1(\rho+2\pi/3)^{n-k} K_-(\zeta)^{n-k} Z^3_{n,k}(T_0,T_1,T_2). \end{aligned} \tag{4.30}$$

This concludes the proof. □

We now have an expression that relates the partition function of the three-colour model to the known partition function of the 8VSOS model. We note, however, that we cannot directly extract the full partition function Z^3_n as there are different coefficients for different number of positive turns. One way to extract the coefficient would be to write (4.21) as a polynomial in $K^\rho_+(\zeta)/K^\rho_-(\zeta)$, invert the relation with ζ and use Cauchy's theorem. In the special case $k = 0$ and $k = n$, we can simply fix the values of ζ.

Corollary 4.12. *The partition functions $Z^3_{n,0}(T_0,T_1,T_2)$ and $Z^3_{n,n}(T_0,T_1,T_2)$ with T_0, T_1 and T_2 as in Theorem 4.11 are*

$$\begin{aligned} Z^3_{n,0}(T_0,T_1,T_2) &= \frac{1}{A_n\Psi(\rho)^{2n(n+1)}} \frac{(-1)^{n(n-1)/2}}{\vartheta_1(2\pi/3)^{2n^2}\vartheta_1(\rho)^{2n+3}} Z_n\left(\frac{2\pi}{3},0,\rho,\frac{2\pi}{3}-\rho\right) \\ Z^3_{n,n}(T_0,T_1,T_2) &= \frac{1}{A_n\Psi(\rho)^{2n(n+1)}} \frac{(-1)^{n(n-1)/2}}{\vartheta_1(2\pi/3)^{2n^2}\vartheta_1(\rho)^{2n+3}} Z_n\left(\frac{2\pi}{3},0,\rho,\frac{2\pi}{3}\right) \end{aligned} \tag{4.31}$$

Proof. If we take $\zeta = 2\pi/3 - \rho$, then $K_+(\zeta) = 0$. Hence, we have by Theorem 4.11

$$\begin{aligned} Z_n\left(\frac{2\pi}{3},0,\rho,\frac{2\pi}{3}-\rho\right) &= \vartheta_1(2\pi/3)^{2n^2}(-1)^{n(n-1)/2}\vartheta_1(\rho)^{n+3}\Psi(\rho)^{2n(n+1)}A_n \\ &\quad \times K^\rho_-\left(\frac{2\pi}{3}-\rho\right)^n Z^3_{n,0}(T_0,T_1,T_2). \end{aligned} \tag{4.32}$$

We compute explicitly $K^\rho_-(2\pi/3-\rho) = \vartheta_1(\rho)$. We substitute this equation into (4.32) and obtain the first part of the theorem. The case $k = n$ is similar with $\zeta = 2\pi/3$. □

4.2.1 Domain of the Parameters for Positive Weights

If we wish to study the statistical properties of the three-colour model, we need to have positive weights. We thus investigate for which range of parameter (if any) we can make the weights T_0, T_1 and T_2 simultaneously positive. In general, the first Jacobi theta function is complex valued. But if each T_i has the same phase, we can extract the phase and define new positive weights. We thus search parameters such that there exist $\alpha, \beta \in \mathbb{R}^+_*$ that satisfy

$$T_0 = \alpha T_1, \quad T_0 = \beta T_2. \tag{4.33}$$

We have two parameters available, ρ and p (or τ). We give a compatible domain in the following proposition.

Proposition 4.13. *When p is real and ρ is on the line $\mathrm{Im}\rho = \pi\mathrm{Im}\tau/2$, the parameters T_0, T_1 and T_2 have the same phase.*

Proof. We write $x = \rho - \pi\tau/2 \in \mathbb{R}$. We compute for $i \in \{0,1,2\}$ by using the relations of the Jacobi theta functions (4.2)

$$\frac{1}{T_i} = \vartheta_1\left(x + \frac{2i\pi}{3} + \frac{\pi\tau}{2}, p\right)^3 = -\mathrm{i}\mathrm{e}^{-3\mathrm{i}x}p^{-3/4}\vartheta_4\left(x + \frac{2i\pi}{3}, p\right). \tag{4.34}$$

As the overall factor multiplying ϑ_4 is the same for T_0, T_1 and T_2, it is irrelevant for their relative phase. Hence, T_0, T_1 and T_2 have the same phase if there exist $\alpha, \beta \in \mathbb{R}_*^+$ such that

$$\vartheta_4(x,p) = \alpha\vartheta_4(x + 2\pi/3, p), \quad \vartheta_4(x,p) = \beta\vartheta_4(x + 4\pi/3, p). \tag{4.35}$$

We can show from the definition of the fourth Jacobi theta function 4.1 that, as x and p are real, $\vartheta_4(x + 2i\pi/3, p)$ is also real. Moreover, the zeros of $\vartheta_4(z)$ are on the lines $\mathrm{Im}z \in \pi\mathrm{Im}\tau/2 + \pi\mathrm{Im}\tau\mathbb{Z}$. Hence, in our case, there is no $x \in \mathbb{R}$ such that $\vartheta_4(x + 2i\pi/3, p) = 0$. Thus, $\vartheta_4(x + 2i\pi/3, p)$ has the same sign for all $x \in \mathbb{R}$ and (4.35) has solutions. This concludes the proof. □

Hence, we can parametrise our weights W_0, W_1 and W_2 with T_0, T_1 and T_2. Numerical results suggest that there are no other set of parameters that satisfy this property. In general, as we are not interested in the cases where one of the weights is zero, we can choose $W_0 = 1$, $W_1 = T_1/T_0$ and $W_2 = T_2/T_0$. It seems that this is enough for all weights, as numerical results indicate that the map ϕ defined by

$$\phi\colon [0,\pi) \times [0,1) \to (\mathbb{R}_*^+)^2\colon (\rho,p) \mapsto \left(\frac{T_1(\rho,p)}{T_0(\rho,p)}, \frac{T_2(\rho,p)}{T_0(\rho,p)}\right) \tag{4.36}$$

is surjective (see figure 4.6). Moreover, for all $\rho \in \mathbb{R}$, $\phi(\rho, 0) = (1,1)$ and we believe that the restriction of ϕ on $[0,\pi) \times (0,1)$ gives a bijection with image $(\mathbb{R}_*^+)^2 \backslash \{(1,1)\}$.

4.3 Partition Function at $\eta = \pi/2$

In this section, we study a simpler specialisation than the one related to the three-colour model. We look at the choice $\eta = \pi/2$ of the partition function. At this point, the determinant factors into a simple product.

We can not have positive weights with this specialisation because we then have $b_+ = -b_-$. To solve this problem, we rewrite part of the parametrisation 4.8 in terms of ϑ_4. By convenience, we write $\bar{z} = z - \pi\tau/2$. We find

$$b_\pm(\lambda,h) = \pm\mathrm{i}\frac{\vartheta_1(x)\vartheta_3(\bar{z})}{\vartheta_4(\bar{z})}, \quad c_\pm(\lambda,h) = \mathrm{e}^{\mp\mathrm{i}\lambda}\frac{\vartheta_1(x)\vartheta_4(\bar{z} \pm \lambda)}{\vartheta_4(\bar{z})} \tag{4.37}$$

If we forget about the factors $\pm\mathrm{i}$ and $\mathrm{e}^{\mp\mathrm{i}\lambda}$, we can take the parameter in such a way that they are all positive. If we write $\alpha_\pm, \beta_\pm$ and $\gamma_\pm$ the new generated weights, the

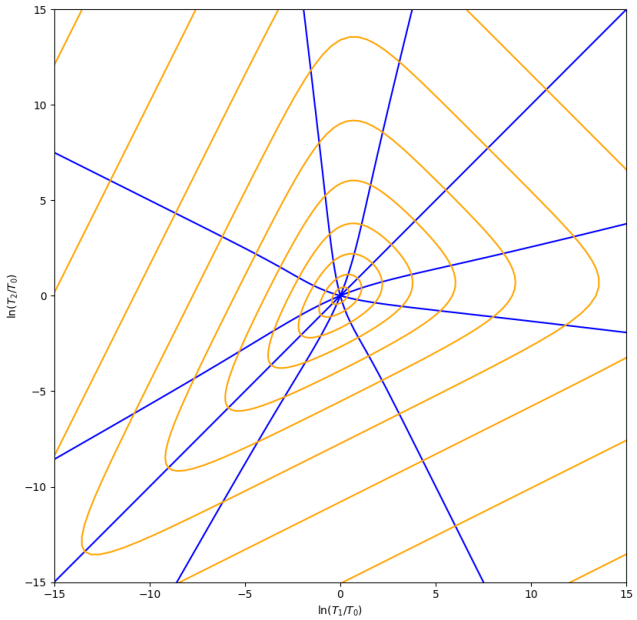

Figure 4.6: The coordinate system $(\ln(T_1/T_0), \ln(T_2/T_0))$. The blue and orange lines are respectively curves with constant p and ρ.

partition function reads

$$Z = \sum_{\omega \in \Omega} \mathrm{i}^{\delta b} \mathrm{e}^{-\mathrm{i}\lambda\delta c} \alpha_{\pm}^{N_{a\pm}} \beta_{\pm}^{N_{b\pm}} \gamma_{\pm}^{N_{c\pm}}. \tag{4.38}$$

By the first proposition 2.1, if we consider the number of k_+ (or k_- constant, then we can extract the constant $\mathrm{i}^{\delta b}\mathrm{e}^{-\mathrm{i}\lambda\delta c}$ and decide to work with the real positive weights independently. We continue to use the original parameterisation in what follows.

We return to the factorisation of the partition function. We define the function

$$\begin{aligned} h(x,y) &= \vartheta_1(x+y+\pi/2)\vartheta_1(x-y+\pi/2)\vartheta_1(x+y)\vartheta_1(x-y) \\ &= \vartheta_1(x+y)\vartheta_2(x+y)\vartheta_1(x-y)\vartheta_2(x-y). \end{aligned} \tag{4.39}$$

We also use the notation $h_{ij} = h(\lambda_i, \mu_j)$. With this nomenclature, the matrix K in theorem 4.9 is the matrix with components $1/h_{ij}$. We first compute the determinant of K at $\eta = \pi/2$. By the duplication formula (4.6), there exists a constant C such that (we do not write the constant explicitly to simplify the notations)

$$\vartheta_1(x)\vartheta_2(x) = C\vartheta_1(2x, p^2). \tag{4.40}$$

We substitute this relation in the expression of h (4.39) and obtain

$$h(x,y) = C^2\vartheta_1(2(x+y), p^2)\vartheta_1(2(x-y), p^2). \tag{4.41}$$

We furthermore use the addition rule (4.5) and find the expression

$$h(x,y) = \frac{C^2}{\vartheta_4(0,p^2)^2}\left[\vartheta_1(2x,p^2)^2\vartheta_4(2y,p^2)^2 - \vartheta_4(2x,p^2)^2\vartheta_1(2y,p^2)^2\right]. \tag{4.42}$$

We define for convenience the set of functions

$$x_i = \vartheta_1(2\lambda_i, p^2)^2, \quad X_i = \vartheta_1(2\lambda_i, p^2)^2, \quad y_i = \vartheta_1(2\mu_i, p^2)^2, \quad Y_i = \vartheta_1(2\mu_i, p^2)^2. \tag{4.43}$$

We have $h_{ij} = (C^2/\vartheta_4(0,p^2)^2)(x_i\, Y_j - X_i\, y_j)$. As stated previously, K is the matrix with components $1/h_{ij}$. Hence, the determinant of K is

$$\begin{aligned} \det K &= \det\left[\frac{\vartheta_4(0,p^2)^2}{C^2}\frac{1}{x_iY_j - X_iy_j}\right]_{1\le i\le n}^{1\le j\le n} \\ &= \left[\frac{\vartheta_4(0,p^2)}{C}\right]^{2n}\left[\prod_{k=1}^{n}\frac{1}{X_kY_k}\right]\det\left[\frac{1}{x_i/X_i - y_j/Y_j}\right]_{1\le i\le n}^{1\le j\le n}. \end{aligned} \tag{4.44}$$

The determinant on the right is a Cauchy determinant, therefore we find

$$\begin{aligned} \det K &= \left[\frac{\vartheta_4(0,p^2)}{C}\right]^{2n}\left[\prod_{k=1}^{n}\frac{1}{X_kY_k}\right]\frac{\prod_{i<j=1}^{n}(x_j/X_j - x_i/X_i)(y_i/Y_i - y_j/Y_j)}{\prod_{ij}(x_i/X_i - y_j/Y_j)} \\ &= \left[\frac{\vartheta_4(0,p^2)}{C}\right]^{2n}\frac{\prod_{i<j=1}^{n}(x_jX_i - x_iX_j)(y_iY_j - y_jY_i)}{\prod_{i,j=1}^{n}(x_iY_j - X_iy_j)}. \end{aligned} \tag{4.45}$$

We rewrite the denominator in terms of h_{ij}

$$\det k = \left[\frac{C}{\vartheta_4(0,p^2)}\right]^{2n(n-1)}\left[\prod_{i,j=1}^{n}\frac{1}{h_{ij}}\right]\prod_{i<j=1}^{n}(x_jX_i - x_iX_j)(y_iY_j - y_jY_i). \tag{4.46}$$

The expressions of the differences are

$$\begin{aligned} x_jX_i - x_iX_j &= \vartheta_1(2\lambda_j,p^2)^2\vartheta_4(2\lambda_j,p^2)^2 - \vartheta_4(2\lambda_j,p^2)^2\vartheta_1(2\lambda_j,p^2)^2, \\ y_iY_j - y_jY_i &= \vartheta_1(2\mu_i,p^2)^2\vartheta_4(2\mu_j,p^2)^2 - \vartheta_4(2\mu_i,p^2)^2\vartheta_1(2\mu_j,p^2)^2. \end{aligned} \tag{4.47}$$

We use the addition rule (4.5) to obtain

$$\begin{aligned} x_jX_i - x_iX_j &= \vartheta_4(0,p^2)^2\vartheta_1(\lambda_j+\lambda_i,p^2)\vartheta_1(\lambda_j-\lambda_i,p^2) \\ y_iY_j - y_jY_i &= \vartheta_4(0,p^2)^2\vartheta_1(\mu_i+\mu_j,p^2)\vartheta_1(\mu_i-\mu_j,p^2) \end{aligned} \tag{4.48}$$

Therefore, we have the expression

$$\begin{aligned} \left[\prod_{i,j=1}^{n}h_{ij}\right]\det K = C^{2n(n-1)}\prod_{i<j=1}^{n}&\vartheta_1(2(\lambda_j+\lambda_i),p^2)\vartheta_1(2(\lambda_j-\lambda_i),p^2) \\ &\times\vartheta_1(2(\mu_i+\mu_j,p^2)\vartheta_1(2(\mu_i-\mu_j),p^2). \end{aligned} \tag{4.49}$$

We finally use the duplication formula (4.40) to obtain

$$\begin{aligned} \left[\prod_{i,j=1}^{n}h_{ij}\right]\det K = \prod_{i<j=1}^{n}&\vartheta_1(\lambda_j+\lambda_i)\vartheta_1(\lambda_j-\lambda_i)\vartheta_1(\mu_i+\mu_j)\vartheta_1(\mu_i-\mu_j) \\ &\times\vartheta_2(\lambda_j+\lambda_i)\vartheta_2(\lambda_j-\lambda_i)\vartheta_2(\mu_i+\mu_j)\vartheta_2(\mu_i-\mu_j). \end{aligned} \tag{4.50}$$

We now compute the full partition function at $\eta = \pi/2$.

Proposition 4.14. *Let Q_n be the function defined by*

$$Q_n(\rho) = \left[\frac{-\vartheta_1(\rho)}{\vartheta_2(\rho)}\right]^{(-1)^n\lfloor n/2\rfloor}. \tag{4.51}$$

When $\eta = \pi/2$, the inhomogeneous partition function specialises to

$$\begin{aligned} Z_n(\vec{\lambda},\vec{\mu},\rho,\zeta) = \vartheta_2(0)^n Q_n(\rho) \prod_{i=1}^{n} \frac{\vartheta_1(2\lambda_i)\vartheta_1(\zeta-\mu_i)\vartheta_1(\rho+\zeta+\mu_i)}{\vartheta_1(\zeta+\lambda_i)\vartheta_1(\rho+\zeta+\lambda_i)} \\ \times \prod_{i<j=1}^{n} \vartheta_1(\lambda_i+\lambda_j)\vartheta_2(\lambda_i-\lambda_j)\vartheta_2(\mu_i+\mu_j)\vartheta_2(\mu_i-\mu_j). \end{aligned} \tag{4.52}$$

Proof. The determinant times the product on the numerator of the second fraction f_0 in the expression of the partition function (4.12) is given by Equation (4.50). Moreover, some of the factors of the product cancel the denominator of the fraction f_0. We compute

$$\begin{aligned} Z_n(\vec{\lambda},\vec{\mu},\rho,\zeta) = \vartheta_1(\eta)^n \prod_{i=1}^{n} \frac{\vartheta_1(2\lambda_i)\vartheta_1(\zeta-\mu_i)\vartheta_1(\rho+\zeta+\mu_i)\vartheta_1(\rho+(2i-n-2)\eta)}{\vartheta_1(\zeta+\lambda_i)\vartheta_1(\rho+\zeta+\lambda_i)\vartheta_1(\rho+(n-i)\eta)} \\ \times \prod_{i<j=1}^{n} \vartheta_1(\lambda_i+\lambda_j)\vartheta_2(\lambda_i-\lambda_j)\vartheta_2(\mu_i+\mu_j)\vartheta_2(\mu_i-\mu_j). \end{aligned} \tag{4.53}$$

With the specialisation $\eta = \pi/2$, we have $\vartheta_1(\eta) = \vartheta_2(0)$. We also simplify the rightmost term of the numerator and the denominator. The product of the numerator is

$$A = \prod_{i=1}^{n} \vartheta_1(\rho+(2i-n-2)\eta) = \prod_{i=0}^{n-1} \vartheta_1(\rho+(i-n/2)\pi). \tag{4.54}$$

We compute A by separating the odd and even cases. When n is even, we write $n = 2p$ and compute

$$A = \prod_{i=0}^{n-1} \vartheta_1(\rho+(i-p)\pi) = \prod_{i=0}^{n-1} (-1)^{i-p}\vartheta_1(\rho) = (-1)^{n/2}\vartheta_1(\rho)^n. \tag{4.55}$$

If n is odd, we write $n = 2p-1$ and then we rewrite the product in terms of ϑ_2 for convenience,

$$A = \prod_{i=0}^{n-1} \vartheta_2(\rho+(i-p)\pi) = \prod_{i=0}^{n-1} (-1)^{i-p}\vartheta_2(\rho) = -\vartheta_2(\rho)^n. \tag{4.56}$$

We compute the product on the denominator in the same way and obtain

$$B = \prod_{i=1}^{n} \vartheta_1(\rho+i\eta) = \begin{cases} \vartheta_1(\rho)^{n/2}\vartheta_2(\rho)^{n/2} & \text{if } n \text{ is even,} \\ (-1)^{(n-1)/2}\vartheta_1(\rho)^{(n+1)/2}\vartheta_2(\rho)^{(n-1)/2} & \text{if } n \text{ is odd.} \end{cases} \tag{4.57}$$

The ratio of the two products is thus

$$Q_n(\rho) = \frac{A}{B} = \begin{cases} [-\vartheta_1(\rho)/\vartheta_2(\rho)]^{n/2} & \text{if } n \text{ is even} \\ [-\vartheta_2(\rho)/\vartheta_1(\rho)]^{(n-1)/2} & \text{if } n \text{ is odd} \end{cases} = \left[\frac{-\vartheta_1(\rho)}{\vartheta_2(\rho)}\right]^{(-1)^n\lfloor n/2\rfloor}. \tag{4.58}$$

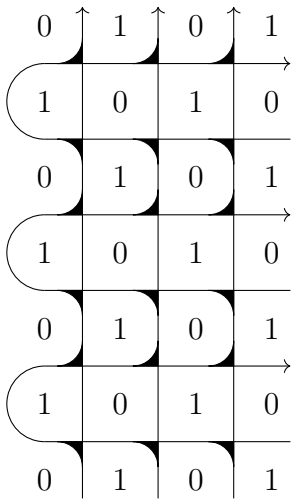

Figure 4.7: The parity of the heights on the domain is 0 for even height and 1 for odd height. The shadow region at each vertex indicates the height associated with its weight. In each column, every vertex sees the same height.

With this notation, the partition function reads

$$\begin{aligned} Z_n(\vec{\lambda},\vec{\mu},\rho,\zeta) = \vartheta_2(0)^n Q_n(\rho) \prod_{i=1}^{n} \frac{\vartheta_1(2\lambda_i)\vartheta_1(\zeta-\mu_i)\vartheta_1(\rho+\zeta+\mu_i)}{\vartheta_1(\zeta+\lambda_i)\vartheta_1(\rho+\zeta+\lambda_i)} \\ \times \prod_{i<j} \vartheta_1(\lambda_i+\lambda_j)\vartheta_2(\lambda_i-\lambda_j)\vartheta_2(\mu_i+\mu_j)\vartheta_2(\mu_i-\mu_j). \end{aligned} \tag{4.59}$$

This concludes the proof. □

4.3.1 Partially Homogeneous Partition Function

The vertex weights are periodic with respect to the parameter z, with period π. Therefore, at $\eta = \pi/2$, the vertex weights depend only on the parity of the height on the adjacent face. As the relevant faces are always on the left of the vertices, above the vertices on even lines, and below on odd lines, the height contributing to the vertex weight can be considered a constant within each column (see figure 4.7.) For the last column, the relevant parameter z is $z_n = \rho + (n-1)\eta$.

We are interested in the refined partition function $Z_{n,k}$. These are the partition functions of the subset of configurations that have a c-vertex on the rightmost vertical line at vertical position k. To this end, we first compute the partially homogeneous partition function

$$\tilde{Z}_n(\lambda,\mu,\rho,\zeta,\xi) = \lim_{\substack{\lambda_1,\ldots,\lambda_n \\ \mu_1,\ldots,\mu_{n-1}\to\mu \\ \mu_n\to\xi}} Z_n(\vec{\lambda},\vec{\mu},\rho,\zeta). \tag{4.60}$$

The homogeneous partition function is $Z_n(\lambda,\mu,\rho,\zeta) = \tilde{Z}_n(\lambda,\mu,\rho,\zeta,\mu)$. We use the expression of the general partition function (4.59) to compute the relation between the two

Proposition 4.15. *When $\eta = \pi/2$, the homogeneous and partially homogeneous partition functions satisfy*

$$\tilde{Z}_n(\lambda,\mu,\rho,\zeta,\xi) = Z_n(\lambda,\mu,\rho,\zeta)\frac{\vartheta_1(\zeta-\xi)\vartheta_1(\rho+\zeta-\xi)}{\vartheta_1(\zeta-\mu)\vartheta_1(\rho+\zeta-\mu)}\left[\frac{\vartheta_2(\xi+\mu)\vartheta_2(\xi-\mu)}{\vartheta_2(2\mu)\vartheta_2(0)}\right]^{n(n-1)/2}. \tag{4.61}$$

Proof. We find the expression by directly computing and comparing the homogeneous and partially homogeneous limits on equation (4.52). □

Proposition 4.16. *Let ω be a configuration with homogeneous horizontal spectral parameter λ such that the only c-vertex on the rightmost column is at horizontal position k. The weight of the vertices on the rightmost column in ω is*

$$\begin{aligned} W_{n,k}(\lambda,\mu_n,\rho) = b_1(\lambda+\mu_n,z_n)^{\lfloor k/2\rfloor}a(\lambda-\mu_n)^{\lceil k/2\rceil-1} \\ \times a(\lambda+\mu_n)^{n-\lceil k/2\rceil}b_1(\lambda-\mu_n,z_n)^{n-\lfloor k/2\rfloor} \\ \times\begin{cases} c_2(\lambda-\mu_n,z_n), & \textit{if } k \textit{ is even,} \\ c_1(\lambda+\mu_n,z_n), & \textit{if } k \textit{ is odd.}\end{cases}\end{aligned} \tag{4.62}$$

Proof. We group vertices on the edge as pairs, numbered from one to n, starting from the bottom. Every pair of vertices at position ℓ above the one containing the c-vertex, i.e. $\ell > \lceil k/2\rceil$, has weight $a(\lambda_\ell+\mu_n)b_1(\lambda_\ell-\mu_n,z_n)$. The pairs below have weights $a(\lambda_\ell-\mu_n)b_1(\lambda_\ell+\mu_n,z_n)$. The weight of the pair containing the c-vertex depends on the parity of k, it is given by (see figure 4.8)

$$\begin{cases} b_1(\lambda_l+\mu_n,z_n)c_2(\lambda_l-\mu_n,z_n), & \text{if } n \text{ is even,} \\ c_1(\lambda_l+\mu_n,z_n)b_1(\lambda_l-\mu_n,z_n), & \text{if } n \text{ is odd.}\end{cases} \tag{4.63}$$

Hence, the total weight $W_{n,k}$ of the right column when every horizontal spectral parameter is equal to λ is

$$\begin{aligned} W_{n,k}(\lambda,\mu_n,\rho) = b_1(\lambda+\mu_n,z_n)^{\lfloor k/2\rfloor}a(\lambda-\mu_n)^{\lceil k/2\rceil-1} \\ \times a(\lambda+\mu_n)^{n-\lceil k/2\rceil}b_1(\lambda-\mu_n,z_n)^{n-\lfloor k/2\rfloor} \\ \times\begin{cases} c_2(\lambda-\mu_n,z_n), & \text{if } k \text{ is even,} \\ c_1(\lambda+\mu_n,z_n), & \text{if } k \text{ is odd.}\end{cases}\end{aligned} \tag{4.64}$$

This concludes the proof. □

We now state the relation between the refined partition function and the partially homogeneous one.

Corollary 4.17. *We define the set of function $\{w_{n,k}\colon k\in\{1,\dots,2n\}\}$ by*

$$\begin{aligned} w_{n,k}(\lambda,\mu,\rho) = \vartheta_1(\lambda+\mu)^{\lfloor k/2\rfloor}\vartheta_2(\lambda-\mu)^{\lceil k/2\rceil-1}\vartheta_2(\lambda+\mu)^{n-\lceil k/2\rceil}\vartheta_1(\lambda-\mu)^{n-\lfloor k/2\rfloor} \\ \times\begin{cases} \vartheta_1(z_n-\lambda+\mu), & \textit{if } k \textit{ is even,} \\ \vartheta_1(z_n+\lambda+\mu), & \textit{if } k \textit{ is odd.}\end{cases}\end{aligned} \tag{4.65}$$

The partially homogeneous partition function is

$$\tilde{Z}_n(\lambda,\mu,\rho,\zeta,\xi) = \sum_{k=1}^{2n} Z_{n,k}(\lambda,\mu,\rho,\zeta)\frac{w_{n,k}(\lambda,\xi,\rho)}{w_{n,k}(\lambda,\mu,\rho)}. \tag{4.66}$$

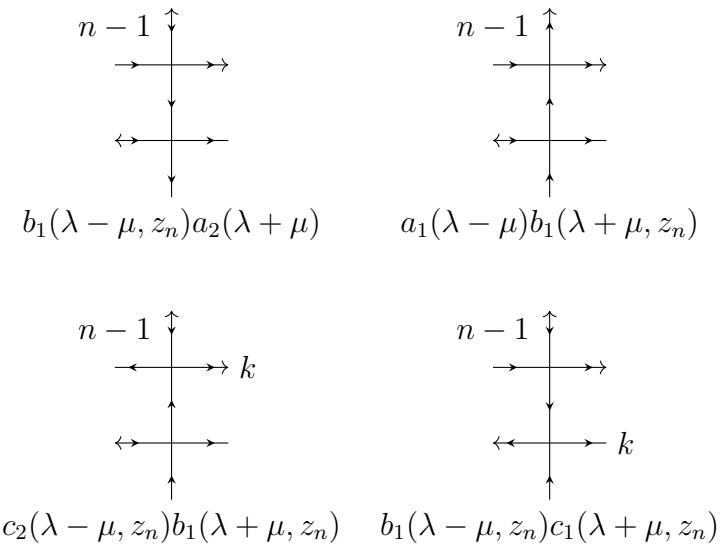

$b_1(\lambda-\mu,z_n)a_2(\lambda+\mu)$ $\quad$ $a_1(\lambda-\mu)b_1(\lambda+\mu,z_n)$

$c_2(\lambda-\mu,z_n)b_1(\lambda+\mu,z_n)$ $\quad$ $b_1(\lambda-\mu,z_n)c_1(\lambda+\mu,z_n)$

Figure 4.8: Illustration of each possible pair of vertices lying on the last column. There is one c-vertex on the column, at horizontal position k. (up left) A pair above the pair containing the c-vertex. (up right) A pair below the pair containing the c-vertex. (down left) The pair containing the c-vertex, with k even. (down right) The pair containing the c-vertex, with k odd.

Proof. As stated previously, the only difference between the weight of the configurations in $\tilde{Z}_n$ and Z_n is the weight of the vertices on the rightmost column. We obtain using proposition 4.16

$$\tilde{Z}_n(\lambda,\mu,\rho,\zeta,\xi)=\sum_{k=1}^{2n} Z_{n,k}(\lambda,\mu,\rho,\zeta)\frac{W_{n,k}(\lambda,\xi,\rho)}{W_{n,k}(\lambda,\mu,\rho)}. \tag{4.67}$$

From the parametrisation of the weights (A.10), we see that $w_{n,k}$ is the only factor of $W_{n,k}$ that depends on the parameter μ (or ξ). Therefore, we have

$$\frac{W_{n,k}(\lambda,\xi,\rho)}{W_{n,k}(\lambda,\mu,\rho)}=\frac{w_{n,k}(\lambda,\xi,\rho)}{w_{n,k}(\lambda,\mu,\rho)}. \tag{4.68}$$

We substitute (4.68) into (4.67) and obtain the theorem. □

We abuse notation and write the functions $\xi\mapsto w_{n,k}(\lambda,\xi,\rho)$ as $w^{\rho}_{n,k}$. As we know the expression of the partially homogeneous partition function, we hope to extract the refined partition functions from equation (4.66). To this end, we use the space of theta functions.

Lemma 4.18. *For all $n\in\mathbb{N}_*$ and $k\in\{1,\dots,2n\}$, the function $w^{\rho}_{n,k}$ is an element of $\Theta_{2n}(\rho)$.*

Proof. By theorem 4.2, we have

$$\vartheta_1(x+\pi)=-\vartheta_1(x),\quad \vartheta_1(x+\pi\tau)=(-p)^{-1}\mathrm{e}^{-2\mathrm{i}x}\vartheta_1(x). \tag{4.69}$$

We apply these relations to each factor of the functions $w^{\rho}_{n,k}$ and find

$$w^{\rho}_{n,k}(\xi+\pi)=(-1)^{2n}\,w^{\rho}_{n,k}(\xi), \tag{4.70}$$

$$w^{\rho}_{n,k}(\xi + \mathrm{i}\pi\tau) = (-p)^{-2n}\mathrm{e}^{-2\mathrm{i}(2n\xi+\rho)}w^{\rho}_{n,k}(\xi). \tag{4.71}$$

Thus, $w^{\rho}_{n,k}$ is a theta function of order $2n$, nome p and norm ρ. □

We aim to extract the refined partition functions. We show that those functions form a basis of $\Theta_{2n}(\rho)$.

Proposition 4.19. *Let $\lambda, \rho \in \mathbb{C}$ such that $\rho, 2\lambda, \rho + 2\lambda \notin \pi/2\mathbb{Z} + \pi\tau\mathbb{Z}$. For all $n \in \mathbb{N}_*$, the set of functions $\{w^{\rho}_{n,k} \colon k \in \{1, \dots, 2n\}\}$ is a basis of $\Theta_{2n}(\rho)$.*

Proof. For all $x \in \mathbb{C}$ and $n \in \mathbb{N}_*$, the set $\Theta_{2n}(x)$ is a vector space of dimension $2n$ by theorem 4.7. We consider first $n = 1$. We compute

$$w^{\rho}_{1,1}(\lambda) = 0, \quad w^{\rho}_{1,2}(\lambda) = \vartheta_1(2\lambda)\vartheta_1(\rho) \neq 0. \tag{4.72}$$

As $w^{\rho}_{1,1}$ is not constant zero, (4.72) implies that the two functions are linearly independent. Therefore, $\{w^{\rho}_{1,1}, w^{\rho}_{1,2}\}$ is a basis of $\Theta_2(\rho)$. The same argument shows that $\{w^{\rho+\pi/2}_{1,1}, w^{\rho+\pi/2}_{1,2}\}$ is a basis of $\Theta_2(\rho + \pi/2)$

Let $n \in \mathbb{N}_*$. We Suppose that $\{w^{\rho}_{n,k} \colon k \in \{1, \dots, 2n\}\}$ is a basis of $\Theta_{2n}(\rho)$ and $\{w^{\rho+\pi/2}_{n,k} \colon k \in \{1, \dots, 2n\}\}$ is a basis of $\Theta_{2n}(\rho + \pi/2)$. For each $x \in \mathbb{C}$, we define a set $V(x)$ by

$$V(x) = \{f \in \Theta_{2(n+1)}(x) \mid f(\lambda) = 0 = f(\pi/2 - \lambda)\}. \tag{4.73}$$

The set $V(x)$ is a subspace of $\Theta_{2(n+1)}(x)$. We define the function $\imath$ on $\Theta_{2n}(\rho)$ by

$$\imath f(\mu) = f(\mu)\vartheta_2(\lambda + \mu)\vartheta_1(\lambda - \mu) \quad \text{for all } f \in \Theta_{2n}(\rho). \tag{4.74}$$

The function $\imath$ is linear injective. Moreover, $\imath$ maps every function in $\Theta_{2n}(\rho)$ to $V(\rho + \pi/2)$. For every $f \in V(\rho + \pi/2)$, the function g defined by

$$g(\mu) = \frac{f(\mu)}{\vartheta_2(\lambda + \mu)\vartheta_1(\lambda - \mu)} \tag{4.75}$$

is a function of $\Theta_{2n}(\rho)$ and satisfies $\imath g = f$. Hence, $\imath$ is a linear isomorphism. Thus, $V(\rho + \pi/2)$ has dimension $2n$.

We compute

$$\imath(w^{\rho}_{n,k})(\mu) = -w^{\rho+\pi/2}_{n+1,k}(\mu). \tag{4.76}$$

The negative sign and the $\pi/2$ in the right side of the equation is there to cancel the change $z_n \mapsto z_{n+1}$. Because $\{w^{\rho}_{n,k} \colon k \in \{1, \dots, 2n\}\}$ is a basis of $\Theta_{2n}(\rho)$ and $\imath$ is a linear isomorphism, $\{w^{\rho+\pi/2}_{n+1,k} \colon k \in \{1, \dots, 2n\}\}$ is a basis of $V(\rho + \pi/2)$.

As $\Theta_{2(n+1)}(\rho + \pi/2)$ has dimension $2(n + 1)$, we only need two additional vectors to construct a basis. We see that $w^{\rho+\pi/2}_{n+1,2n-1}$ has only one of the roots defining $V(\rho + \pi/2)$, whereas $w^{\rho+\pi/2}_{n+1,2n}$ has none

$$\begin{aligned}
w^{\rho+\pi/2}_{n+1,2n-1}(\lambda) &= 0, \\
w^{\rho+\pi/2}_{n+1,2n-1}(\pi/2 - \lambda) &= -\vartheta_2(0)^{n-1}\vartheta_1(2\lambda)^{n-1}\vartheta_2(2\lambda)\vartheta_2(z_n) \neq 0, \\
w^{\rho+\pi/2}_{n+1,2n}(\lambda) &= \vartheta_1(2\lambda)^{n}\vartheta_2(0)^{n-1}\vartheta_1(z_n) \neq 0, \\
w^{\rho+\pi/2}_{n+1,2n}(\pi/2 - \lambda) &= \vartheta_2(0)^{n}\vartheta_1(2\lambda)^{n-1}\vartheta_2(z_n + 2\lambda) \neq 0.
\end{aligned} \tag{4.77}$$

Both functions are not in $V(\rho+\pi/2)$. As λ is a root of only one of the functions, they are linearly independent in $\Theta_{2(n+1)}(\rho+\pi/2)/V(\rho+\pi/2)$. Therefore, $\{w_{n+1,k}^{\rho+\pi/2}\colon k \in \{1,\dots,2(n+1)\}\}$ is a basis of $\Theta_{2(n+1)}(\rho+\pi/2)$. We use the same argument on the other basis and the relation $\Theta_{2(n+1)}(\rho+\pi/2) = \Theta_{2(n+1)}(\rho-\pi/2)$ to show that $\{w_{n+1,k}^{\rho}\colon k \in \{1,\dots,2(n+1)\}\}$ is a basis of $\Theta_{2(n+1)}(\rho)$.

By induction, the statement holds for all $n \in \mathbb{N}_*$. □

4.3.2 Future Steps

The next step would be to compute the coefficients C_k of $\tilde{Z}_n(\lambda,\mu,\rho,\zeta,\xi)$ in this basis. The coefficients are, up to a factor, the refined partition functions. We define the two vector spaces of $\Theta_{2n}(\rho)$

$$\begin{aligned} V_n^+ &= \operatorname{span}\{w_{n,k}\colon k \in \{2,4,\dots,2n\}\}, \\ V_n^- &= \operatorname{span}\{w_{n,k}\colon k \in \{1,3,\dots,2n-1\}\}. \end{aligned} \tag{4.78}$$

We write $P^{\pm}$ the projector associated to $V_n^{\pm}$. One way to extract the coefficients would be to find how to explicitly write $P^{\pm}\tilde{Z}_n(\lambda,\mu,\rho,\zeta,\xi)$. Then, we would have

$$\begin{aligned} P^+ Z_n(\lambda,\mu,\rho,\zeta,\xi) &= \sum_{k=1}^{n} C_{2k} w_{n,2k}(\lambda,\xi,\rho) \\ &= w_{n,2}(\lambda,\xi,\rho) \sum_{k=1}^{n} C_{2k} \left(\frac{\vartheta_1(\lambda-\xi)\vartheta_2(\lambda+\xi)}{\vartheta_1(\lambda+\xi)\vartheta_2(\lambda-\xi)}\right)^{k-1}. \end{aligned} \tag{4.79}$$

A similar equation holds for $P^- Z_n(\lambda,\mu,\rho,\zeta,\xi)$. Up to a factor $w_{n,2}(\lambda,\xi,\rho)$, the last line of Equation (4.79) is a polynomial in the parameter $t(\xi) = \vartheta_1(\lambda-\xi)\vartheta_2(\lambda+\xi)/\vartheta_1(\lambda+\xi)\vartheta_2(\lambda-\xi)$. We could then extract the coefficient by inverting the relation $t = t(\xi)$ and then use Cauchy's theorem.

In parallel, we need to find the partition function of the free path in the extendend domain. We can use the same technique as in Section 3.1.6, but the matrix E is bigger. Because of the double parity dependence of the weights, the matrix is of size $2^3 = 8$. We inverted E with symbolic computation during this work, but we did not simplify it enough to be able to use the results.

Chapter 5

Conclusion

In this thesis, we studied the arctic curve with the help of the tangent method. We examined the computation of this curve in the case of the six-vertex model with domain-wall boundary conditions with and without a reflecting end. We also generated random configurations numerically to compare the results. We noticed that in the case of the reflecting end, the tangent method does not allow us to compute the western branches of the curve.

We then considered the three-colour model and its relation to the eight-vertex solid-on-solid model. The sampled three-colouring indicates that, when the colour weights are different, the three-colour model has a third phase in the center of the square. This behaviour is similar to the anti-ferroelectric phase of the six-vertex model. We saw that the partition function of the latter model is similar to the six-vertex model with domain-wall boundary conditions. However, we were not yet able to use this relation to make a step towards the computation of the arctic curve in the three-colour model. We were additionally interested in a simpler model, specifically when the parameter η takes the value $\pi/2$. We still have to extract the refined partition functions of the latter model.

Looking forward, the main challenge remains the search for the arctic curve in the three-colour model. Moreover, if a third phase really exists, the tangent method cannot give us information about its arctic curve. Additionally, we still do not know how to obtain the arctic curve's expression on the left side of the six-vertex model with a reflecting end.

Appendix A

Eight-Vertex Solid-on-Solid Model Partition Function

In this section, we rewrite the partition function of Hietala's thesis [20] in terms of the weight parametrisation of definition 4.8. We begin by writting Hietala's parametrization. Let $q = \mathrm{e}^{\mathrm{i}\eta}$ and $p = \mathrm{e}^{\mathrm{i}\tau}$. We define two functions

$$\vartheta(x,p) = \prod_{k=0}^{\infty}(1-p^k x)(1-p^{k+1}/x) \quad \text{and} \quad [x] = q^{-x}\vartheta(q^{2x},p^2). \tag{A.1}$$

We write $z^H = \rho + h$. Hietala's weight parametrization is

$$a^H(\lambda,h) = \frac{[\lambda+1]}{[1]}, \quad b^H_{\pm}(\lambda,h) = \frac{[\lambda]}{[1]}\frac{[z^H \mp 1]}{[z^H]}, \quad c^H_{\pm}(\lambda,h) = \frac{[z^H \pm \lambda]}{[z^H]}. \tag{A.2}$$

The weights for the turns are

$$k_+(\lambda,\rho,\zeta) = \frac{[\rho+\zeta-\lambda]}{[\rho+\zeta+\lambda]}, \quad k_-(\lambda,\rho,\zeta) = \frac{[\zeta-\lambda]}{[\zeta+\lambda]}. \tag{A.3}$$

With this parametrisation, the partition function is given in the following theorem.
Theorem A.1 (Partition function [19, p. 7])**.** *For $n \in \mathbb{N}$, define the matrix $K \in \mathbb{C}^{n\times n}$ with components*

$$K_{ij} = \frac{1}{[\lambda_i+\mu_j+1][\lambda_i-\mu_j+1][\lambda_i+\mu_j][\lambda_i-\mu_j]}. \tag{A.4}$$

The partition function of the 8VSOS with domain-wall boundary condition and a reflecting end with weight as in equation (A.2) *and* (A.3) *is*

$$\begin{aligned} Z^H_n(\vec{\lambda},\vec{\mu},\rho,\zeta) = [1]^{n-2n^2}\prod_{i=1}^{n}\frac{[2\lambda_i][\zeta-\mu_i][\rho+\zeta+\mu_i][\rho+(2i-n-2)]}{[\zeta+\lambda_i][\rho+\zeta+\lambda_i][\rho+(n-i)]} \\ \times\frac{\prod_{i,j=1}^{n}[\lambda_i+\mu_j+1][\lambda_i-\mu_j+1][\lambda_i+\mu_j][\lambda_i-\mu_j]}{\prod_{i<j}^{n}[\lambda_i+\lambda_j+1][\lambda_i-\lambda_j][\mu_j+\mu_i][\mu_j-\mu_i]}\det K. \end{aligned} \tag{A.5}$$

To prove theorem 4.9, we use the infinite product expression of the Jacobi theta function.

Theorem A.2. *We write $G(p) = \prod_{k=1}^{\infty}(1-p^{2k})$. The product form of the first and fourth Jacobi theta functions are*

$$\vartheta_4(x,p) = G(p)\prod_{n\in\mathbb{N}}(1-p^{2n+1}\mathrm{e}^{\mathrm{i}2x})(1-p^{2n+1}\mathrm{e}^{-\mathrm{i}2x}). \tag{A.6}$$

Proof of theorem 4.9. We compare the infinite product of ϑ_4 (A.6) with the definition of ϑ (A.1) and obtain

$$\vartheta_4(x,p) = G(p)\vartheta(p\mathrm{e}^{\mathrm{i}2x}, p^2). \tag{A.7}$$

In terms of ϑ_1, we use (4.4) and the expression becomes

$$\begin{aligned}\vartheta_1(x,p) &= \mathrm{i}\mathrm{e}^{-\mathrm{i}x}p^{1/4}\vartheta_4(x-\pi\tau/2,p)\\ &= \mathrm{i}\mathrm{e}^{-\mathrm{i}x}p^{1/4}G(p)\vartheta(\mathrm{e}^{\mathrm{i}2x},p^2) = \mathrm{i}p^{1/4}G(p)[x/\eta].\end{aligned} \tag{A.8}$$

For any $i\in\{1,2,3,4\}$, we write $\vartheta_i(x) = \vartheta_i(x,p)$. We rewrite the weight parametrised by Linnea Hietala in terms of ϑ_1 using (A.8)

$$a^H(\lambda,z) = \frac{\vartheta_1(\eta\lambda+\eta)}{\vartheta_1(\eta)}, \quad b^H_{\pm}(\lambda,z) = \frac{\vartheta_1(\eta\lambda)}{\vartheta_1(\eta)}\frac{\vartheta_1(\eta z\mp\eta)}{\vartheta_1(\eta z)}, \tag{A.9}$$

$$c^H_{\pm}(\lambda,z) = \frac{\vartheta_1(\eta z\pm\eta\lambda)}{\vartheta_1(\eta z)}. \tag{A.10}$$

We could do the same thing with the turns and the partition function Z^H. To simplify the notations, we consider a new parametrization. We absorb the factor η in λ, z and ζ and multiply each vertex weight by $\vartheta_1(\eta)$. We find

$$a(\lambda,z) = \vartheta_1(\lambda+\eta), \quad b_{\pm}(\lambda,z) = \frac{\vartheta_1(\lambda)\vartheta_1(z\mp\eta)}{\vartheta_1(z)}, \tag{A.11}$$

$$c_{\pm}(\lambda,z) = \frac{\vartheta_1(\eta)\vartheta_1(z\pm\lambda)}{\vartheta_1(z)}. \tag{A.12}$$

This is exactly the vertex weight parametrisation of definition (4.8). The same results holds for the turns k_+ and k_-. We use again (A.8) to rewrite the partition function of the system with this choice of weight

$$\begin{aligned}Z_n(\vec{\lambda},\vec{\mu},\rho,\zeta) &= \vartheta_1(\eta)^{2n^2}Z^H_n(\vec{\lambda}/\eta,\vec{\mu}/\eta,\rho/\eta,\zeta/\eta)\\ &= \vartheta_1(\eta)^n\prod_{i=1}^{n}\frac{\vartheta_1(2\lambda_i)\vartheta_1(\zeta-\mu_i)\vartheta_1(\rho+\zeta+\mu_i)\vartheta_1(\rho+(2i-n-2)\eta)}{\vartheta_1(\zeta+\lambda_i)\vartheta_1(\rho+\zeta+\lambda_i)\vartheta_1(\rho+(n-i)\eta)}\\ &\times\frac{\prod_{i,j=1}^{n}\vartheta_1(\lambda_i+\mu_j+\eta)\vartheta_1(\lambda_i-\mu_j+\eta)\vartheta_1(\lambda_i+\mu_j)\vartheta_1(\lambda_i-\mu_j)}{\prod_{i<j}\vartheta_1(\lambda_i+\lambda_j+\eta)\vartheta_1(\lambda_i-\lambda_j)\vartheta_1(\mu_j+\mu_i)\vartheta_1(\mu_j-\mu_i)}\det K,\end{aligned} \tag{A.13}$$

and K is

$$K_{ij} = \frac{1}{\vartheta_1(\lambda_i+\mu_j+\eta)\vartheta_1(\lambda_i-\mu_j+\eta)\vartheta_1(\lambda_i+\mu_j)\vartheta_1(\lambda_i-\mu_j)}. \tag{A.14}$$

This concludes the proof. □

We conclude with the appendix with the proofs of the two properties 4.4 and 4.5.

Proof of proposition 4.4. We use A.8 to obtain

$$\vartheta_1(x,p)\vartheta_1(x+\pi/2,p) = \mathrm{i}\mathrm{e}^{-2\mathrm{i}x}p^{1/2}\vartheta(\mathrm{e}^{2\mathrm{i}x},p^2)\vartheta(-\mathrm{e}^{2\mathrm{i}x},p^2). \tag{A.15}$$

We use the definition of ϑ (A.1) on the product

$$\vartheta(\mathrm{e}^{2\mathrm{i}x},p^2)\vartheta(-\mathrm{e}^{2\mathrm{i}x},p^2) = \prod_{k=0}^{\infty}(1-p^{4k}\mathrm{e}^{4\mathrm{i}x})(1-p^{4k+4}\mathrm{e}^{-4\mathrm{i}x}) = \vartheta(\mathrm{e}^{4\mathrm{i}x},p^4). \tag{A.16}$$

We use the relation between ϑ_1 and ϑ_2 from Proposition 4.2 and A.8 a second time to find

$$\vartheta_1(x,p)\vartheta_2(x,p) = \frac{G(p)^2}{G(p^2)}\vartheta_1(2x,p^2). \tag{A.17}$$

□

Proof of proposition 4.5. We write $\delta = \mathrm{e}^{2\pi\mathrm{i}/3}$. We use A.8 and $\delta^3 = 1$ to obtain

$$\begin{aligned}\vartheta_1(x,p)\vartheta_1(x+2\pi/3,p)\vartheta_1(x+4\pi/3,p)&\\ = \mathrm{i}\mathrm{e}^{-3\mathrm{i}x}p^{3/4}\vartheta(\mathrm{e}^{2\mathrm{i}x},p^2)\vartheta(\mathrm{e}^{2\mathrm{i}x}\delta,p^2)\vartheta(\mathrm{e}^{2\mathrm{i}x}\delta^2,p^2).&\end{aligned} \tag{A.18}$$

For each $k \in \mathbb{N}$ and $X \in \mathbb{C}$, we have

$$(1-p^{2k}X)(1-p^{2k}X\delta)(1-p^{2k}X\delta^2) = 1-p^{2k}X^3. \tag{A.19}$$

We use the definition of ϑ (A.1) on the product and (A.19)

$$\begin{aligned}\vartheta(\mathrm{e}^{2\mathrm{i}x},p^2)\vartheta(\mathrm{e}^{2\mathrm{i}x}\delta,p^2)\vartheta(\mathrm{e}^{2\mathrm{i}x}\delta^2,p^2)&\\ = \prod_{k=0}^{\infty}(1-p^{6k}\mathrm{e}^{6\mathrm{i}x})(1-p^{6k+6}\mathrm{e}^{-6\mathrm{i}x}) = \vartheta(\mathrm{e}^{6\mathrm{i}x},p^6).&\end{aligned} \tag{A.20}$$

We use proposition 4.2 and A.8 a second time to find

$$\vartheta_1(x,p)\vartheta_1(x+2\pi/3,p)\vartheta_1(x+4\pi/3,p) = \frac{G(p)^3}{G(p^3)}\vartheta_1(2x,p^2). \tag{A.21}$$

□

Appendix B

Computation of the Boundary Factor

In this section, we compute the factor A_n of the proof of Theorem 4.11. We recall (4.26)

$$\prod_{v\in V(\mathcal{B})} \tilde{w}_\omega(v) = B_n \Psi(\rho)^{2n^2} \prod_{f\in F(\mathcal{B})} \frac{1}{\vartheta_1(\rho + 2h_\omega(f)\pi/3)^3}. \tag{B.1}$$

To find this equation, we counted that every vertiex gives a factor $1/\vartheta_1$ to each face. The factor B_n accounts for the boundary. We write L_n, R_n, U_n and D_n the part of B_n that comes respectively from the left column, the right column, the upper line and the lower line. We count the factor arising from the corner of the grid in the column, not the lines. We compute the factors with the help of figure B.1. On the left column, we overcounted $n+3$ time the faces outside the turns, which have all zero height, and two times for each face inside the turns. We thus obtain

$$L_n = \vartheta_1(\rho)^{n+3} \vartheta_1\left(\rho + \frac{2\pi}{3}\right)^{n-k} \vartheta_1\left(\rho + \frac{4\pi}{3}\right)^{k}. \tag{B.2}$$

On the right column, we overcounted once the faces that are on the same lines as the faces outside the turns, and the other are counted two times to much, except the bottom right corner that we need to count once more. We thus obtain

$$R_n = \vartheta_1\left(\rho - \frac{2n\pi}{3}\right) \prod_{k=0}^{2n} \vartheta_1\left(\rho - \frac{2n\pi}{3} + \frac{2k\pi}{3}\right) \prod_{k=0}^{n} \vartheta_1\left(\rho - \frac{2n\pi}{3} + \frac{4k\pi}{3}\right). \tag{B.3}$$

For U_n, we counted each factor one time two much and for D_n two times two much.

$$U_n = \prod_{k=1}^{n-1} \vartheta_1\left(\rho + \frac{2k\pi}{3}\right), \quad D_n = \prod_{k=1}^{n-1} \vartheta_1\left(\rho - \frac{2k\pi}{3}\right)^2. \tag{B.4}$$

We recall that we use the notation

$$\Psi(\rho) = \frac{G(p)^3}{G(p^3)} \vartheta_1(3\rho, p^3) = \prod_{k=0}^{2} \vartheta_1\left(\rho + \frac{2k\pi}{3}\right). \tag{B.5}$$

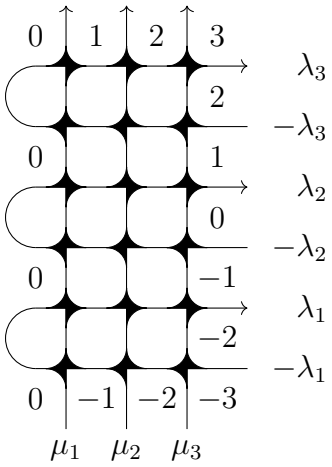

Figure B.1: Configuration of the 8VSOS model on a rectangular grid with $n = 3$ with a reflecting end. The shadow region near each vertex v indicates the faces a, b, and d.

With the help of (B.5), we can replace the product involved in R_n, U_n and D_n by $\Psi(\rho)$ when the product has a multiple of 3 terms. We compute the factors R_n, U_n and D_n depending on the values of n modulo 3. If $n \equiv 0 \mod 3$, there exist $m \in \mathbb{N}$ such that $n = 3m$ and

$$\begin{aligned} R_n &= \vartheta_1(\rho) \prod_{k=0}^{6m} \vartheta_1\left(\rho + \frac{2k\pi}{3}\right) \prod_{k=0}^{3m} \vartheta_1\left(\rho + \frac{4k\pi}{3}\right) = \vartheta_1(\rho)^3 \Psi(\rho)^{3m}, \\ U_n &= \frac{1}{\vartheta_1(\rho)} \prod_{k=0}^{3m-1} \vartheta_1\left(\rho + \frac{2k\pi}{3}\right) = \frac{\Psi(\rho)^m}{\vartheta_1(\rho)}, \\ D_n &= \frac{1}{\vartheta_1(\rho)^2} \prod_{k=0}^{3m-1} \vartheta_1\left(\rho + \frac{4k\pi}{3}\right)^2 = \frac{\Psi(\rho)^{2m}}{\vartheta_1(\rho)^2}. \end{aligned} \tag{B.6}$$

So the product is $R_n U_n D_n = \Psi(\rho)^{2n}$. If $n \equiv 1 \mod 3$, there exist $m \in \mathbb{N}$ such that $n = 3m + 1$ and

$$\begin{aligned} R_n &= \vartheta_1\left(\rho + \frac{4\pi}{3}\right) \prod_{k=0}^{6m+2} \vartheta_1\left(\rho + \frac{2(k+2)\pi}{3}\right) \prod_{k=0}^{3m+2} \vartheta_1\left(\rho + \frac{4(k+1)\pi}{3}\right) \frac{1}{\vartheta_1(\rho)} \\ &= \frac{1}{\vartheta_1(\rho)} \vartheta_1\left(\rho + \frac{4\pi}{3}\right) \Psi(\rho)^{3m+2}, \\ U_n &= \prod_{k=1}^{3m} \vartheta_1\left(\rho + \frac{2k\pi}{3}\right) = \Psi(\rho)^m, \\ D_n &= \prod_{k=1}^{3m} \vartheta_1\left(\rho + \frac{4k\pi}{3}\right)^2 = \Psi(\rho)^{2m}. \end{aligned} \tag{B.7}$$

So with $n = 3m + 1$ the product $R_n U_n D_n$ is

$$R_n U_n D_n = \frac{1}{\vartheta_1(\rho)} \vartheta_1\left(\rho + \frac{4\pi}{3}\right) \Psi(\rho)^{2n}. \tag{B.8}$$

Finally, for $n \equiv 2 \mod 3$, there exist $m \in \mathbb{N}$ such that $n = 3m + 2$ and

$$\begin{aligned}
R_n &= \vartheta_1\left(\rho + \frac{2\pi}{3}\right) \prod_{k=0}^{6m+5} \vartheta_1\left(\rho + \frac{2(k+1)\pi}{3}\right) \frac{1}{\vartheta_1(\rho)} \prod_{k=0}^{3m+2} \vartheta_1\left(\rho + \frac{4(k-1)\pi}{3}\right) \\
&= \frac{1}{\vartheta_1(\rho)} \vartheta_1\left(\rho + \frac{2\pi}{3}\right) \Psi(\rho)^{3m+3}, \\
U_n &= \prod_{k=1}^{3m} \vartheta_1\left(\rho + \frac{2k\pi}{3}\right) \vartheta_1\left(\rho + \frac{2\pi}{3}\right) = \vartheta_1\left(\rho + \frac{2\pi}{3}\right) \Psi(\rho)^m, \\
D_n &= \prod_{k=1}^{3m} \vartheta_1\left(\rho + \frac{4k\pi}{3}\right)^2 \vartheta_1\left(\rho + \frac{4\pi}{3}\right)^2 = \vartheta_1\left(\rho + \frac{4\pi}{3}\right)^2 \Psi(\rho)^{2m}.
\end{aligned} \tag{B.9}$$

So the product $R_n U_n D_n$ is

$$\begin{aligned}
R_n U_n D_n &= \frac{1}{\vartheta_1(\rho)} \vartheta_1\left(\rho + \frac{2\pi}{3}\right)^2 \vartheta_1\left(\rho + \frac{4\pi}{3}\right)^2 \Psi(\rho)^{6m+3} \\
&= \frac{1}{\vartheta_1(\rho)^2} \vartheta_1\left(\rho + \frac{2\pi}{3}\right) \vartheta_1\left(\rho + \frac{4\pi}{3}\right) \Psi(\rho)^{2n}.
\end{aligned} \tag{B.10}$$

Bibliography

[1] A. Aggarwal. Arctic boundaries of the ice model on three-bundle domains. *Invent. Math.*, 220:611–671, 2022.

[2] D. Allison and N. Reshetikhin. Numerical study of the 6-vertex model with domain wall boundary conditions. *Ann. I. Fourier*, 55(6):1847–1869, 2005.

[3] R. J. Baxter. *Exactly solved models in statistical mechanics*. Academic Press, 1982.

[4] P. Bleher and T. Bothner. Exact solution of the six-vertex model with domain wall boundary conditions: Critical line between disordered and antiferroelectric phases. *Random Matrices-Theo.*, 01(04):1250012, 2012.

[5] P. Bleher and K. Liechty. Exact solution of the six-vertex model with domain wall boundary conditions. critical line between ferroelectric and disordered phases. *J. Stat. Phys.*, 134(3):463–485, 2009.

[6] P. Bleher and K. Liechty. Exact solution of the six-vertex model with domain wall boundary conditions. ferroelectric phase. *Commun. Math. Phys.*, 286(2):777–801, 2009.

[7] P. Bleher and K. Liechty. Exact solution of the six-vertex model with domain wall boundary conditions. antiferroelectric phase. *Commun. Pure Appl. Math.*, 63(6):779–829, 2010.

[8] P. Bleher and K. Liechty. *Random matrices and the six-vertex model*, volume 32 of *CRM Monograph Series*. Amer. Math. Soc., 2013.

[9] P. M. Bleher and V. V. Fokin. Exact solution of the six-vertex model with domain wall boundary conditions. disordered phase. *Commun. in Math. Phys.*, 268(1):223–284, 2006.

[10] S. Brasseur. *The eight-vertex model on its combinatorial line*. Master's thesis, UCLouvain, 2019.

[11] D. M. Bressoud. *Proofs and confirmations: the story of the alternating-sign matrix conjecture*. Cambridge University Press, 1999.

[12] I. V. Cherednik. Factorizing Particles on a Half Line and Root Systems. *Theor. Math. Phys.*, 61:977–983, 1984.

[13] F. Colomo and A. Sportiello. Arctic curves of the six-vertex model on generic domains: The tangent method. *J. Stat. Phys.*, 164(6):1488–1523, 2016.

[14] J.-F. de Kemmeter. *Fluctuations et courbes arctiques dans le modèle à 6 vertex*. Master's thesis, UCLouvain, 2020.

[15] B. Debin, E. Granet, and P. Ruelle. Concavity analysis of the tangent method. *J. Stat. Mech.-Theory E*, 2019(11):113107, 2019.

[16] P. Di Francesco. Arctic curves of the reflecting boundary six vertex and of the twenty vertex models. *J. Phys. A: Math. Theor.*, 54(35):355201, 2021.

[17] R. Diestel. *Graph theory*. GTM. Springer, fifth edition, 2017.

[18] P. L. Ferrari and H. Spohn. Domino tilings and the six-vertex model at its free-fermion point. *J. Phys. A: Math. Gen.*, 39(33):10297–10306, 2006.

[19] L. Hietala. A combinatorial description of certain polynomials related to the xyz spin chain. *SIGMA*, 16(101):1–26, 2020.

[20] L. Hietala. *Combinatorics of solvable lattice models with a reflecting end*. PhD thesis, University of Gothenburg, 2021.

[21] A. G. Izergin, D. A. Coker, and V. E. Korepin. Determinant formula for the six-vertex model. *J. Phys. A: Math. Gen.*, 25(16):4315, 1992.

[22] T. R. Jensen and B. Toft. *Graph coloring problems*. John Wiley & Sons, 2011.

[23] V. Korepin and P. Zinn-Justin. Thermodynamic limit of the six-vertex model with domain wall boundary conditions. *J. Phys. A: Math. Gen.*, 33(40):7053–7066, 2000.

[24] V. E. Korepin. Calculation of norms of Bethe wave functions. *Commun. Math. Phys.*, 86:391–418, 1982.

[25] G. Kuperberg. Another proof of the alternative-sign matrix conjecture. *Int. Math. Res. Notices*, 1996(3):139–150, 01 1996.

[26] G. Kuperberg. Symmetry classes of alternating-sign matrices under one roof. *Ann. Math.*, 156(3):835–866, 2002.

[27] J. Lamers et al. *On elliptic quantum integrability: vertex models, solid-on-solid models and spin chains*. PhD thesis, Utrecht University, 2016.

[28] D. A. Levin and Y. Peres. *Markov chains and mixing times*. Amer. Math. Soc., 2017.

[29] E. H. Lieb. Residual entropy of square ice. *Phys. Rev.*, 162:162–172, 1967.

[30] E. H. Lieb and F. Y. Wu. Two-dimensional ferroelectric models. In *Phase transitions and critical phenomena*, volume 1, pages 331–490. 1972.

[31] L. Pauling. The structure and entropy of ice and of other crystals with some randomness of atomic arrangement. *J. Am. Chem. Soc.*, 57(12):2680–2684, 1935.

[32] G. M. Phillips. *Interpolation and approximation by polynomials*, volume 14 of *CMS Books in Mathematics*. Springer, 2003.

[33] H. Rosengren and M. Schlosser. Elliptic determinant evaluations and the macdonald identities for affine root systems. *Compos. Math.*, 142(4):937–961, 2006.

[34] E. K. Sklyanin. Boundary conditions for integrable quantum systems. *J. Phys. A: Math. Gen.*, 21(10):2375, 1988.

[35] B. Sutherland. Exact solution of a two-dimensional model for hydrogen-bonded crystals. *Phys. Rev. Lett.*, 19(3):103, 1967.

[36] E. T. Whittaker and G. N. Watson. *A Course of Modern Analysis*. Cambridge Mathematical Library. Cambridge University Press, fourth edition, 1996.

UNIVERSITE CATHOLIQUE DE LOUVAIN

Faculté des sciences

Place des sciences, 2 bte L6.06.01, 1348 Louvain-la-Neuve, Belgique — **www.uclouvain.be/sc**